UNIVERSITÀ DEGLI STUDI DI TRIESTE

XXX CICLO DEL DOTTORATO DI RICERCA IN

Scienze della Riproduzione e dello Sviluppo

Role of Patrolling Monocytes in Diabetic Retinopathy in an animal model of Type 1 Diabetes

Settore scientifico-disciplinare: **MED/13 ENDOCRINOLOGIA**

DOTTORANDO
Francesco Tecilazich

COORDINATORE
PROF. Alessandro Ventura

SUPERVISORE DI TESI
PROF. Mara Lorenzi

SUPERVISORE DI TESI
PROF. Tarcisio Not

ANNO ACCADEMICO 2016/2017

Table of Contents

I. INTRODUCTION

1. Diabetic Retinopathy

Diabetic retinopathy is the leading cause of legal blindness among adults in the Western World, and a personal catastrophe to the individual. Epidemiological data predict a dramatic increase in the prevalence of diabetes in Europe, rising from 55 million in 2010, to over 66 million in 2030 (International Diabetes Federation, 2015). It is reasonable to assume there will be a parallel increase in all its complications, including diabetic retinopathy, the most common complication of diabetes. In this perspective it is imperative to develop better means to identify, prevent, and treat diabetic retinopathy in its early stages.

The hallmarks of the early stages of diabetic retinopathy are pericyte loss, thickening of vascular basal lamina, breakdown of blood retinal barrier, and acellular capillaries. As the diabetic retinal microvascular disease progresses, saccular microaneurysms and hemorrhages appear, and increasingly larger areas of non-perfused capillaries become evident; this non-perfusion – in combination with the loss of the blood retinal barrier – facilitates the formation of retinal exudates and retinal edema in the macula with loss of vision. When non-perfused areas of the retina become large enough, neovascularization may develop and may lead to vitreal hemorrhages, scarring, and retinal detachment with subsequent severe vision loss.

2. Vascular repair

The concept of vascular repair encompasses the restoration of normal vascular function and structure, and the reversal of vascular senescence. Regeneration by stem cells and progenitor cells has been recognized as a system for the maintenance and recovery of vascular homeostasis; given their theoretical capacity to replicate, differentiate, and form new blood vessels, stem cells and progenitor cells have been considered as ideal candidates for delivering therapeutic activities on damaged vessels. The occurrence of vascular repair, at least in the early stages of diabetes, is suggested by the long latency period observed between the onset of the metabolic abnormalities, and the clinical appearance of microvascular disease. In human diabetes, clinical signs of diabetic retinopathy – usually the first microvascular complication to become apparent – develop after a period of time that was 5-8 years before the implementation of tight glycemic control, and may currently reach 15-20 years (Hammes et al., 2011). Symmetrically, in rodents with experimental diabetes apoptosis of vascular cells that precedes development of acellular capillaries – a cumulative measure of retinal microangiopathy (Mizutani et al., 1996) – does not become detectable until at least 6-9 months after the induction of diabetes (Gerhardinger et al., 2001, Zheng et al., 2007), despite hyperglycemia in the range of 400-500 mg/dl.

3. From Endothelial Progenitor Cells to Patrolling monocytes

We first approached the concept of vascular repair in diabetes by studying the role of endothelial progenitor cells

(EPCs), both in early diabetic retinopathy, and in diabetic wound healing. The former project contrasted different types of EPCs in patients with type 1 diabetes and very early or absent retinopathy. It showed an increased number of clonogenic EPCs (CFU-Hill), but not of EPCs that integrate into the vascular wall, in patients with initial retinopathy (Zerbini et al., 2012). We hypothesized that the selectively increased number may represent a response to vessels signalling a need for repair (Zerbini et al., 2012). We also found that some of the specifications needed for “homing” were defective in the cells from diabetic patients (Zerbini et al., 2012). This combination of findings highlighted the need for a systematic evaluation of the agents and mechanisms of vascular repair in diabetes. The study of EPCs in diabetic wound healing focused instead on how EPCs changed in the progression of wound healing in diabetes; whether EPC levels correlated with wound healing, and whether diabetes induced an unfavorable EPC profile that could negatively impact the wound outcome (Tecilazich et al., 2013). We found that EPCs were reduced in patients with ulcerations, suggesting possible increased homing.

Pursuing CFU-Hill cells appeared risky because their lineage was not well defined, and they were accessible only through their clonogenic activity in vitro. The fact that CFU-Hill cells exert their pro-angiogenic role via the paracrine provision of cytokines and growth factors (Yoder et al., 2007) – and have both endothelial and monocytic characteristics (Zerbini et al., 2012, Yoder et al., 2007, Rohde et al., 2006) – brought the attention to the potential repair roles of a discrete subset of circulating monocytes named “Patrolling”.

4. Inflammation and vascular disease

The relationship between inflammation and vascular disease is so robust that the measurement of high-sensitivity C-reactive protein – a measure of subclinical inflammation – is used in clinical medicine as a potent and independent predictor of future vascular events (Ridker, 2003). Moreover, the Canakinumab Antiinflammatory Thrombosis Outcome Study, a clinical trial of more than 10,000 heart attack patients, has recently confirmed that reducing inflammation reduces the risk of cardiovascular disease, and thereby provides the proof of principle of the pivotal role of inflammation in the pathogenesis of cardiovascular disease (Ridker et al., 2017). Notably, early in the inflammatory process, circulating leukocytes bind to the endothelium; among them monocytes are prominent (Woollard and Geissmann, 2010).

5. Monocytes

Monocytes are non-dividing cells, they represent ~2% of the total bone marrow mononuclear cells and are the largest phagocytic cells (12-20μ) in the bone marrow. They are capable of differentiating into dendritic cells (DCs), and macrophages during inflammation. The fate of monocytes depends both on their antigenic profile and also on the environment.

i. Development

Mononuclear phagocytes can be separated into two groups of cells: the circulating mononuclear phagocytes, or monocytes, in the peripheral blood, and tissue macrophages in organs, such as the spleen, lymphnodes, liver (Kupffer's cells), the lung (alveolar

macrophages), the peritoneal cavity, and the subcutaneous tissues (van Furth and Cohn, 1968).

Monocytes continuously derive from the bone marrow from dividing monoblasts (Auffray et al., 2007). Hematopoietic stem cells can give rise to monoblasts (via the common myeloid progenitor) and lymphoblasts (via the common lymphoid progenitor) on one hand, and vascular cells on the other hand. The monocyte direct precursors (promonocytes) divide at least twice before maturing to the monocyte stage.

ii. Kinetics

Most monocytes leave the bone marrow immediately after being originated, even though a minority appears to stay in the bone marrow for several hours or even days (Williams, 1977). Once released into the blood stream, monocytes circulate for several days (t½ ~3 days) before entering tissues and replenishing the macrophage populations (71 hours in humans; 17 hours in rodents). Monocytes typically assume a triangular shape as they move, with one point trailing behind and the other two points advancing before the cell. In a steady state monocytes do not proliferate and constitute 5-9% of circulating leukocytes in human adults (285-500/mm^3) (van Furth, 1989).

iii. Classification

Morphologically, monocytes are a heterogeneous population with varying size, degree of granularity and nuclear morphology. Functionally, monocytes can be divided in two principal subsets (Geissmann et al., 2003, Ziegler-Heitbrock et al., 2010, Passlick et al., 1989); the salient identifying characteristics of the two subsets are listed in Table 1. One is the “classical” or “inflammatory”

subset, whose cells are actively recruited to inflamed tissues, are phagocytic, and produce reactive oxygen species (ROS) and pro-inflammatory cytokines. The second is the “nonclassical” or “patrolling” subset, whose cells survey normal blood vessels, accumulate poorly in tissues, are weak phagocytes, do not produce ROS, produce non-inflammatory or anti-inflammatory cytokines, and have housekeeping functions for the endothelium.

The common monocyte progenitor (cMoP) is the common precursor of inflammatory and patrolling monocytes, and is defined as [Lin^- C-Kit^+ M-$CSFR^+$ $Flt3^-$ $Ly6C^+$ $CD11b^-$ CX_3CR1^+]. cMoP is a monocyte-restricted progenitor and represents the missing link between MDP (monocyte macrophage DC progenitor) and mature monocytes. Notably, cMoP gives rise also to macrophages and monocyte-derived DCs, but not to classical DCs and to lymphoid cell types (T cells, B cells and natural killer cells) (Hettinger et al., 2013).

iv. Patrolling monocytes

PMo have round or bean shaped nuclei; a granule-poor cytoplasm; present mobile filopedia-like structures, pseudopodia (to attach endothelial cells), and large endosomes (that contain endogenous debris/microparticles). Notably, PMo have been shown to uptake submicrometric and micrometric particles.

PMo have higher expression of pro-apoptotic and lower expression of anti-apoptotic transcripts than inflammatory monocytes. Both monocyte subsets are susceptible of caspase-dependent apoptosis, however this pathway is more pronounced in PMo and more specifically the intrinsic (mitochondrial) pathway. PMo present also lower levels of anti-oxidants than the

inflammatory subset; the inhibition of glutathione activity showed an increase of H_2O_2 induced apoptosis in inflammatory monocytes, suggesting that this mechanism is involved in the protection of oxidant induced death in these monocytes (Zhao et al., 2010). PMo present higher mitochondrial metabolic activity that induces cell death through increased production of reactive oxygen species (ROS), notably inhibition of ROS significantly reduced apoptosis (Zhao et al., 2010).

A functional characteristic that distinguishes PMo from inflammatory monocytes is their motility pattern defined as “crawling”. PMo possess a constitutive crawling against the midstream blood flow and are tightly adherent to the endothelium. The instantaneous velocity of crawling monocytes is between 4-20 μm/min (average 12).

Dr. Geissman’s group has extensively studied the functional characteristics of PMo, and unveiled the endothelium monitoring activity of these monocytes. They initially reported that these monocytes possess a high confinement ratio, as the distance they travel is generally half their path length (Auffray et al., 2007). In addition, they assessed the motility of monocytes with intravital confocal microscopy imaging in vivo in real time in branches of mesenteric vein and artery and in dermal ear vessels. They used mice expressing green fluorescent protein (GFP) at the locus of the CX_3CR1 gene ($CX_3CR1^{GFP/+}$, the expression of CX_3CR1 is bi-allelic). In this model all monocytes (but not granulocytes) express GFP, inflammatory monocytes and PMo were distinguished by the level of GFP expression (GFP^{lo}: CX_3CR1^{lo}; $GFP^{hi}\rightarrow$ CX_3CR1^{hi}, respectively). The function of CX_3CR1 was established comparing

$CX_3CR1^{GFP/+}$ to $CX_3CR1^{GFP/GFP}$ (CX_3CR1 deficient mice). Crawling has been shown to be impaired in CX_3CR1 deficient mice. Ly-6C induces clustering of LFA-1, that binds to ICAM-1, and that is required for crawling; indeed, LFA-1 inhibition causes the release of monocytes from the endothelium (Liaskou et al., 2012). Conversely, the inhibition of MAC-1, which is another ligand of ICAM-1, does not induce the detachment of monocytes from vessels. Notably, LFA-1 deficiency does not affect early recruitment of inflammatory monocytes (Tacke et al., 2007).

In addition Dr. Geissman's group has shown that there is a constant exchange of PMo between the bloodstream and the endothelium (Carlin et al., 2013). They reported that the dwell time of PMo (i.e. the time these cells were attached to the endothelium) is of 9 minutes; and showed that the blockage of LFA-1 reduced the attachment to the EC to 1%. In addition, CD11a (αL integrin) appeared absolutely necessary for crawling, and the binding of LFA-1 with ICAM-1 mediated the adhesion and crawling of PMo. Furthermore, CCR2 deficiency did not affect circulating number and crawling of PMo, but reduced number of circulating inflammatory monocytes by 50%. CX_3CR1 deficiency did not impair the motility and filopedia of PMo, but reduced their number. Hence, the authors concluded that crawling does not require CX_3CR1 nor CCR2.

Notably, a growing wealth of data documents remarkable conservation of biosynthetic and functional characteristics between human and rodents (Ingersoll et al., 2010, Ziegler-Heitbrock et al., 2010).

A. Patrolling monocytes and cardiovascular disease

Dr. Nahrendorf's group has demonstrated that PMo are fundamental in the second phase (reparative) post-myocardial infarction, as their removal impairs myocardial repair in a model of acute myocardial infarction in rodents. At baseline, the heart contains mostly CD11b^{hi} F4/80^{int} I-Ab^{+} CD11c^{lo} cells. Healing of myocardial infarction requires leukocytes through the activation of inflammatory signals. During the first week after coronary ligation, heart contains mostly monocytes (total monocytes: 4-5x10^4 cells/mg of tissue). The first cells to be recruited are neutrophils (within 24 hours, ~10^5 cells/mg of tissue), short after monocytes. In mice, the monocytes present in the infarcted zone are distinguished into two different populations: Ly-6C^{hi} (inflammatory), and Ly-6C^{lo} (PMo). The former are detectable from day 1 to day 4, when they represent 75% of total monocytes (phase 1: Ly-6C^{hi} peak day 3: 4x10^4 cells/mg of tissue; Ly-6C^{lo} ~1-2 x 10^4 cells/mg of tissue). The latter are present from day 5 to day 7, when they represent 75% of total monocytes (phase 2: Ly-6C^{lo} peak on day 7: 0.5 x 10^4 cells/mg of tissue; Ly-6C^{hi} peak on day 7: 0.5 x 10^4 cells/mg of tissue). Monocytes returned to baseline levels 16 days after coronary ligation (total monocytes: 0.3x10^4 cells/mg of tissue). Notably, macrophages in the infarcted tissue stayed at low levels from day 1 to day 7 (<1x10^4 cells/mg of tissue). By 2-3 weeks after myocardial infarction, monocytes and macrophages disappear from the tissue. CCR2 and CX_3CR1 play a pivotal role in recruiting monocytes: MCP-1 levels increase during phase 1 and its receptor is CCR2 expressed only on Ly-6C^{hi}. CCR2$^{-/-}$ mice show a 50% decrease of monocytes in phase 1, which is secondary also to

decreased bone marrow recruitment. Fractalkine (CX_3CL1) levels increase during phase 1 and its receptor is CX_3CR1 majorly expressed on PMo. $CX_3CR1^{-/-}$ mice had 6-fold reduction in PMo in phase 2, and normal levels of inflammatory monocytes in phase 1. Infarction of the myocardium did not substantially modify the levels of total circulating leukocytes; however, it induced Ly-$6C^{hi}$ monocytosis limited to phase 1. The levels of Ly-$6C^{lo}$ monocytes instead remained unchanged after MI. During phase 1, Ly-$6C^{hi}$ are 4.5-fold higher than Ly-$6C^{lo}$; instead, during phase 2 the circulating levels of the two subgroups are comparable. MI induced also a 4.8-fold increase in the infiltrating capacity limited to Ly-$6C^{lo}$ monocytes during phase 2. The infiltrating capacity of Ly-$6C^{hi}$ and Ly-$6C^{lo}$ was similar during phase 1. Therefore, Dr. Nahrendorf's group elegantly showed that the mechanisms of monocyte recruitment are different in phase 1 and phase 2 post MI, and that the dominance of Ly-$6C^{hi}$ in phase 1 is driven by the selective expansion of this circulating subtype (Ly-$6C^{hi}$ pre-MI 250 ± 200/mg tissue, day 1 post-MI 24,000 ± 6,000/mg tissue; Ly-$6C^{lo}$ pre-MI 1,400 ± 1,000/mg tissue, day 1 post-MI 5,800 ± 2,000/mg tissue). Conversely, the predominance of Ly-$6C^{lo}$ is mainly driven by preferential recruitment of this subtype. Interestingly, it has been clearly showed that Ly-$6C^{lo}$ monocytes in phase II do not derive from Ly-$6C^{hi,}$ since the number of newly recruited Ly-$6C^{lo}$ matched the number of Ly-$6C^{lo}$ in the infarcted area. In addition, $CCR2^{-/-}$ mice had low levels of Ly-$6C^{hi}$ in phase 2, and normal levels of Ly-$6C^{lo}$ in phase 2. The depletion of monocytes in phase 1 (but not phase 2) determined an increase in infarcted area and necrotic tissue, which removal depends on the proteolytic and phagocytic

actions of Ly-6C^{hi}. Conversely, the depletion of monocytes in phase 2 (but not phase 1) caused a decrease in collagen deposition and in the number of microvascular α-actin^{+} smooth muscle cells and CD31^{+} endothelial cells. Of interest, the induction of MI in Apo e$^{-/-}$ mice induced an increased recruitment of monocytes at the wound area (presumably secondary to circulating monocytosis); moreover, these mice exhibited large areas of debris and necrotic tissue (probably reflecting impaired phagocytosis). Finally, the authors observed an increased number of microvessels, but impaired deposition of new extracellular matrix. Taken together this data suggests that patients with atherosclerosis and monocytosis present impaired myocardial healing, possibly secondary to increased levels of Ly-6C^{hi} that could delay or even prevent the start of phase 2. Another possible explanation proposed by the authors could be the dysfunction of either one or both monocyte subsets (Nahrendorf et al., 2007, Hilgendorf et al., 2014).

The levels of circulating monocyte subsets were measured by Tsujioka et al. (Tsujioka et al., 2009) in the peripheral whole blood of human subjects with increasing degree of coronary artery disease: myocardial infarction (MI), unstable angina (UA) and stable angina (SA). Of note, SA days post event were defined as days post hospital admission. The inflammatory monocytes were defined as [CD14^{+}/CD16^{-}], meanwhile PMo were defined as [CD14^{hi}/CD16^{+}] and [CD14^{int}/CD16^{+}]. At day 1 post event: inflammatory monocytes showed no differences among the three groups, while PMo were lower in MI when compared to SA subjects. In the MI group the levels of the monocyte subsets were

not significantly different during the 12 days post event, but somehow consistently with Dr. Nahrendorf's findings, inflammatory monocytes peaked at 2.8 ± 0.8 days post event, and PMo peaked 4.8 ± 2.9 days after event. In the UA group the levels of the monocyte subsets were not significantly different during the 3 days post event. Notably, nor inflammatory nor PMo levels correlated with indicators of MI severity. In addition, the authors sought correlation of the monocyte subsets with myocardial salvage (defined as the ratio myocardium at risk-myocardium necrosis, assessed by cardiac MRI): the peak levels of inflammatory monocytes negatively correlated with myocardial salvage ($r=-0.68$; $p<0.001$), while PMo were not correlated; and sought correlation of monocyte subsets with the left ventricular ejection fraction (LVEF) at 6 months post event: peak levels of inflammatory monocytes negatively correlated with LVEF ($r=-0.60$; $p=0.001$), while PMo were not correlated.

B. Patrolling monocytes and cancer

Dr. Hedrick has shown that PMo play a critical role in the prevention of multiple tumor metastasis in the lung (Hanna et al., 2015). The authors found that after tumor injection (Lewis lung carcinoma cells or B16F10 melanoma cells): (i) PMo were recruited within 30 minutes, and for at least 7 days; (ii) PMo maintained their phenotype; (iii) PMo exhibited decreased crawling speed in the vasculature and arrested near lung tumor sites by 24 hours; (iv) PMo number in the lung was significantly increased 24 hours post tumor injection, and after 7 days there were significantly higher numbers of PMo (~24/100 mm^3) associated with tumor areas compared with tumor-free areas; (v) CX_3CR1 is critical for

sensing and up-taking tumor material; and (vi) the crawling of PMo on the vasculature 4 hours after tumor injection appeared to move toward tumor cells, and inhibit their attachment to the lung microvasculature. To learn whether PMo play a role in regulating tumor invasion, metastasis, and growth in the lungs, the authors injected intravenously B16F10 melanoma cells or Lewis lung carcinoma cells in an animal model of selective loss of PMo (the NR4A1$^{-/-}$ mice, see below). The authors found increased tumor invasion and spontaneous metastases in the lungs of NR4A1$^{-/-}$ mice compared with control mice, while not detecting differences in lung vascular permeability between the two groups, nor did not find differences in either Ly6C^{+} monocyte or Ly6G^{+} granulocyte populations. The authors then tested the role of PMo in an animal model of spontaneous mammary tumor — the mouse mammary tumor virus–polyoma middle T — and report findings consistent with the previous tumor models. These findings were confirmed by using three complementary approaches of specific lack of PMo: the NR4A1$^{-/-}$ bone marrow chimeras, and two different myeloid-specific NR4A1 conditional knockout models (CSF1RCre^{+} NR4A1$^{fl/fl}$ and LysM-Cre^{+} NR4A1$^{fl/fl}$). To confirm a direct role for PMo in regulating tumor metastasis, Ly6C^{+} or Ly6C^{-} monocytes from wild-type mice were adoptively transferred into recipient NR4A1$^{-/-}$ mice before tumor injection. Reconstitution of PMo into NR4A1$^{-/-}$ mice prevented lung tumor metastasis, but only if already present and active in the vasculature at the moment of tumor injection. In contrast, transfer of inflammatory monocytes into NR4A1$^{-/-}$ mice actually promoted tumor metastasis, consistent with their known protumoral properties. Collectively, these data

illustrate increased lung metastasis burden in the absence of PMo in multiple cancer models, and directly demonstrate that PMo inhibit tumor metastasis to the lung.

Recently, Dr. Fukumura's group has demonstrated that PMo are responsible for resistance to anti-VEGFR2 treatment in an animal model of colon cancer, and that the underlying mechanism is dependent on a CXCR4-mediated immunosuppressive function of PMo, (Jung et al., 2017). The authors report that 5 days after anti-VEGFR2 therapy the infiltration of PMo was increased into colon cancer carcinomas, while inflammatory monocytes and neutrophils subsets did not change significantly; on day 12, authors observed a further increase in PMo and also a significant increase in neutrophils, whereas inflammatory monocytes remained at similar levels between treatment groups. Consistently, the authors found that anti-VEGFR2 therapy significantly increased the number of rolling and crawling PMo compared with the control on day 6, while there was no significant change in the leukocyte-endothelial cell interaction in the control tumors over time. These results show that the blood serves as the source of tumor-infiltrated PMo, rather than local proliferation of in the tumor parenchyma; in addition, authors report that the PMo interaction with the tumor vessels and the subsequent transmigration across the endothelium during antiangiogenic treatment, are CX_3CL1/CX_3CR1 dependent. Notably, starting from day 2 post blockade of VEGF/VEGFR2 signaling, CX_3CL1 is upregulated in both human and mouse endothelial cells isolated from colon rectal carcinomas, and causes active recruitment of PMo to tumors. Interestingly, anti-VEGFR2 treated tumors in an animal model of

lack of PMo ($CX_3CR1^{-/-}$ mice, see below) showed also significantly reduced infiltration of neutrophils; conversely, the pharmacological depletion of neutrophils did not affect PMo. These data indicate that early infiltration of PMo during anti-VEGFR2 treatment promotes subsequent recruitment of neutrophils to tumors. The authors report that the underlying mechanism is the CXCL5 secretion by PMo that recruits neutrophils expressing CXCR2. Using the $CX_3CR1^{-/-}$ mouse model, the authors improved efficacy of anti-VEGFR2 therapy by blocking the CX_3CR1-dependent infiltration of PMo*;* furthermore, the adoptive transfer of PMo in the same animals abrogated the improved efficacy of anti-VEGFR2 therapy and determined tumor growth. The authors next investigated the mechanism of PMO mediated resistance to anti-VEGFR2 therapy and tumor growth, and observed vessel regression on days 5 and 12 after treatment without any rebound of vessel density, suggesting that tumor-infiltrating PMo or neutrophils did not seem to promote tumor angiogenesis. Hence, the authors questioned whether the mechanism relied on the modulation of the tumor immune microenvironment by PMo. The authors report higher levels of immunosuppressive cytokines (IL-10) and more $PD\text{-}1^+$ lymphocytes in treated tumors, together with downregulated immunostimulatory cytokines (TNF) and fewer effector $CD4^+$ and $CD8^+$ T cells. These data – coupled with in vitro assays on PMo regulatory effects on lymphocytes – support the mechanism that PMo directly regulate the adaptive immunity, and suggest that anti-VEGFR2-treatment induces the recruitment of PMo and neutrophils that inhibit effector T cell activation with a IL-10-dependent mechanism, which leads to a shift of the tumor

microenvironment toward immunosuppression, and thus to an attenuated immune response against the tumor. Their findings are so relevant and innovative that the authors claim to have been the first to report an immunosuppressive function of PMo in any context.

In a follow-up study, Dr. Fukumura's group found a significant increase in CXCR4 and CXCL12 expression after anti-VEGFR2 treatment in colorectal cancer, and that the mechanism of resistance to anti-VEGFR2 treatment was abolished by the blockade of CXCR4. Interestingly, the authors report that CXCR4 is not involved in the regulation of colorectal cancer cell proliferation, but the positive anti-tumor effect of its blockade on anti-VEGFR2 therapy is mediated by the modulation of the tumor immune microenvironment via restoration of the levels of T cells. Notably, in the colorectal cancer microenvironment, T lymphocytes express negligible levels of CXCR4, suggesting an indirect effect mediated by other immune cell types expressing CXCR4. Indeed, the blockade of CXCR4 treatment inhibited the anti-VEGFR2 induced accumulation in the tumor microenvironment of PMo and neutrophils. Consistently, the antitumor efficacy of combinatorial blockade of CXCR4 and anti-VEGFR2 in wild-type mice was comparable to that of anti-VEGFR2 monotherapy in mice lacking PMo ($CX_3CR1^{-/-}$ mice). Moreover, there was no further improvement in antitumor efficacy by blockade of CXCR4 in mice lacking PMo ($CX_3CR1^{-/-}$ mice). Finally, the pharmacological depletion of neutrophils did not induce any significant improvement in antitumor efficacy when combined to anti-VEGFR2 treatment when compared with anti-VEGFR2 monotherapy. Meanwhile, the

combind blockade of CXCR4 along with anti-VEGFR2 induced a dramatic enhancement in antitumor efficacy compared with anti-VEGFR2 monotherapy, suggesting that PMo are a critical target to improve anti-VEGFR2 therapy efficacy.

C. Patrolling monocytes and acute vascular injury

Dr. Geismann's group has unveiled the mechanism of PMo housekeeping function on vascular endothelium in a model of glomerulo-nephritis (Carlin et al., 2013). Dr. Geissman's group has also studied the role of PMo in acute glomerulonephritis, using Resiquimod (R848), an imidazoquinoline compound with potent anti-viral activity that activates the immune cells via a TLR7/TLR8 MyD88-dependent signaling pathway. After R848, PMo increased the length and decreased the velocity of crawling, determining a 2-3 fold increase in dwell time (Cros et al., 2010). R848 caused an increase in the number of PMo in the peritubular capillaries; of note, the mechanism is TLR7 mediated, even though at steady state crawling is TLR7 independent. Importantly, using labeled Ab anti CD11b (MAC-1), PMo were shown to be inside the lumen after R848 administration (i.e. PMo exerted their activities on the luminal side of endothelial cells). In this same study, the authors showed that neutrophils crawl and cluster close to PMo, and that the recruitment of neutrophils was greatly decreased in animal models of absence of PMo, and proposed a model in which PMo recruit neutrophils after their retention in the microvasculature of the kidney. The authors also reported that after TLR7 stimulus, in areas of PMo and neutrophil recruitment the endothelium appeared increased in thickness, and the endothelial cells were swollen with: i) rarefaction of cytoplasm, ii) blebbing from plasmatic

membrane of cytoplamatic fragments, iii) loss of plasma membrane integrity and iv) release of cellular debris and damaged organelles (such as altered mitochondria). The PMo adjacent to the damaged endothelial cells phagocyted cell debris and organelles. Altogether, their data suggested that the expression of TLR7 on the endothelium is required for the recruitment of PMo; neutrophils are required for endothelial cell killing; and patrolling monocytes. Two reports supported the above described role of PMo as activators of neutrophils, one in acute glomerular nephritis (Finsterbusch et al., 2016), the second in acute mesenteric vasculitis (Imhof et al., 2016).

D.Patrolling monocytes and neurocognitive dysfunction

An interesting study by Michaud et al. has shown that PMo remove beta-amyloid from cortical vessels in a mouse model of Alzheimer disease. With live intravital two-photon microscopy, the authors demonstrated that PMo are attracted to and crawl onto the luminal walls of amyloid beta (Aβ) positive microvessels. Additionally, the authors reported the presence of crawling monocytes carrying Aβ and their ability to circulate back into the bloodstream. Moreover, the selective removal of PMo in an animal model of Alzheimer disease (the APP/PS1 mouse) induced a significant increase of Aβ load in the cortex and hippocampus, when compared to wild-type littermate controls (Michaud et al., 2013). Altogether, these data uncovered the ability of PMo to target and eliminate Aβ within the lumen of cerebral microvessels.

E. Patrolling monocytes and glucose metabolism

Nagareddy et al. (Nagareddy et al., 2013) analyzed the levels of circulating WBC in two models of diabetes in mice (B6 +

STZ; Akita) at baseline and after hypoglycemic treatment (sodium glucose cotransporter 2 inhibitor). They found that hyperglycemia (~500mg/dl) induces leukocytosis and therapy (~260 in Akita; ~320 in B6+STZ) reversed it, in both models. Circulating Ly6C^{hi} were increased in both models and therapy brought the levels to normality. On the other hand, patrollers were not affected by hyperglycemia in the B6+STZ model (even though therapy appears to reduce their numbers), whereas in the Akita model their levels were increased and then reduced by therapy. Leucocytosis was associated with increased myelopoiesis (in bone-marrow, not spleen) as seen by increased numbers of progenitor cells (CMP, GMP), this effect was reversed by therapy. The authors measured the levels of hematopoietic cytokines (M-CSF, G-CSF, GM-CSF and IL-1β) and only G-CSF was affected by diabetes (hyperglycemia increased the levels; therapy reduced them). They also assessed the transcriptional profile of circulating and BM myeloid cells and found increased levels of damage associated molecular patterns (DAMPs) specifically S100a8 and s100a9 (neutrophils primary source) in diabetes and their restoration with therapy. ROS and transcription factors (Klf-5 and C/ebp-α) levels were going in the same directions and are known to promote S100a8/s100a9 expression (Fujiu et al., 2011). Of note, the depletion of neutrophils normalized the levels of monocytes in diabetes; decreased DAMPs levels; decreased levels of CMP and GMP. DAMPs play a central role in DM induced myelopoiesis (S100a9$^{-/-}$, lack also s100a8, no myelopoiesis after DM induction) and they signal through the RAGEs (RAGE$^{-/-}$ do not develop leucocytosis in DM). The authors show that this mechanism is

mediated by inflammatory cytokines that increase the levels of M-CSF and GM-CSF (effect inhibited by anti-NFKb).

F. Models for the study of Patrolling monocytes

There are two well-established mouse models of lack of PMo: the $CX_3CR1^{-/-}$ and the $NR4A1^{-/-}$.

a. $CX_3CR1^{-/-}$

CX_3CR1 is the receptor for fractalkine (CX_3CL1), a membrane-bound glycoprotein functioning as a cell-adhesion receptor capable of arresting cells under physiological flow conditions (Bazan et al., 1997). Chemokines are subdivided into four subfamilies, C, CC, CXC, and CX_3C chemokine (where C is a cysteine and X any amino-acid residue), based on the number and spacing of the first two cysteines in a conserved cysteine structural motif. The CXC molecules seem biased in targeting neutrophils (and to a lesser extent lymphocytes); the CC molecules mainly target monocytes, and also lymphocytes, basophils, and eosinophils, with varying selectivity, but not neutrophils; and the C chemokine (only member is lymphotactin) appears to act preferentially on lymphocytes.

CX_3CL1 [also called fractalkine (FKN)] is the sole member of the chemokine CX_3C family. CX_3CL1 is furthermore structurally unique in that it is synthesized as a type I transmembrane protein with the CX_3C (Cys-X-X-X-Cys) chemokine domain presented on top of an extended mucin-like stalk as a part of the protein (Bazan et al., 1997). FKN presents another unique characteristic among chemokines: exists both in a transmembrane and in a soluble form (Imai et al., 1997). The region of homology of CX_3CR1 to other chemokines is located at the amino terminus from residues 23 to 92 (Pan et al., 1997). CX_3CL1 contains a stretch of 19 conserved

hydrophobic residues towards the carboxy terminus, suggesting that it is a membrane protein. Three additional cysteines are present at the C-terminal portion of the CX_3CL1: one in the transmembrane domain and two in the cytoplasmic domain FKN is expressed on endothelial cells (Bazan et al., 1997), vascular smooth muscle cells (Ludwig et al., 2002), dendritic cells (Papadopoulos et al., 1999) and neurons (Schwaeble et al., 1998). Interestingly, FKN may be cleaved by ADAM17 [aka: TNF-α-converting enzyme (TACE)] and released from cells and act in this soluble form as a potent leukocyte chemoattractant at CX_3CR1 (Garton et al., 2001). Fractalkine is expressed by the inflamed endothelium and induces leukocyte adhesion and migration; it is in fact expressed in a membrane-bound form on TNF-a- and IL-1-activated endothelial cells (Bazan et al., 1997). FKN is a key molecule for the interaction of monocytes and ECs through both integrin-dependent and integrin–independent mechanisms (EDTA does not affect adhesion) (Goda et al., 2000, Fong et al., 1998). CX_3CR1 is a G-coupled signaling receptor expressed on monocytes, T lymphocytes and natural killer cells (Imai et al., 1997). The adhesive activity of CX_3CR1 does not require activation of Gi-signaling nor Calcium (Pertussis toxin does not affect adhesion) (Fong et al., 1998). FKN induces rapid capture (efficacy decreases with shear stress increase) and firm adhesion of CX_3CR1 expressing leukocytes (Fong et al., 1998). The captured leukocytes did not exhibit rolling motility on the endothelial surface (Fong et al., 1998) [adhesion is 15-fold stronger in TNF-alpha then control HUVECs] (Imai et al., 1997).

CX_3CR1 activation upregulates cell adhesion to fibronectin and ICAM-1. Genetic variants of FKN and CX_3CR1 have been shown to be associated with AMD (Tuo et al., 2004), coronary endothelium dysfunction and atherosclerosis (McDermott et al., 2001). Genetic variants of CX_3CR1 responsible of reduced monocytic adhesion were associated with decreased coronary artery disease and endothelium dependent vasodilation, and correlated with protection from cardiovascular disease (McDermott et al., 2003).

During inflammation, FKN shedding increases as a result of its increased gene induction. The soluble released FKN functions as attractant for WBC. There is a reduction of the adhesiveness of the endothelial surface for WBC (for resolving inflammation but also for allowing firmly adherent WBC to proceed with lateral migration and diapedesis) The remaining cellular fragment can undergo further proteolysis in the membrane: the c-terminal is released in the cytoplasm and acts as a transcription factor involved in the differentiation of vascular precursors (true for Notch, not sure for FKN). FKN shedding occurs only on the apical site and the major control of its cleavage is by ADAM10 and ADAM17. ADAM10 and 17 are both highly expressed in atherosclerotic lesions (ADAM10 especially in microvessels and areas of neovascularization).

Unfortunately, the $CX_3CR1^{-/-}$ mice are in the C57BL/6N substrain which poses the risk of homozygosity for the *rd8* mutation (Mattapallil et al., 2012). This mutation is autosomal recessive, and when present in the homozygous form, causes retinal degeneration. Retinal degeneration would be a confounder

in our experiments because retinal vessels respond and adapt to changes in the neural retina.

b. NR4A1$^{-/-}$

The NR4A1 (Nur77) orphan nuclear receptor is a master regulator of differentiation and survival of patrolling Ly6C^{low} monocytes (Hanna et al., 2011). Patrollings express abundant NR4A1 mRNA and protein, whereas over 95% of inflammatory monocytes manifest very low expression. NR4A1 deficiency interferes with later stages of monocyte development and results in the absence of patrollings from the circulation (Hanna et al., 2011). This observation has established independence between the patrolling and inflammatory subsets of monocytes (Hanna et al., 2011).

Nuclear hormone receptor (NR)4A1 (Nur77), 2, and 3 constitute the NR4A subfamily of orphan nuclear receptors in the steroid-thyroid receptor family 4 A. NRs are the largest class of transcription factor; they are regulated by lipophilic ligands, allowing rapid ligand-dependent control of the various developmental and metabolic processes. This family includes receptors for: fat-soluble vitamins, hormones (thyroid, and others), bile acids, etc. The NR4A subfamily is defined as orphan nuclear receptors since currently no endogenous/native *bona fide* ligands have been identified. Their transcriptional activity is thought to be mainly dependent on their expression levels. In addition: co-repressors, co-activators, and post translational modifications modulate their transcriptional activity.

The NR4A subfamily has three functionally distinct domains: signs activation trans-activation, DNA binding, and ligand binding.

Members of the NR4A subgroup bind to DNA binding sites, as: monomers, and homodimers or heterodimers (when two members are bound together, the same or different respectively) As monomers they bind to the NGFI-B response element (NBRE); as homodimers and heterodimers they (a) bind to the Nur – responsive element, NurRE, (b) heterodimerize with the retinoid X receptor (RXR) and the resulting NR4A/RXR complex binds to a combination of an NBRE and retinoid acid response element, called DR5.

Functionally, the NR4A subgroup is involved in various hormonal, physiological, and pathophysiological processes including: cardio vascular disease, apoptosis, inflammation, metabolic disease, oncogenesis and neurological disease. The expression of all three members of the NR4A subgroup is rapidly and transiently induced by: various receptor agonists (G protein-coupled receptors, tyrosine kinase receptors), activators of cAMP and protein kinase signaling, mechanical stress, exercise, and UV light.

The expression of the NR4A subgroup is induced in the skeletal muscle by β-adrenergic signaling via cAMP, protein kinase A, MAPK, and cAMP response element-binding protein.

Metabolism: In vivo NR4A1 regulates the expression of metabolic genes specifically involved in glucose transport, insulin signaling (Glut 4), glycolysis, and glycogenolysis (Chao et al., 2007). Importantly, NR4A1 KO mice exhibited limited metabolic changes on a normal diet. The alterations observed (increased weight, decreased energy usage, and insulin resistance) were observed only after high fat diet (Chao et al., 2009). It has been

shown that NR4A1 and 3 were repressed in rodent models of obesity and diabetes (Fu et al., 2007). Of note, mice lacking NR4A1 present a dramatic increase in NR4A3 (Nor-1) expression. Furthermore, in vivo the three members of the NR4A subgroup are induced by glucagon and fasting, and the over expression of NR4A1 induced expression of genes involved in hepatic gluconeogenesis, stimulated glucose production, and increased glycemia (Pei et al., 2006). Finally, the expression of NR4A1 in skeletal muscle also enhances oxidative metabolism and mitochondrial function (Chao et al., 2012).

Vasculature: The NR4A subgroup is induced by atherogenic stimuli; it is expressed in atherosclerotic plaques (particularly in areas of plaque activation and remodeling, suggesting their involvement in plaque progression); it is activated in smooth muscle cells by vascular disease. NR4A1 is up regulated in the inflamed vasculature, specifically in endothelial cells, smooth muscle cells, and monocytes NR4A1 KO mice exhibited larger arterial lesions, while NR4A1 overexpression caused reduced arterial lesions (Arkenbout et al., 2002).

In endothelial cells the NR4A subgroup is induced by stimuli such as: hypoxia, TNF-alfa, IL-1beta and VEGF. The only gene known to be directly regulated by NR4A1 in endothelial cells is PAI-1: NR4A1 induces PAI-1 through direct binding to an NRBE in the promoter region of the PAI-1 gene; NR4A1-/- ECs show abrogated PAI-1 expression in response to TNF-alfa (Pols et al., 2007) (Gruber et al., 2003).

Basal vascular permeability (BVP) is reduced in the skin of NR4A1 KO vs WT mice. In addition, acute vascular

hyperpermeability (AVH) post VEGF-A, histamine, serotonin, and platelet-activating factor (all potent vascular permeabilizing molecules) is reduced in the skin of KO vs WT mice. Also the permeability in the peritoneum post VEGF ip injection is reduced. Zhao et al. used Fvb mice to selectively overexpress NR4A1 full-length DNA (NR4A1-S) or NR4A1 dominant negative mutant (NR4A1-DN). They found that NR4A1-S exhibited increased BVP and AVH, and increased vessels size but not density. Converesely, in NR4A1-DN BVP and AVH were reduced (Zhao et al., 2011).

Zeng et al. found that HUVEC cells overexpressing NR4A1 had increased levels of eNOS (comparable to HUVEC stimulated with VEGF-A). Silencing NR4A1 increased eNOS expression via inhibitition of VEGF-A. eNOS protein expression was greatly reduced in NR4A1 KO mice. HUVEC transduced with NR4A1-S exhibited increase in monolayer permeability; interestingly, the effect was abolished when transducing also VE-cadherin and claudin 5 (Zeng et al., 2006).

Interferon Stimulated Gene 12 (ISG12) is a modulator of the activity of NR4A1. Under normal conditions it is expressed at low levels, while it is strongly upregulated in response to inflammatory stimuli. ISG12 is upregulated in the vasculature upon injury and contributes to vascular pathologies by inhibiting the transcriptional activities of protective nuclear receptors such as NR4A1. ISG12 KO mice are completely protected from restenosis in vascular injury models (Papac-Milicevic et al., 2012).

Immune System: in human macrophages, NR4A1 has been shown to recuse the expression of pro-inflammatory genes (Bonta et al., 2006). In contrast, it has been also reported that NR4A1 is

up-regulated by inflammatory stimuli in a mouse macrophage cell line and that its overexpression induces the expression of inflammatory response genes (Pei et al., 2005). Therefore, even though there is agreement that NR4A1 is up-regulated in vascular pathologies, there are conflicting data and hypothesis on its functional role in inflammatory responses.

NR4A1 has a crucial function in the survival of $Ly6C^-$ monocytes (Hanna et al., 2011). There is no difference instead, in $Ly6C^+$ monocytes between WT and NR4A1 KO mice. NR4A1 KO mice show increased expression of SDF-1alfa by bone marrow derived macrophages, secondary to absent inhibition of NR4A1. Moreover, NR4A1 deficiency results in an impressive increase in atherosclerotic lesion formation; accumulation of T cells, macrophages, and smooth muscle cells is increased; the extent of necrotic core formation is enhanced indicating a different lesion composition in NR4A1 KO mice (Arkenbout et al., 2002).

TGF-beta: (Palumbo-Zerr et al., 2015) mRNA levels of NR4A1 (but not of NR4A2 and 3) are higher in patients with systemic sclerosis, liver fibrosis, and in various mouse models of fibrosis. “Pan-NR4A1” (all NR4A1 detected by Ab against NR4A1 regardless of post-translational modifications) is located predominantly in fibroblasts of fibrotic skin (normal skin has weak expression). Overexpression of TGF-beta receptor type I (TBRI) induces pan-NR4A1 expression in vivo (B6 mice); block of TGF-beta signaling with selective inhibitor of TBRI (SD-208) does not up-regulate pan-NR4A1 in fibroblasts. Likewise, also block of SP1 (knockdown or pharmacologically) prevented TGF-beta mediated increase of NR4A1. The TGF-beta induction of NR4A1 is

abrogated by inhibition of SMAD3 or SMAD4, and of SP1, showing that the NR4A1 induction is SMAD and SP1 mediated. Overexpression of SMAD3, SMAD4, and SP1 enhanced the activity of NR4A1 promoter constructs. Thus, TGF-beta induces NR4A1 by recruiting SMAD3-SMAD4-SP1 complexes to the NR4A1 promoter. NR4A1 has been shown to interact with SP1, and SP1 signaling regulates the transcription of type I collagen.

Mouse models of fibrosis (overexpression of TGF-beta; tight skin-1 mouse; bleomycin induced skin fibrosis) and NR4A1 KO show greater degree of collagen when compared to WT littermates (more pronounced dermal thickening, deposition of collagen, higher myofibroblast counts). NR4A1 KO fibroblasts when compared to WT fibroblasts show: (i) more pronounced TGF-beta stimulatory effects on Pai-1 and SMAD7; (ii) enhanced TGF-beta induced myofibroblast differentiation (with higher expression of alfa-SMA); and, (iii) upregulation of Col1a1 and 2, and increased release of collagen. This phenotype was rescued by re-expression of NR4A1. Neither overexpression nor knockdown of NR4A1 altered total amount, affected phosphorylation, or changed subcellular localization of SMAD3, nor the amount of AXIN-2 (shown to promote degradation of SMAD7) in cultured fibroblasts. Amount of SMAD3 and pSMAD3 does not differ between NR4A1 KO and WT. Chronically elevated TGF-beta induces phosphorylation of NR4A1 (pNR4A1) at Ser351 (steadily high over time) which decreases transcriptional activity of NR4A1. Overexpression of TBRI (that induces pan-NR4A1 expression in vivo, see above) and other causes of fibrosis, induce accumulation of pNR4A1. pNR4A1 accumulates in fibrotic tissues, and thus

accounts for the increased pan-NR4A1. Protein kinase B (AKT), glycogen synthase kinase 3-beta, and c-jun N-terminal kinase, phosphorylate NR4A1. The knockdown of AKT (but not of the other two enzymes), prevent TGF-beta induced phosphorylation of NR4A1. pNR4A1 does not bind to SP1 and thus prevents the NR4A1-mediated SP1-dependent (Palumbo-Zerr et al., 2015) repression of TGF-beta target genes. In mice: during physiologic wound healing, pan-NR4A1 expression increases (peaks during final phases); however, during wound healing pNR4A1 levels remain lower than in experimental fibrosis. In humans not affected by fibrotic disease, during wound healing (surgical) ratio pan-NR4A1/pNR4A1 is higher than in patients affected by scleroderma disease. This suggests that chronic high TGF-beta signaling (in fibrotic disease) inactivates physiologic NR4A1 negative feed-back through AKT-induced phosphorylation and HDAC-mediated epigenetic silencing. The $NR4A1^{-/-}$ mice are available in C57BL/6J substrain and therefore do not carry the *rd8* mutation; are fertile, and do not manifest overt abnormalities, but show abnormalities when challenged. Notably, human PMo ($CD14^{dim}$ $CD16^{+}$) express NR4A1 (Hanna et al., 2012).

II. HYPOTHESIS

Diabetes is characterized by chronic low grade inflammation, which is involved in molecular and structural alterations associated with microangiopathy. However, in diabetes there is a long latency period between the onset of metabolic abnormalities and appearance of microangiopathy; this latency does not imply, but is consistent with the occurrence of vascular repair at least in the early stages of diabetes. Previous work by Dr. Lorenzi demonstrated that even subclinical vascular abnormalities signal to EPCs that carry monocytic markers, a need for repair (Zerbini et al., 2012). The possibility that PMo may be involved in the repair of diabetic retinal microangiopathy was suggested to us by the work of Dr. Geissman's group (Carlin et al., 2013, Cros et al., 2010, Auffray et al., 2007); while the possibility that PMo may be involved in early diabetes was suggested to us by the observations of Serra et al related to leukostasis (Serra et al., 2012). Leukostasis is a phenomenon observed in retinal vessels of rodents after short duration of diabetes, and characterized by an increased number of white blood cells firmly adherent to the vascular endothelium. It is classically interpreted as a pro-inflammatory event (Joussen et al., 2004); however, the observation by Serra et al. that the adherent cells expressed typical characteristics of PMo ($CD11b^{+}$ and CX_3CR1^{++}, but not $GR1^{+}$; see Table 1) suggested to us a different interpretation of leukostasis, where PMo may be the main protagonists. Such different interpretation for leukostasis was not entertained by the authors, but fits their additional observation that diabetes-induced changes in the endothelium were a prerequisite for its development (Serra et al., 2012).

III. SPECIFIC AIMS

We tested the hypothesis that PMo exert protective and repairing functions in retinal microvessels in physiology and in early diabetes. The specific aims were:

1. To test if diabetes alters quantitatively the circulating monocyte subsets, and in particular the PMo.
2. To test the relation of PMo to the phenomenon of retinal leukostasis observed after a few weeks of experimental diabetes. Determine (i) whether the number of patrolling monocytes that appear “arrested” in the retinal vessels is larger in diabetic than in control mice, and (ii) which proportion of total leukocytes participating in diabetic leukostasis is represented by PMo.
3. To test if the profound reduction in endothelial crawling and vessel patrolling documented to occur when monocytes lack the transcription factor NR4A1, accelerates the retinal capillary changes observed in healthy aging.
4. To test if the profound reduction in endothelial crawling and vessel patrolling documented to occur when monocytes lack the transcription factor NR4A1, accelerates the retinal capillary damage induced by diabetes.

IV. METHODS

1. Animals

Female and male NR4A1$^{+/-}$ mice (heterozygous) were purchased from The Jackson Laboratory to serve as breeders. Heterozygous mice were intercrossed to generate mice carrying the NR4A1 mutation in homozygous (NR4A1$^{-/-}$) or being wild-type littermates (NR4A1$^{+/+}$). Only male mice were studied, and entered the experiments at 8 weeks of age. Diabetes mellitus was induced at 8 weeks of age in a subset of the WT and KO mice, using streptozotocin (STZ). Mice received daily intraperitoneal injections of STZ (50 mg/kg body weight) freshly prepared in citrate buffer (0.1M) for 5 consecutive days. 4 days after the last STZ injection, blood glucose was measured to verify the development of diabetes. A drop of blood was obtained by needle (25 G) puncture of the tail vein, and applied directly to a glucose strip and read in a glucometer (One Touch UltraMini). A blood glucose equal or greater than 250 mg/dl was diagnostic of diabetes. The diabetic mice were weighed 3-4 times per week to determine the need for insulin administration and treated with insulin as needed to prevent weigh loss (0.1-0.3 U NPH sc 3-4 times/week). All animals had unlimited access to food and water and were checked daily for infections or other problems. Age and sex matched controls received citrate buffer (0.1M) i.p. injections. All procedures involving animals conformed to guidelines on the use of animals in research and were approved by the Schepens Eye Research Institute animal use and care committee.

2. Flowcytometry

Peripheral blood was collected by submandibular bleeding. Blood was subjected to red blood cell lysis, incubated with anti-mouse FcγRII/III (2.4G2) and a viability dye (Zombie UV), and then stained with the following anti-mouse antibodies: Alexa700-coupled CD45 (clone 30-F11, Biolegend); APC-coupled CD11b (clone M1/70, Biolegend); PE-coupled CD3 (clone 145-2C11, Biolegend), CD19 (clone eBio1D3, eBioscience), and NK1.1 (clone PK136, Biolegend); BV785-coupled Ly6G (clone 1A8, Biolegend); BV605-coupled CD115 (clone AFS98, eBioscience); FITC-coupled Ly6C (clone AL-21, BD Bioscience). PMo were identified as $CD45^{hi}$/$CD11b^{hi}$/Lin (CD3/CD19.9/NK1.1)^{neg}/Ly-$6G^{neg}$/$CD115^{hi}$/Ly-$6C^{neg}$, using a FACSAria II (BD Biosciences).

3. Leukostasis

The mice were deeply anesthetized with ketamine-xylazine, and positioned under the microscope on a heating pad to maintain physiological body temperature. The anterior chest wall was cut open, a 26G needle – already connected to tubing filled with warm phosphate buffered saline (PBS) – was inserted into the left ventricle at the apex, and a large incision made into the right atrium. The perfusion fluids were maintained at 37ºC and delivered via a peristaltic pump: 10 ml PBS to wash away blood (pre-wash); 10 ml PBS containing Concanavalin A (1 mg) bound to fluorescein (FITC-ConA) to label luminal endothelium and the cells remaining adherent; and 10 ml PBS to wash out the excess FITC-ConA (post-wash). The checkpoints monitored during the procedure and

used to determine technical success were (i) duration of each individual phase of perfusion (each phase was timed to last ~33”, the complete procedure lasted ~1’39”), (ii) time to blanching of the liver (less than 4”), (iii) absence of visible lung edema, and (iv) absence of blood at enucleation of the eyes.

The enucleated eyes were rinsed in PBS and immediately fixed in 4% paraformaldehyde for 1 hour. The retinas were dissected under the dissecting microscope and whole-mounted. The FITC-ConA^{+} cells were counted on the retinal whole-mounts surveyed systematically throughout the three capillary layers under a Zeiss Axiophot (Karl Zeiss Inc., Thornwood, NY) fluorescence microscope. In some experiments, one of the two retinas was further processed for immunohistochemistry to identify the nature of the cells remaining adherent to the vessels after perfusion.

4. Acellular Capillaries

Mice were euthanized by CO_2 inhalation and death confirmed by cervical dislocation. Eyes were immediately removed after sacrifice and fixed in 10% buffered formalin for 48 hours. The retinas were dissected and the neural elements digested with trypsin to yield the intact microvascular network. Cell nuclei and acellular capillaries were counted in retinal trypsin digests stained with periodic acid Schiff hematoxylin and viewed at 20× magnification. Counts were performed in eight fields in mid-retina using the AxioVision4 program (Carl Zeiss, Göttingen, Germany). Acellular capillaries were those that had *(1*) no visible nuclei along the vessel between bifurcations, *(2*) length of at least 40 μm, and *(3*) width equal to at least 20% of an average capillary. Acellular

capillaries counts are reported as number of acellular capillaries per mm^2 retinal trypsin digest. The counts were performed on masked slides independently by three observers. In most cases the three values were consistent; if a value departed by more than two SD from the mean of two consistent counts was excluded from computation.

5. Fluorescein Angiography

All experiments were performed in the Visual Assessment Core of the Schepens Animal Facility, with the assistance of the specialized Core technician. Briefly, after anesthesia with Ketamine/Xylazine, pupil dilation with 1% Tropicamide, and application of lubricant GenTeal gel to the eye, the mice were placed on the stand of the Micron III Retinal Imaging Microscope (Phoenix Research Laboratories, Pleasanton, California) to examine the front of the eye and capture fundus images. Mice were then injected intraperitoneally with 0.05 ml of 2% Fluorescein/10g body weight, and retinal photographs were taken at 1, 2, 3, 4, and 5 minutes post fluorescein injection using the Micron III Retinal Imaging Microscope.

6. RNA extraction and gene expression profiling

Circulating PMo were identified as above, and sorted with a FACSAria II (BD Biosciences). Total RNA was isolated using Trizol-LS from, approximately 20,000 cells per sample. cDNA was synthesized and RNA-Seq libraries were constructed using SMARTer v. 3 kit from Clontech. Next Generation Sequencing

(NGS), cells were collected from animals with 5 months duration of diabetes and non-diabetic sex and age matched littermate controls. Sequencing was performed on Illumina HiSeq 2500 instrument, resulting in approximately 30 million of paired-end 50 bp reads per sample. A splice-aware alignment program (STAR) was used to map sequencing reads to the mouse reference transcriptome (mm9 assembly) (Dobin et al., 2013). Read counts over transcripts were calculated using HTSeq v.0.6.0 (Anders et al., 2015) based on a current Ensemble annotation file for NCBI37/mm9 assembly. For differential expression analysis we performed calculations by using the package EdgeR (Robinson et al., 2010) and classified genes as differentially expressed when the expression value of a gene is changed at least 2-fold and their false discovery rates (FDR) were below 0.05. Real-Time qPCR, cells were collected from a group of animals with 3 months of diabetes duration, one with 5 months of diabetes duration, and another group with 7 months of diabetes duration; and from correspondent non-diabetic sex and age matched littermate controls. Determination of gene expression levels of *CXCR4*, *TNF-α*, *IL-1β*, *ANGPTL4*, *CD28*, *CD81*, *CXCL4*, *ITGA2B*, and *PPPr19a* was performed using Applied Biosystems™ TaqMan® Gene Expression Assays, which consisted of a pair of unlabeled PCR primers and a TaqMan® probe with an Applied Biosystems™ FAM™ dye label on the 5' end and minor groove binder (MGB) and nonfluorescent quencher (NFQ) on the 3' end. Data were analyzed and presented on the basis of the relative expression method. Relative expression was determined by the comparative $\Delta\Delta C_T$ method, representing the change in cycling threshold

between the gene of interest and the “housekeeping” gene *Gapdh* (encoding glyceraldehyde phosphate dehydrogenase). Pathway enrichment and Network analysis: Analysis of enriched functional categories among detected genes was performed using Gene Set Enrichment Analysis (GSEA) and Ingenuity Pathway Analysis (IPA). We used the package for GSEA to analyze the enrichment of functional gene groups among differentially expressed transcripts. Normalized enrichment score (NES) and enrichment plots were calculated based on gene lists ranked by the expression ratio between diabetic and non-diabetic control PMo (Subramanian et al., 2005). GSEA was run with 10,000 permutations by using Java interface, following the developer’s protocol (http://www.broad.mit.edu/gsea/). The list of DEGs was uploaded to the IPA software to investigate the biological networks associated with these proteins (http://www.ingenuity.com). Networks are ranked in the Ingenuity analysis according to the fit of the network. IPA uses the proteins from the highest-scoring network to extract a connectivity pathway that relates candidate proteins to each other based on their interactions. The proteins corresponding to the obtained gene sets were searched against the version 10.0 of the STRING database to display functional protein-association networks (Szklarczyk et al., 2015). Interactions were considered with a STRING confidence score ≥ 0.4 (medium confidence). Unsupervised functional interaction network analysis was carried out considering each protein as a node and permitting ≤5 *s*-order interactions to maximize connectivity (http://string.embl.de/).

7. Statistical analysis

The specific tests used to analyze each set of experiments are indicated in the figure legends. For each statistical analysis, data were analyzed for normality using the Shapiro-Wilk and the Shapiro-Francia tests; normally distributed data were summarized with the mean ± SD, nonnormally distributed data with the median and interquartile range. Continuous data normally distributed were analyzed using a two-tailed Student’s t test to compare between two groups, and one-way ANOVA was used to compare several groups, followed by the Bonferroni post-hoc procedure for pairwise comparison of groups after the null hypothesis was rejected. Categorical data were analyzed using Fisher's exact test. *P* values of less than 0.05 were considered significant. All statistical analyses were performed using the Stata 12 software (Stata Statistical Software: Release 12; StataCorp LP, College Station, TX, USA).

V. RESULTS

The results of this work are currently under revision, and therefore have not been published yet. We have in fact just recently concluded all the real-time qPCR experiments, that were necessary in order to validate the transcriptome data acquired by NGS, and therewith start understanding the mechanisms through which PMo exert their activities on retinal microvessels.

1. Diabetes induction

It was a critical requirement for our project that the NR4A1$^{-/-}$ mice develop diabetes in response to streptozotocin (STZ). All mice injected with STZ, successfully developed diabetes. Notably, in both the NR4A1$^{-/-}$ mice and the WT controls, the STZ-induced diabetes is of the insulin-requiring type, as the mice become severely dehydrated and die unless treated with small doses of insulin (0.15 – 0.3 U) s.c. every other day. The characteristics of the mice used in the different experiments (see below) are reported in Tables 2 (A through D) and 3.

2. Circulating WBC and PMo

To learn if diabetes alters quantitatively the circulating monocyte subsets, and in particular PMo, we determined the number of leukocyte populations by flowcytometry. (Table 3, Figure 1) In parallel, we performed counts of total circulating white blood cells (WBC) by hemocytometer on a separate aliquot of the same blood sample. We found that diabetes determined a significant reduction of WBC (C: 7.4±2.2 x 10^9/L, DM: 4.1±0.9, $p<0.0001$; Figure 2), and that this reduction was apparently driven

by a reduction of circulating lymphocytes (C: 74.8±6.5% of WBC, DM: 64.4±11.4, p=0.015) (r^2=0.33, p=0.007), while granulocytes (C: 29.4±9.9% of myeloid cells, DM: 37.5±11.2, p=NS) and total monocytes (C: 55.4±8.3% of myeloid cells, DM: 48.5±13.9, p=NS) were unchanged (Figure 3). Interestingly, diabetes determined a rearrangement of the monocyte subpopulations (Figure 4): intermediate monocytes were increased (C: 13.2±2.7%, DM: 26.2±7.4%, p<0.0001), PMo were decreased (C: 54.6±13.9%, DM: 37.1±14.6%, p=0.008), whereas inflammatory monocytes were unchanged (C: 25.4±15.1%, DM: 25.9±14.5%, p=NS). Based on the results of diminished circulating PMo – contextually with their increase in the microcirculatory compartment, and the increased retinal microvascular pathology observed in diabetic mice lacking PMo – it is tempting to speculate that diabetes induces the "sequestration" of PMo in the retinal microvessels.

3. Leukostasis

We dedicated a substantial amount of time to set up a perfusion procedure with satisfactory reproducibility. The method entails delivering through the left ventricle a total volume of 20 ml at a rate of 0.3 ml/sec via a peristaltic pump. We compared the number of "arrested" FITC-ConA$^+$ cells in perfused retinal microvessels. (Figure 5) The characteristics of the animals examined are reported in Table 2.A. We tested the correspondence between FITC-ConA$^+$ cells and the pan-leukocyte marker CD45, and found almost 100% correspondence (r=0.96, p<0.0001), indicating that the cells arrested in the vessels are WBC (Figure 6). The critical finding is presented in Figure 7: the

number of FITC-ConA^{+} cells almost doubled in retinal vessels of WT-DM when compared to WT-C; in contrast, the number did not increase in NR4A1$^{-/-}$-DM vs. NR4A1$^{-/-}$-C. Is to be noted that (i) in the retinal vessels of the WT diabetic (D) mice the number of FITC-ConA+ cells almost doubled when compared to the WT control (C) mice, whereas in the diabetic (D) NR4A1$^{-/-}$ mice the number did not increase versus controls (C) despite levels of hyperglycemia comparable to those of the WT D mice.

To identify which proportion of the leukostatic WBC were PMo, it was critical to identify a marker for PMo usable in immunohistochemical studies on fixed tissue, so as to be able to enumerate specifically PMo in the retinal vessels. Several antibodies can identify PMo in flow cytometry, but the large majority does not react or has not been tested in fixed tissue. It was recently reported that the activating IgG Fc receptor called FCγgamma RIV (also named CD16.2) (Nimmerjahn et al., 2005) is expressed, among circulating WBC, only on neutrophils and LyC^{lo} monocytes, i.e., PMo. Importantly, the expression level on PMo is 10-fold higher than on neutrophils (Biburger et al., 2011). We identified one antibody (monoclonal Armenian Hamster anti-mouse CD16.2) able to successfully stain FITC-ConA+ cells in fixed retinal vessels (Figure 8). We validated its specificity by testing it in our NR4A1$^{-/-}$ mice lacking PMo. Flow cytometry confirmed the specificity (Fig. 9). Only the WT mice (control and diabetic) manifest the very high intensity signal for CD16.2 characteristic of PMo; whereas, CD16.2 immunohistochemistry in retinal vessels of KO mice failed to stain any FITC-ConA+ cells. In contrast, the low-level intensity signal for CD16.2 in the granulocytes is present in

both WT and KO mice. The findings presented in Fig. 8 suggest that PMo are important players, if not the protagonists, of diabetic leukostasis. In fact, we found over 3-fold increase in the number of FITC-ConA^{+}/CD16.2^{+} cells in WT-DM when compared to WT-C ($P<0.0001$), representing a percentage increase from 20% to 43%. Notably, the increase in absolute number (approximately 27 cells/retina) can quantitatively account for the increase in FITC-ConA^{+} cells recorded in the WT diabetic mice and presented in Figure 10. These data show that i) PMo are a large portion of the cells adherent to retinal vessels, ii) the number of "leukostatic" PMo increases in DM, and notably, iii) the extent of increase of PMo matches precisely the increase in total adherent WBC in DM.

In summary, these observations indicate a prominent numerical contribution of patrolling monocytes to the cells adherent to retinal vessels in early diabetes. This changes the functional meaning of the phenomenon of leukostasis. Diabetic leukostasis can no longer be interpreted as a pro-inflammatory event as currently proposed, but it may rather represent an attempt to bring healing influences to the distressed cells of retinal vessels.

4. Retinal microvascular disease

i. Healthy aging

We tested whether the lack of PMo accelerates the retinal capillary changes observed in healthy aging. The characteristics of the animals examined are reported in Table 2.B. The NR4A1$^{-/-}$ mice survived to 18 months in the same proportion as the WT siblings, and did not show evidence of obesity (as measured by body weight) or diabetes (as measured by blood glucose and

HbA1c). This is worthy of note because the NR4A1 (Nur77) orphan nuclear receptor, in addition to being a master regulator of the differentiation and survival of PMo, is known to have roles in metabolism and energy balance in a context- and tissue-dependent manner. Most of the metabolic abnormalities developed by the NR4A1$^{-/-}$ mice have been observed upon the application of challenges. Aging does not appear to be a sufficient challenge to alter baseline metabolic parameters. With regard to retinal vessels, aging did not detectably increase permeability in the WT mice, nor in the NR4A1$^{-/-}$ mice (Fig 11). Aging did not affect the density and viability of the microvasculature in the WT mice, nor in the NR4A1$^{-/-}$ mice, also when assessed quantitatively at the microscopic level by counting the number of acellular capillaries. (Figure 12 and 13) In summary, the retinal vessels of WT mice appear very stable in the face of increasing age up to 18 months of age; and the lack of PMo (and/or other characteristics) in NR4A1$^{-/-}$ mice does not detectably impact on such stability.

ii. Diabetes

We tested whether the lack of PMo accelerates the retinal capillary damage induced by 4 and by 6 months duration of diabetes. As detailed above in the description of the animal model, we induced diabetes in male mice using the standard protocol of multiple STZ injections.

A. Diabetes of 4-months duration

The severity of the hyperglycemia and the insulin requirement were similar in the WT and NR4A1$^{-/-}$ mice. The characteristics of the animals examined are reported in Table 2.C. The WT and NR4A1$^{-/-}$ diabetic mice were perfectly matched for the

severity of diabetes, as measured by the comparisons of body weight, blood glucose and HbA1c at sacrifice. Figure 14 shows representative images of fluorescein angiograms performed in one WT and one NR4A1$^{-/-}$ mouse after 4 months of diabetes. Comparison of multiple frames in the WT diabetic mouse with those of the WT control mice presented in Fig. 14 show that the structure of the main vessels, and the density and permeability of the microvasculature were not visibly affected by 4 months of diabetes. The NR4A1 deletion did not alter vascular patterns and did not induce leakage. Figure 15 shows the counts of acellular capillaries in mice with 4 months of diabetes. As anticipated in accordance with published observations, the WT diabetic mice did not show as yet a significant increase in the number of acellular capillaries when compared to nondiabetic controls; and also the NR4A1$^{-/-}$ diabetic mice failed to show a significant increase versus the NR4A1$^{-/-}$ control mice.

B. Diabetes of 6-month duration

When diabetes duration was prolonged to 6 months, some of the diabetes-induced changes in the retinal vessels showed an accelerated course in the absence of patrolling monocytes. The characteristics of the animals examined are reported in Table 2.D. The WT and NR4A1$^{-/-}$ diabetic mice were very well matched for the severity of diabetes, as measured by the comparisons of body weight, blood glucose and HbA1c at sacrifice. Figure 16 shows representative images of fluorescein angiograms performed in 2 WT and 2 NR4A1$^{-/-}$ mice, respectively, after 6 months of diabetes (a total of four mice per group were studied). Comparison of multiple frames in the WT diabetic mouse with those of the WT

control mice presented in Fig.16 showed that the structure of the main vessels, and the density and permeability of the microvasculature were not visibly affected by 6 months of diabetes. The NR4A1 deletion did not alter vascular patterns and did not induce leakage. Fig. 17 shows representative images of trypsin digests from WT and NR4A1-/- mice after 6 months of diabetes. The trypsin digest of each of the two WT diabetic mice shows three acellular capillaries, similar to the number appearing in the non-diabetic WT vessels presented in Fig. 17. On the other hand, comparable fields in the two NR4A1$^{-/-}$ diabetic mice immediately seize attention for the much larger number of acellular capillaries -- 9 in one mouse, and 6 in the other. Fig.18 accordingly shows statistically significant differences in the counts of acellular capillaries. WT mice with 6 months of diabetes manifest a number of acellular capillaries not different from nondiabetic WT controls, again in accordance with published data that place at 6-9 months of diabetes the beginning of an increase in retinal acellular capillaries. In contrast, the NR4A1$^{-/-}$ diabetic mice now have more than doubled the number of acellular capillaries when compared to nondiabetic NR4A1$^{-/-}$ as well as WT control mice.

In summary, diabetes of up to 6 months duration does not affect the permeability of mouse retinal vessels. Instead, 6, but not 4-month duration, is uncovering in mice lacking PMo an accelerated development of acellular capillaries in the retinal vasculature. These results support our hypothesis, and suggest the existence of mechanisms of vascular protection against diabetes.

5. Gene expression profiling

To learn if and how diabetes alters the biosynthetic profile of PMo we performed Next Generation Sequencing (NGS) on these cells. We studied WT mice with 5 months duration of DM and non-diabetic sex and age-matched littermate controls; the duration of diabetes was based on the previous observation that KO mice without PMo showed increased retinal microangiopathy as compared to WT controls after 6, but not 4, months of diabetes. Hence, we reasoned that an intermediate time point would have been ideal for capturing changes in the transcriptome of PMo. In Table 3 the characteristics of the mice used for transcriptome analysis, the number of sorted PMo, and the quality of the extracted RNA (RNA integrity number, RIN). First, we performed Principal Component Analysis (PCA, Figure 19) in order to visualize the sample-to-sample distances. PCA is a method that identifies patterns in high dimensional data and expresses these data in a way that highlights their similarities and differences among samples. The procedure uses an orthogonal transformation to convert the observations, which are presented as functions of possibly correlated variables, into a set of values of linearly uncorrelated variables called Principal Components (Smith, 2002). The PCA analysis showed good separation between the control and diabetic samples, indicating that the changes found in the transcriptome are reliable. Analyzing the signature of the differentially expressed genes (DEGs) between diabetic and control mice (Table 4 and Figure 20), we found that 5 months of diabetes determined changes in 114 genes (at logFC>1 and FDR<0.05), inducing a comprehensive anti-inflammatory, anti-

apoptotic, pro-adesive/pro-migratory, and vasculo-protective signature in PMo (Tables 4 and 5). Specifically,

The overall anti-inflammatory pattern included:

--) the downregulation of pro-inflammatory cytokines (TNFalfa, its receptor CD40, IL1beta);

--) the downregulation of genes (CD6, CD28, CD81, CXCL4, PRKCCQ, Clec4n, ACHE, EGR1) that upregulate pro-inflammatory cytokines;

--) the upregulation of genes (IFIT2, Cldn-1, Hp) that downregulate pro-inflammatory genes; and, finally,

--) the inhibition of neutrophil recruitment via upregulation of Angptl4, and downregulation of CXCL7.

The overall anti-apoptotic pattern included:

--) the downregulation of pro-apoptotic mediators (Clu, Phlda3, Apbb1, Cd24, Niacr1, ACHE, EGR1, Nab2);

--) the upregulation of anti-apoptotic mediators (Claudin1, RCN, Ddit4).

The overall pro-adesive and pro-migratory pattern included:

--) the downregulation of the anti-adhesive mediator (CD81);

--) the upregulation of pro-adesive and pro-migratory mediators (CXCR4, PPP1r9A, Claudin1, Shootin1).

The overall vasculo-protective pattern included:

--) the downregulation of mediators of vascular injury and angiostatins (CD6, CXCL4, Niacr), and

--) the upregulation of vasculoprotective mediators (Angptl4, RCN3).

Notatly, diabetes increased the expression of CXCR4 and Cldn-1, that are involved in the chemotactic response to SDF-1/CXCL12, a “stress” molecule expressed by endothelial cells in response to injury.

Taken together, these findings support the hypothesis that diabetes activates a healing/protective transcriptional program in PMo. To confirm this finding, we analyzed enriched functional categories among detected genes using GSEA and IPA. GSEA analysis showed that PMo sorted form diabetic animals had significantly less enriched pathways related to immune response and activation of apoptosis, such as “GO positive regulation of immune response” (FDR<0.0001), “Zhou inflammatory response LPS up” (FDR<0.05) and “GO regulation of cell death” (FDR<0.05). (Table 6) Consistently, IPA Canonical Pathway analysis showed that PMo sorted form diabetic animals had significantly less enriched CD28 (-log pvalue=3.07), PKC-θ (-log pvalue=2.48) signaling and pro-apoptotic (-log pvalue=2.11) pathways (Table 7). In addition, we looked for an over-representation of protein–protein interactions (PPIs) within our top-ranking genes using the STRING software; we found considerable functional coherence, with many genes forming a single large interconnected subnetwork of medium-confidence (STRING score > 0.4) protein–protein interactions, the degree of interconnection of which was significantly higher than expected by chance (PPI enrichment *p-value* <0.0001). Key hubs were *Tnf, IL1b, CXCR4, PF4 and IFIT2* (Table 8 and Figure 21). Based on these data, we planned the real-time qPCR of a selection of genes chosen from the RNAseq data, on PMo sorted from WT mice after 3, 5, and 7

months of diabetes duration, and their age and sex-matched littermate controls. We found that an anti-inflammatory, pro-adhesive, and vasculo-protective program is activated in mice as early as after 3 months of diabetes, and as up to 7 months of diabetes duration. However, CXCR4 is upregulated in mice with 3 and 5 months – but not 7 months – of diabetes duration.

VI. DISCUSSION

Our main findings are: (i) PMo play a pivotal role in diabetic leukostasis; (ii) the absence of PMo is detrimental for retinal microvessels; (iii) diabetes activates a protective/healing transcriptional program in PMo, and (iv) PMo's protective activities are CXCR4-dependent.

1. PMo play a pivotal role in diabetic leukostasis

Classically, diabetic leukostasis has been interpreted as a detrimental phenomenon, and for this reason intensive investigation has been oriented to inhibit leukostasis to prevent or cure diabetic retinopathy. In fact, when in 1991 Schroder et al described for the first time the phenomenon of leukostasis in retinal microvessels of diabetic rats, they also suggested it may play a key role in the pathogenesis of diabetic retinopathy via induction of capillary occlusion and endothelial damage; in addition, the authors identified monocytes and granulocytes as the main protagonists of this phenomenon (Schroder et al., 1991). Soon after, McLeod et al measured the expression of ICAM-1 – an adhesion molecule that enhances leukocyte adhesion to vessels – in the retinal blood vessels of postmortem human tissue sections, and found that it was increased in diabetic subjects with early or no retinopathy, this finding indirectly supports the hypothesis that diabetic leukostasis is an early phenomenon present also in human diabetes (McLeod et al., 1995). Subsequently, an interesting publication by Adamis' group reported that the inhibition of ICAM-mediated leukocyte adhesion significantly improved retinopathy in mice with long duration of diabetes (11-15 months)

(Joussen et al., 2004). Further to the above, increased leukostasis in the retinal microvasculature has been reported in vivo after short and long-term diabetes, by acridine orange fluorography (Tamura et al., 2005, Abiko et al., 2003).

The fact that the overall effect of leukostatic cells may become at some point detrimental for microvessels, does not imply that leukostasis is *per se* a detrimental phenomenon; i.e. leukostasis may not be detrimental during all stages of diabetes, and not all the participating leukostatic populations may be acting detrimentally. There is mounting evidence demonstrating on the one hand the existence of a multitude of leukocyte subpopulations, each with its peculiar role and activity, and on the other hand demonstrating the ability of leukocytes to modulate their phenotype and biosynthetic profile over time and with progression of disease. Altogether, these evidences suggest that leukostasis is probably a much more complex and dynamic event than what was initially thought. It is conceivable that leukostasis is characterized by an extremely articulated interplay between leukocytes, that continuously adapt and react to a multitude of stimuli, such as the altered metabolic environment, the evolving vascular damage, and the neighboring leukocytes. In this picture, it is reasonable to believe that different leukostatic cells play different roles, where some cells try to orchestrate the response of the other immune cells to the stressed microvessels in order to repair the damage/alterations and maintain vascular homeostasis. Indeed, our findings strongly suggest that diabetic leukostasis represents at least in part a protective/healing phenomenon in which PMo are protagonists and in the context of which they appear to deliver

protection to endothelial cells from the hyperglycemic stress. Notably, a very recent paper reports that diabetic retinal leukostasis is an ICAM-dependent phenomenon that is present as early as after 3 weeks of diabetes duration; of note, the authors report that at this duration no signs of retinopathy were present yet (Frimmel et al., 2017), somehow supporting our hypothesis.

Therefore, our work on diabetic leukostasis now calls for an official re-interpretation of diabetic leukostasis. The next step is to unveil the other players involved in leukostasis, and to understand if their representation is altered by diabetes. In addition it is mandatory to explore the nature of the physical and molecular interactions occurring among leukostatic cells, and specifically in the setting of leukostasis. This knowledge has the potential to foster the discovery of new pharmacological targets for the prevention and the treatment of diabetic microvascular disease in the retina, as well as in other tissues and organs, such as kidney, heart, and central and peripheral nervous system.

2. Absence of PMo is detrimental for retinal microvessels

Most groups have reproducibly reported that the first signs of diabetic retinal microvascular disease in rodents start to appear after 6-9 months of diabetes (Kern et al., 2010, Zheng et al., 2007, Hazra et al., 2012, Feng et al., 2008, Gerhardinger et al., 2001). We found that PMo apparently are not involved in the maintenance of vascular homeostasis in healthy aging, nor after 4 months of diabetes. We found instead that the absence of PMo significantly worsens the damage occurring after 6 months of diabetes in control (WT diabetic) mice. One possible interpretation is that the

protective/healing mechanism operated by PMo is not activated in the absence of microvascular stress and damage; instead, once microvessels start being/showing diabetes-related damage, PMo are activated and become operative in their protective/healing activities. Our findings strongly support the hypothesis that PMo represent a protective mechanism of the vessels. In addition, solid literature showing protective and healing activities of PMo on microvessels in the kidney (Carlin et al., 2013, Cros et al., 2010), in the cortex (Michaud et al., 2013), in the lung (Hanna et al., 2015), etc. further supports our hypothesis.

3. Diabetes activates a protective/healing transcriptional program in PMo

To the best of our knowledge PMo are the only leukocytes that respond to diabetes by activating a protective/healing transcriptional program, that comprises an overall anti-inflammatory, anti-apoptotic, pro-adhesive/pro-migratory, and vasculo-protective program. The evidence that diabetes exerts an ubiquitous pro-inflammatory effects is so solid that it has become a paradigm in Medicine.

Since the early 1980's it is known that monocyte metabolic activation is increased in diabetic patients (Kitahara et al., 1980), and recently this aberrant behavior has been linked to vascular complications (Devaraj et al., 2006). Notably, monocytes from type 1 and type 2 diabetic patients secrete more superoxide and pro-inflammatory cytokines (such as IL-1β, IL-6, and TNF-α**),** than monocytes from healthy control subjects (Giulietti et al., 2004, Devaraj et al., 2006). Besides playing a pivotal role in the

pathogenesis of type 1 (Burkart and Kolb, 1996) and type 2 (Morris, 2015) diabetes, macrophages are also altered by diabetes itself. In fact, macrophages isolated from both type 1 and type 2 diabetic mice exhibit an inflammatory phenotype (Kanter et al., 2012, Kraakman et al., 2014). In addition, macrophages have been proposed as key players in the development of diabetic complications (Tesch, 2007). We have previously studied ourselves the role of macrophage polarization (M1: pro-inflammatory; M2: anti-inflammatory) in diabetic wound healing, and found that diabetes increases the skin M1/M2 ratio at baseline, and prevents post-wounding changes in macrophage polarization (Leal et al., 2015).

Neutrophils from diabetic mice have been shown to be primed for marginalization and superoxide production (Gyurko et al., 2006); moreover, neutrophils from diabetic patients produce more superoxide and cytokines (Karima et al., 2005, Hanses et al., 2011), and are induced to release Neutrophil Extracellular Traps (Wong et al., 2015), which are known to contribute to inflammatory and vascular diseases (Yipp and Kubes, 2013).

It has been shown that B lymphocytes from diabetic subjects secrete a comprehensive proinflammatory cytokine profile, that includes the inability to secrete the anti-inflammatory cytokine IL-10, and an increased production of the proinflammatory cytokine IL-8 (Jagannathan et al., 2010). In a follow-up study, the authors showed that B lymphocytes regulate inflammation in diabetes, both directly via their altered secretory profile, and indirectly via the modulation of T lymphocytes (DeFuria et al., 2013). It has been shown that lymphocytes from diabetic patients display features of

oxidative stress, and alterations of intracellular Calcium homeostasis (Belia et al., 2009); in addition, it has been shown that diabetes induces specific structural chromosomal aberrations in lymphocytes (Boehm et al., 2008).

Early studies by Pozzilli et al. demonstarted that T1DM of long duration caused an alteration in the absolute number of total T lymphocytes (Pozzilli et al., 1983); more specifically, the levels of total T lymphocytes and of T-helpers were decreased, while the levels of T-suppressor/cytotoxic were increased (Andreani et al., 1984). Notably, the authors observed no relationship between high levels of T-suppressor/cytotoxic lymphocytes and microvascular disease. More recently, the study of NK cell in newly diagnosed T1DM patients showed that the levels of these cells are reduced (Rodacki et al., 2007); in addition, functional abnormalities have also been reported in NK cells of patients with T1DM (Lorini et al., 1994). Intriguingly, these alterations may represent a link to the increased risk of infections and neoplasia in diabetic patients.

Herein, we found instead a peculiar response of PMo to diabetes, these cells decrease the expression of pro-inflammatory cytokines, and increase the expression of anti-inflammatory cytokines. In addition, PMo respond to diabetes by shutting down pro-apoptotic mediators, and by activating anti-apoptotic signaling. Another peculiar response of PMo is the upregulation of the homing machinery (namely CXCR4) which has ben shown to be usually impired by diabetes. Finally, PMo respond to diabetes with the activation of vasculo-protection through indirect upregulation of VEGF signaling and the direct upregulation of vasculogenic molecules.

4. PMo's protective activities are CXCR4-dependent

The fact that diabetes activates a protective transcriptional program (namely anti-inflammatory, pro-adhesive, and vasculo-protective) as early as after 3 months and up to 7 months of diabetes duration, whereas CXCR4 is upregulated only up to 5 months of diabetes duration – together with the morphological observation that signs of retinal microangiopathy become apparent in mice only after 6 months of diabetes – strongly suggests that CXCR4 may be the critical mechanism allowing PMo to deliver their protective/healing activities on retinal vessels. The hypothesis that CXCR4 is a critical molecule for the delivery of protection of microvessels in diabetes is not new, work from Maria Grant's laboratory has in fact previously shown its role for guiding the recruitment of EPCs to areas of ischemia, allowing these cells to participate in compensatory angiogenesis (Bhatwadekar et al., 2010, Segal et al., 2006). Moreover, Dr. Lorenzi's group has previously demonstrated that patients with T1DM with initial retinopathy – but not the ones without retinopathy – had decreased expression of CXCR4 on CHU-Hills (see above) (Zerbini et al., 2012). Consistently to this hypothesis, there is mounting evidence in the literature, that the SDF1/CXCR4 axis plays a pivotal role in the maintainance of tissue homeostasis (Penn, 2010). Our data clearly show that as long as CXCR4 is upregulated (3 and 5 months of diabetes-duration) retinal microvessels do not develop damage; instead, after 7 months of diabetes, when CXCR4 is no longer up-regulated, signs of microvascular disease appear in the retina, even though the anti-inflammatory profile is activated in PMo. Notably, our findings appears extremely consistent with a

recent report from Dr. Fukumura's group in which the authors demonstrate that the anti-inflammatory activities of PMo are CXCR4-dependent (Jung et al., 2017).

Dr. Bianchi's group has extensively studied the role of CXCR4 in tissue repair, and has shown that CXCR4 binds the heterocomplex formed by the high mobility group box 1 (HMGB1) protein and CXCL12. Once activated, CXCR4 orchestrates tissue regeneration on the one hand by inducing leukocyte migration to the site of tissue damage, and on the other hand by inducing a tissue-healing microenvironment through the modulation of the monocyte-macrophage polarization status toward a tissue-healing phenotype (Tirone et al., 2017, Schiraldi et al., 2012).

Dr. Kubes' group (Wang et al., 2017) has recently shown that CXCR4 plays a key role in the repair of hepatic sterile inflammation exerted by neutrophils, by facilitating clearance of debris from the injury site and revascularization of damaged tissue, via dismantling of injured vessels and the creation of channels for vascular regrowth. In addition, the authors showed that CXCR4 plays a critical role in "reverse migration", a preprogrammed pathway of neutrophils that leave the injury site, reenter the vasculature, and travel through the lungs to the bone marrow, where they "educate" other immune cells to further contribute to the resolution of the sterile inflammatory condition, or even to prepare the host for future sterile injuries.

VII. CONCLUSIONS

Epidemiological data predict a dramatic increase in the prevalence of diabetes worldwide; it is reasonable to assume there will be a parallel increase in all its complications, including diabetic retinopathy, the most common microvascular complication of diabetes. Indeed, great progress has been made in decreasing the impact of all complications, and in particular of retinopathy as a sight-threatening condition. Nevertheless, the persistent occurrence of microvascular complications more than twenty years into the implementation of intensive insulin treatment, and the lack of tools to achieve predictable prevention, strongly indicate the need to continue the quest for interventions and the urge to identify a biomarker of disease.

Two groundbreaking concepts arise from this work, both with far reaching potential. The first novel concept is the discovery of mechanisms that protect and repair retinal microvascular cells. Thereby indicating that the degree of diabetic retinal microangiopathy appears to reflect the balance of damage and repair. Our data demonstrate in fact that Patrolling monocytes protect retinal microvessels – and reasonably other microvascular compartments – from diabetes. The second novel concept is that leukostasis represents an attempt to bring healing influences to the distressed cells of retinal vessels, rather than a pro-inflammatory event as currently proposed, thereby changing the functional meaning of this phenomenon. Our data demonstrate in fact that PMo are prominent contributors to diabetic leukostasis.

Our data now calls (1) to understand whether decreased interactions with PMo alters the biosynthetic activity of vessels and

accelerates the vascular alterations caused by diabetes; (2) to learn whether the biosynthetic profile of PMo changes in relation to increasing duration of DM and evolving retinal vascular damage; and, most importantly, (3) to bring the study of PMo to clinical investigation.

Indeed the results of this work have the far reaching potential to change the clinical management of retinopathy. In fact our results have the potential to foster the development on the one hand of a biomarker of risk for the onset and progression of retinopathy, and on the other hand new targeted therapeutic interventions for diabetic microvascular disease, and in particular of retinopathy.

VIII. REFERENCES

ABIKO, T., ABIKO, A., CLERMONT, A. C., SHOELSON, B., HORIO, N., TAKAHASHI, J., ADAMIS, A. P., KING, G. L. & BURSELL, S. E. 2003. Characterization of retinal leukostasis and hemodynamics in insulin resistance and diabetes: role of oxidants and protein kinase-C activation. *Diabetes,* 52**,** 829-37.

ANDERS, S., PYL, P. T. & HUBER, W. 2015. HTSeq--a Python framework to work with high-throughput sequencing data. *Bioinformatics,* 31**,** 166-9.

ANDREANI, D., DI MARIO, U., ZUCCARINI, O., FRANCO, M., SENSI, M., IAVICOLI, M. & POZZILLI, P. 1984. Lymphocyte subsets and immune complexes in long-standing diabetic patients: relation with the presence of microangiopathy. *Immunology Letters,* 8**,** 17-21.

ARKENBOUT, E. K., DE WAARD, V., VAN BRAGT, M., VAN ACHTERBERG, T. A., GRIMBERGEN, J. M., PICHON, B., PANNEKOEK, H. & DE VRIES, C. J. 2002. Protective function of transcription factor TR3 orphan receptor in atherogenesis: decreased lesion formation in carotid artery ligation model in TR3 transgenic mice. *Circulation,* 106**,** 1530-5.

AUFFRAY, C., FOGG, D., GARFA, M., ELAIN, G., JOIN-LAMBERT, O., KAYAL, S., SARNACKI, S., CUMANO, A., LAUVAU, G. & GEISSMANN, F. 2007. Monitoring of blood vessels and tissues by a population of monocytes with patrolling behavior. *Science,* 317**,** 666-70.

BAZAN, J. F., BACON, K. B., HARDIMAN, G., WANG, W., SOO, K., ROSSI, D., GREAVES, D. R., ZLOTNIK, A. & SCHALL, T. J. 1997. A new class of membrane-bound chemokine with a CX3C motif. *Nature,* 385**,** 640-4.

BELIA, S., SANTILLI, F., BECCAFICO, S., DE FEUDIS, L., MORABITO, C., DAVI, G., FANO, G. & MARIGGIO, M. A. 2009. Oxidative-induced membrane damage in

diabetes lymphocytes: effects on intracellular Ca(2 +) homeostasis. *Free Radical Research,* 43**,** 138-48.

BHATWADEKAR, A. D., GUERIN, E. P., JARAJAPU, Y. P., CABALLERO, S., SHERIDAN, C., KENT, D., KENNEDY, L., LANSANG, M. C., RUSCETTI, F. W., PEPINE, C. J., HIGGINS, P. J., BARTELMEZ, S. H. & GRANT, M. B. 2010. Transient inhibition of transforming growth factor-beta1 in human diabetic CD34+ cells enhances vascular reparative functions. *Diabetes,* 59**,** 2010-9.

BIBURGER, M., ASCHERMANN, S., SCHWAB, I., LUX, A., ALBERT, H., DANZER, H., WOIGK, M., DUDZIAK, D. & NIMMERJAHN, F. 2011. Monocyte subsets responsible for immunoglobulin G-dependent effector functions in vivo. *Immunity,* 35**,** 932-44.

BOEHM, B. O., MOLLER, P., HOGEL, J., WINKELMANN, B. R., RENNER, W., ROSINGER, S., SEELHORST, U., WELLNITZ, B., MARZ, W., MELZNER, J. & BRUDERLEIN, S. 2008. Lymphocytes of type 2 diabetic women carry a high load of stable chromosomal aberrations: a novel risk factor for disease-related early death. *Diabetes,* 57**,** 2950-7.

BONTA, P. I., VAN TIEL, C. M., VOS, M., POLS, T. W., VAN THIENEN, J. V., FERREIRA, V., ARKENBOUT, E. K., SEPPEN, J., SPEK, C. A., VAN DER POLL, T., PANNEKOEK, H. & DE VRIES, C. J. 2006. Nuclear receptors Nur77, Nurr1, and NOR-1 expressed in atherosclerotic lesion macrophages reduce lipid loading and inflammatory responses. *Arteriosclerosis, thrombosis, and vascular biology,* 26**,** 2288-94.

BURKART, V. & KOLB, H. 1996. Macrophages in islet destruction in autoimmune diabetes mellitus. *Immunobiology,* 195**,** 601-13.

CARLIN, L. M., STAMATIADES, E. G., AUFFRAY, C., HANNA, R. N., GLOVER, L., VIZCAY-BARRENA, G., HEDRICK, C. C., COOK, H. T., DIEBOLD, S. & GEISSMANN, F. 2013. Nr4a1-Dependent Ly6C(low)

Monocytes Monitor Endothelial Cells and Orchestrate Their Disposal. *Cell,* 153**,** 362-75.

CHAO, L. C., WROBLEWSKI, K., ILKAYEVA, O. R., STEVENS, R. D., BAIN, J., MEYER, G. A., SCHENK, S., MARTINEZ, L., VERGNES, L., NARKAR, V. A., DREW, B. G., HONG, C., BOYADJIAN, R., HEVENER, A. L., EVANS, R. M., REUE, K., SPENCER, M. J., NEWGARD, C. B. & TONTONOZ, P. 2012. Skeletal muscle Nur77 expression enhances oxidative metabolism and substrate utilization. *Journal of lipid research,* 53**,** 2610-9.

CHAO, L. C., WROBLEWSKI, K., ZHANG, Z., PEI, L., VERGNES, L., ILKAYEVA, O. R., DING, S. Y., REUE, K., WATT, M. J., NEWGARD, C. B., PILCH, P. F., HEVENER, A. L. & TONTONOZ, P. 2009. Insulin resistance and altered systemic glucose metabolism in mice lacking Nur77. *Diabetes,* 58**,** 2788-96.

CHAO, L. C., ZHANG, Z., PEI, L., SAITO, T., TONTONOZ, P. & PILCH, P. F. 2007. Nur77 coordinately regulates expression of genes linked to glucose metabolism in skeletal muscle. *Molecular endocrinology,* 21**,** 2152-63.

CROS, J., CAGNARD, N., WOOLLARD, K., PATEY, N., ZHANG, S. Y., SENECHAL, B., PUEL, A., BISWAS, S. K., MOSHOUS, D., PICARD, C., JAIS, J. P., D'CRUZ, D., CASANOVA, J. L., TROUILLET, C. & GEISSMANN, F. 2010. Human CD14dim monocytes patrol and sense nucleic acids and viruses via TLR7 and TLR8 receptors. *Immunity,* 33**,** 375-86.

DEFURIA, J., BELKINA, A. C., JAGANNATHAN-BOGDAN, M., SNYDER-CAPPIONE, J., CARR, J. D., NERSESOVA, Y. R., MARKHAM, D., STRISSEL, K. J., WATKINS, A. A., ZHU, M., ALLEN, J., BOUCHARD, J., TORALDO, G., JASUJA, R., OBIN, M. S., MCDONNELL, M. E., APOVIAN, C., DENIS, G. V. & NIKOLAJCZYK, B. S. 2013. B cells promote inflammation in obesity and type 2 diabetes through regulation of T-cell function and an inflammatory cytokine

profile. *Proceedings of the National Academy of Sciences of the United States of America,* 110**,** 5133-8.

DEVARAJ, S., GLASER, N., GRIFFEN, S., WANG-POLAGRUTO, J., MIGUELINO, E. & JIALAL, I. 2006. Increased monocytic activity and biomarkers of inflammation in patients with type 1 diabetes. *Diabetes,* 55**,** 774-9.

DOBIN, A., DAVIS, C. A., SCHLESINGER, F., DRENKOW, J., ZALESKI, C., JHA, S., BATUT, P., CHAISSON, M. & GINGERAS, T. R. 2013. STAR: ultrafast universal RNA-seq aligner. *Bioinformatics,* 29**,** 15-21.

FENG, Y., PFISTER, F., SCHREITER, K., WANG, Y., STOCK, O., VOM HAGEN, F., WOLBURG, H., HOFFMANN, S., DEUTSCH, U. & HAMMES, H. P. 2008. Angiopoietin-2 deficiency decelerates age-dependent vascular changes in the mouse retina. *Cellular physiology and biochemistry : international journal of experimental cellular physiology, biochemistry, and pharmacology,* 21**,** 129-36.

FINSTERBUSCH, M., HALL, P., LI, A., DEVI, S., WESTHORPE, C. L., KITCHING, A. R. & HICKEY, M. J. 2016. Patrolling monocytes promote intravascular neutrophil activation and glomerular injury in the acutely inflamed glomerulus. *Proc Natl Acad Sci U S A,* 113**,** E5172-81.

FONG, A. M., ROBINSON, L. A., STEEBER, D. A., TEDDER, T. F., YOSHIE, O., IMAI, T. & PATEL, D. D. 1998. Fractalkine and CX3CR1 mediate a novel mechanism of leukocyte capture, firm adhesion, and activation under physiologic flow. *The Journal of experimental medicine,* 188**,** 1413-9.

FRIMMEL, S., ZANDI, S., SUN, D., ZHANG, Z., SCHERING, A., MELHORN, M. I., NAKAO, S. & HAFEZI-MOGHADAM, A. 2017. Molecular Imaging of Retinal Endothelial Injury in Diabetic Animals. *Journal of ophthalmic & vision research,* 12**,** 175-182.

FU, Y., LUO, L., LUO, N., ZHU, X. & GARVEY, W. T. 2007. NR4A orphan nuclear receptors modulate insulin action and the glucose transport system: potential role in insulin resistance. *The Journal of biological chemistry,* 282**,** 31525-33.

FUJIU, K., MANABE, I. & NAGAI, R. 2011. Renal collecting duct epithelial cells regulate inflammation in tubulointerstitial damage in mice. *The Journal of clinical investigation,* 121**,** 3425-41.

GARTON, K. J., GOUGH, P. J., BLOBEL, C. P., MURPHY, G., GREAVES, D. R., DEMPSEY, P. J. & RAINES, E. W. 2001. Tumor necrosis factor-alpha-converting enzyme (ADAM17) mediates the cleavage and shedding of fractalkine (CX3CL1). *The Journal of biological chemistry,* 276**,** 37993-8001.

GEISSMANN, F., JUNG, S. & LITTMAN, D. R. 2003. Blood monocytes consist of two principal subsets with distinct migratory properties. *Immunity,* 19**,** 71-82.

GERHARDINGER, C., MCCLURE, K. D., ROMEO, G., PODESTA, F. & LORENZI, M. 2001. IGF-I mRNA and signaling in the diabetic retina. *Diabetes,* 50**,** 175-83.

GIULIETTI, A., STOFFELS, K., DECALLONNE, B., OVERBERGH, L. & MATHIEU, C. 2004. Monocytic expression behavior of cytokines in diabetic patients upon inflammatory stimulation. *Annals of the New York Academy of Sciences,* 1037**,** 74-8.

GODA, S., IMAI, T., YOSHIE, O., YONEDA, O., INOUE, H., NAGANO, Y., OKAZAKI, T., IMAI, H., BLOOM, E. T., DOMAE, N. & UMEHARA, H. 2000. CX3C-chemokine, fractalkine-enhanced adhesion of THP-1 cells to endothelial cells through integrin-dependent and -independent mechanisms. *Journal of immunology,* 164**,** 4313-20.

GRUBER, F., HUFNAGL, P., HOFER-WARBINEK, R., SCHMID, J. A., BREUSS, J. M., HUBER-BECKMANN, R., LUCERNA, M., PAPAC, N., HARANT, H., LINDLEY, I., DE MARTIN, R. & BINDER, B. R. 2003.

Direct binding of Nur77/NAK-1 to the plasminogen activator inhibitor 1 (PAI-1) promoter regulates TNF alpha -induced PAI-1 expression. *Blood,* 101**,** 3042-8.

GYURKO, R., SIQUEIRA, C. C., CALDON, N., GAO, L., KANTARCI, A. & VAN DYKE, T. E. 2006. Chronic hyperglycemia predisposes to exaggerated inflammatory response and leukocyte dysfunction in Akita mice. *Journal of Immunology,* 177**,** 7250-6.

HAMMES, H. P., KERNER, W., HOFER, S., KORDONOURI, O., RAILE, K., HOLL, R. W. & GROUP, D. P.-W. S. 2011. Diabetic retinopathy in type 1 diabetes-a contemporary analysis of 8,784 patients. *Diabetologia,* 54**,** 1977-84.

HANNA, R. N., CARLIN, L. M., HUBBELING, H. G., NACKIEWICZ, D., GREEN, A. M., PUNT, J. A., GEISSMANN, F. & HEDRICK, C. C. 2011. The transcription factor NR4A1 (Nur77) controls bone marrow differentiation and the survival of Ly6C- monocytes. *Nature immunology,* 12**,** 778-85.

HANNA, R. N., CEKIC, C., SAG, D., TACKE, R., THOMAS, G. D., NOWYHED, H., HERRLEY, E., RASQUINHA, N., MCARDLE, S., WU, R., PELUSO, E., METZGER, D., ICHINOSE, H., SHAKED, I., CHODACZEK, G., BISWAS, S. K. & HEDRICK, C. C. 2015. Patrolling monocytes control tumor metastasis to the lung. *Science*.

HANNA, R. N., SHAKED, I., HUBBELING, H. G., PUNT, J. A., WU, R., HERRLEY, E., ZAUGG, C., PEI, H., GEISSMANN, F., LEY, K. & HEDRICK, C. C. 2012. NR4A1 (Nur77) deletion polarizes macrophages toward an inflammatory phenotype and increases atherosclerosis. *Circulation research,* 110**,** 416-27.

HANSES, F., PARK, S., RICH, J. & LEE, J. C. 2011. Reduced neutrophil apoptosis in diabetic mice during staphylococcal infection leads to prolonged Tnfalpha production and reduced neutrophil clearance. *PLoS One,* 6**,** e23633.

HAZRA, S., RASHEED, A., BHATWADEKAR, A., WANG, X., SHAW, L. C., PATEL, M., CABALLERO, S., MAGOMEDOVA, L., SOLIS, N., YAN, Y., WANG, W., THINSCHMIDT, J. S., VERMA, A., LI, Q., LEVI, M., CUMMINS, C. L. & GRANT, M. B. 2012. Liver X receptor modulates diabetic retinopathy outcome in a mouse model of streptozotocin-induced diabetes. *Diabetes,* 61**,** 3270-9.

HETTINGER, J., RICHARDS, D., HANSSON, J., BARRA, M., JOSCHKO, A.-C., KRIJGSVELD, J. & FEUERER, M. 2013. Origin of monocytes and macrophages in a committed progenitor. *Nature immunology,* 14**,** 821-830.

HILGENDORF, I., GERHARDT, L. M., TAN, T. C., WINTER, C., HOLDERRIED, T. A., CHOUSTERMAN, B. G., IWAMOTO, Y., LIAO, R., ZIRLIK, A., SCHERER-CROSBIE, M., HEDRICK, C. C., LIBBY, P., NAHRENDORF, M., WEISSLEDER, R. & SWIRSKI, F. K. 2014. Ly-6Chigh monocytes depend on Nr4a1 to balance both inflammatory and reparative phases in the infarcted myocardium. *Circ Res,* 114**,** 1611-22.

IMAI, T., HIESHIMA, K., HASKELL, C., BABA, M., NAGIRA, M., NISHIMURA, M., KAKIZAKI, M., TAKAGI, S., NOMIYAMA, H., SCHALL, T. J. & YOSHIE, O. 1997. Identification and molecular characterization of fractalkine receptor CX3CR1, which mediates both leukocyte migration and adhesion. *Cell,* 91**,** 521-30.

IMHOF, B. A., JEMELIN, S., BALLET, R., VESIN, C., SCHAPIRA, M., KARACA, M. & EMRE, Y. 2016. CCN1/CYR61-mediated meticulous patrolling by Ly6Clow monocytes fuels vascular inflammation. *Proc Natl Acad Sci U S A,* 113**,** E4847-56.

INGERSOLL, M. A., SPANBROEK, R., LOTTAZ, C., GAUTIER, E. L., FRANKENBERGER, M., HOFFMANN, R., LANG, R., HANIFFA, M., COLLIN, M., TACKE, F., HABENICHT, A. J., ZIEGLER-HEITBROCK, L. & RANDOLPH, G. J. 2010.

Comparison of gene expression profiles between human and mouse monocyte subsets. *Blood*, 115**,** e10-9.

INTERNATIONAL DIABETES FEDERATION, I. 2015. IDF Diabetes Atlas, 7th edn. . International Diabetes Federation.

JAGANNATHAN, M., MCDONNELL, M., LIANG, Y., HASTURK, H., HETZEL, J., RUBIN, D., KANTARCI, A., VAN DYKE, T. E., GANLEY-LEAL, L. M. & NIKOLAJCZYK, B. S. 2010. Toll-like receptors regulate B cell cytokine production in patients with diabetes. *Diab tologia*, 53**,** 1461-71.

JOUSSEN, A. M., POULAKI, V., LE, M. L., KOIZUMI, K., ESSER, C., JANICKI, H., SCHRAERMEYER, U., KOCIOK, N., FAUSER, S., KIRCHHOF, B., KERN, T. S. & ADAMIS, A. P. 2004. A central role for inflammation in the pathogenesis of diabetic retinopathy. *FASEB J*, 18**,** 1450-2.

JUNG, K., HEISHI, T., INCIO, J., HUANG, Y., BEECH, E. Y., PINTER, M., HO, W. W., KAWAGUCHI, K., RAHBARI, N. N., CHUNG, E., KIM, J. K., CLARK, J. W., WILLETT, C. G., YUN, S. H., LUSTER, A. D., PADERA, T. P., JAIN, R. K. & FUKUMURA, D. 2017. Targeting CXCR4-dependent immunosuppressive Ly6Clow monocytes improves antiangiogenic therapy in colorectal cancer. *Proceedings of the National Academy of Sciences of the United States of America*.

KANTER, J. E., KRAMER, F., BARNHART, S., AVERILL, M. M., VIVEKANANDAN-GIRI, A., VICKERY, T., LI, L. O., BECKER, L., YUAN, W., CHAIT, A., BRAUN, K. R., POTTER-PERIGO, S., SANDA, S., WIGHT, T. N., PENNATHUR, S., SERHAN, C. N., HEINECKE, J. W., COLEMAN, R. A. & BORNFELDT, K. E. 2012. Diabetes promotes an inflammatory macrophage phenotype and atherosclerosis through acyl-CoA synthetase 1. *Proceedings of the National Academy of Sciences of the United States of America*, 109**,** E715-24.

KARIMA, M., KANTARCI, A., OHIRA, T., HASTURK, H., JONES, V. L., NAM, B. H., MALABANAN, A., TRACKMAN, P. C., BADWEY, J. A. & VAN DYKE, T. E. 2005. Enhanced superoxide release and elevated protein kinase C activity in neutrophils from diabetic patients: association with periodontitis. *Journal of Leukocyte Biology,* 78**,** 862-70.

KERN, T. S., TANG, J. & BERKOWITZ, B. A. 2010. Validation of structural and functional lesions of diabetic retinopathy in mice. *Molecular vision,* 16**,** 2121-31.

KITAHARA, M., EYRE, H. J., LYNCH, R. E., RALLISON, M. L. & HILL, H. R. 1980. Metabolic activity of diabetic monocytes. *Diabetes,* 29**,** 251-6.

KRAAKMAN, M. J., MURPHY, A. J., JANDELEIT-DAHM, K. & KAMMOUN, H. L. 2014. Macrophage polarization in obesity and type 2 diabetes: weighing down our understanding of macrophage function? *Frontiers in immunology,* 5**,** 470.

LEAL, E. C., CARVALHO, E., TELLECHEA, A., KAFANAS, A., TECILAZICH, F., KEARNEY, C., KUCHIBHOTLA, S., AUSTER, M. E., KOKKOTOU, E., MOONEY, D. J., LOGERFO, F. W., PRADHAN-NABZDYK, L. & VEVES, A. 2015. Substance P Promotes Wound Healing in Diabetes by Modulating Inflammation and Macrophage Phenotype. *Am J Pathol*.

LIASKOU, E., ZIMMERMANN, H. W., LI, K. K., HTUN OO, Y., SURESH, S., STAMATAKI, Z., QURESHI, O., LALOR, P. F., SHAW, J., SYN, W. K., CURBISHLEY, S. M. & ADAMS, D. H. 2012. Monocyte subsets in human liver disease show distinct phenotypic and functional characteristics. *Hepatology*.

LORINI, R., MORETTA, A., VALTORTA, A., D'ANNUNZIO, G., CORTONA, L., VITALI, L., BOZZOLA, M. & SEVERI, F. 1994. Cytotoxic activity in children with insulin-dependent diabetes mellitus. *Diabetes Research and Clinical Practice,* 23**,** 37-42.

LUDWIG, A., BERKHOUT, T., MOORES, K., GROOT, P. & CHAPMAN, G. 2002. Fractalkine is expressed by smooth muscle cells in response to IFN-gamma and TNF-alpha and is modulated by metalloproteinase activity. *Journal of immunology,* 168**,** 604-12.

MATTAPALLIL, M. J., WAWROUSEK, E. F., CHAN, C. C., ZHAO, H., ROYCHOUDHURY, J., FERGUSON, T. A. & CASPI, R. R. 2012. The Rd8 mutation of the Crb1 gene is present in vendor lines of C57BL/6N mice and embryonic stem cells, and confounds ocular induced mutant phenotypes. *Investigative ophthalmology & visual science,* 53**,** 2921-7.

MCDERMOTT, D. H., FONG, A. M., YANG, Q., SECHLER, J. M., CUPPLES, L. A., MERRELL, M. N., WILSON, P. W., D'AGOSTINO, R. B., O'DONNELL, C. J., PATEL, D. D. & MURPHY, P. M. 2003. Chemokine receptor mutant CX3CR1-M280 has impaired adhesive function and correlates with protection from cardiovascular disease in humans. *The Journal of clinical investigation,* 111**,** 1241-50.

MCDERMOTT, D. H., HALCOX, J. P., SCHENKE, W. H., WACLAWIW, M. A., MERRELL, M. N., EPSTEIN, N., QUYYUMI, A. A. & MURPHY, P. M. 2001. Association between polymorphism in the chemokine receptor CX3CR1 and coronary vascular endothelial dysfunction and atherosclerosis. *Circulation research,* 89**,** 401-7.

MCLEOD, D. S., LEFER, D. J., MERGES, C. & LUTTY, G. A. 1995. Enhanced expression of intracellular adhesion molecule-1 and P-selectin in the diabetic human retina and choroid. *Am J Pathol,* 147**,** 642-53.

MICHAUD, J. P., BELLAVANCE, M. A., PREFONTAINE, P. & RIVEST, S. 2013. Real-time in vivo imaging reveals the ability of monocytes to clear vascular amyloid Beta. *Cell reports,* 5**,** 646-53.

MIZUTANI, M., KERN, T. S. & LORENZI, M. 1996. Accelerated death of retinal microvascular cells in human

and experimental diabetic retinopathy. *Journal of Clinical Investigation,* 97**,** 2883-90.

MORRIS, D. L. 2015. Minireview: Emerging Concepts in Islet Macrophage Biology in Type 2 Diabetes. *Molecular Endocrinology,* 29**,** 946-62.

NAGAREDDY, P. R., MURPHY, A. J., STIRZAKER, R. A., HU, Y., YU, S., MILLER, R. G., RAMKHELAWON, B., DISTEL, E., WESTERTERP, M., HUANG, L. S., SCHMIDT, A. M., ORCHARD, T. J., FISHER, E. A., TALL, A. R. & GOLDBERG, I. J. 2013. Hyperglycemia promotes myelopoiesis and impairs the resolution of atherosclerosis. *Cell metabolism,* 17**,** 695-708.

NAHRENDORF, M., SWIRSKI, F. K., AIKAWA, E., STANGENBERG, L., WURDINGER, T., FIGUEIREDO, J. L., LIBBY, P., WEISSLEDER, R. & PITTET, M. J. 2007. The healing myocardium sequentially mobilizes two monocyte subsets with divergent and complementary functions. *The Journal of experimental medicine,* 204**,** 3037-47.

NIMMERJAHN, F., BRUHNS, P., HORIUCHI, K. & RAVETCH, J. V. 2005. FcgammaRIV: a novel FcR with distinct IgG subclass specificity. *Immunity,* 23**,** 41-51.

PALUMBO-ZERR, K., ZERR, P., DISTLER, A., FLIEHR, J., MANCUSO, R., HUANG, J., MIELENZ, D., TOMCIK, M., FURNROHR, B. G., SCHOLTYSEK, C., DEES, C., BEYER, C., KRONKE, G., METZGER, D., DISTLER, O., SCHETT, G. & DISTLER, J. H. 2015. Orphan nuclear receptor NR4A1 regulates transforming growth factor-beta signaling and fibrosis. *Nat Med*.

PAN, Y., LLOYD, C., ZHOU, H., DOLICH, S., DEEDS, J., GONZALO, J. A., VATH, J., GOSSELIN, M., MA, J., DUSSAULT, B., WOOLF, E., ALPERIN, G., CULPEPPER, J., GUTIERREZ-RAMOS, J. C. & GEARING, D. 1997. Neurotactin, a membrane-anchored chemokine upregulated in brain inflammation. *Nature,* 387**,** 611-7.

PAPAC-MILICEVIC, N., BREUSS, J. M., ZAUJEC, J., RYBAN, L., PLYUSHCH, T., WAGNER, G. A., FENZL, S., DREMSEK, P., CABARAVDIC, M., STEINER, M., GLASS, C. K., BINDER, C. J., UHRIN, P. & BINDER, B. R. 2012. The interferon stimulated gene 12 inactivates vasculoprotective functions of NR4A nuclear receptors. *Circulation research,* 110**,** e50-63.

PAPADOPOULOS, E. J., SASSETTI, C., SAEKI, H., YAMADA, N., KAWAMURA, T., FITZHUGH, D. J., SARAF, M. A., SCHALL, T., BLAUVELT, A., ROSEN, S. D. & HWANG, S. T. 1999. Fractalkine, a CX3C chemokine, is expressed by dendritic cells and is up-regulated upon dendritic cell maturation. *European journal of immunology,* 29**,** 2551-9.

PASSLICK, B., FLIEGER, D. & ZIEGLER-HEITBROCK, H. W. 1989. Identification and characterization of a novel monocyte subpopulation in human peripheral blood. *Blood,* 74**,** 2527-34.

PEI, L., CASTRILLO, A., CHEN, M., HOFFMANN, A. & TONTONOZ, P. 2005. Induction of NR4A orphan nuclear receptor expression in macrophages in response to inflammatory stimuli. *The Journal of biological chemistry,* 280**,** 29256-62.

PEI, L., WAKI, H., VAITHEESVARAN, B., WILPITZ, D. C., KURLAND, I. J. & TONTONOZ, P. 2006. NR4A orphan nuclear receptors are transcriptional regulators of hepatic glucose metabolism. *Nature medicine,* 12**,** 1048-55.

PENN, M. S. 2010. SDF-1:CXCR4 axis is fundamental for tissue preservation and repair. *The American journal of pathology,* 177**,** 2166-8.

POLS, T. W., BONTA, P. I. & DE VRIES, C. J. 2007. NR4A nuclear orphan receptors: protective in vascular disease? *Current opinion in lipidology,* 18**,** 515-20.

POZZILLI, P., ZUCCARINI, O., IAVICOLI, M., ANDREANI, D., SENSI, M., SPENCER, K. M., BOTTAZZO, G. F., BEVERLEY, P. C., KYNER, J. L. & CUDWORTH, A. G. 1983. Monoclonal antibodies defined abnormalities of T-

lymphocytes in type I (insulin-dependent) diabetes. *Diabetes,* 32**,** 91-4.

RIDKER, P. M. 2003. Clinical application of C-reactive protein for cardiovascular disease detection and prevention. *Circulation,* 107**,** 363-9.

RIDKER, P. M., EVERETT, B. M., THUREN, T., MACFADYEN, J. G., CHANG, W. H., BALLANTYNE, C., FONSECA, F., NICOLAU, J., KOENIG, W., ANKER, S. D., KASTELEIN, J. J. P., CORNEL, J. H., PAIS, P., PELLA, D., GENEST, J., CIFKOVA, R., LORENZATTI, A., FORSTER, T., KOBALAVA, Z., VIDA-SIMITI, L., FLATHER, M., SHIMOKAWA, H., OGAWA, H., DELLBORG, M., ROSSI, P. R. F., TROQUAY, R. P. T., LIBBY, P. & GLYNN, R. J. 2017. Antiinflammatory Therapy with Canakinumab for Atherosclerotic Disease. *New England Journal of Medicine*.

ROBINSON, M. D., MCCARTHY, D. J. & SMYTH, G. K. 2010. edgeR: a Bioconductor package for differential expression analysis of digital gene expression data. *Bioinformatics,* 26**,** 139-40.

RODACKI, M., SVOREN, B., BUTTY, V., BESSE, W., LAFFEL, L., BENOIST, C. & MATHIS, D. 2007. Altered natural killer cells in type 1 diabetic patients. *Diabetes,* 56**,** 177-85.

ROHDE, E., MALISCHNIK, C., THALER, D., MAIERHOFER, T., LINKESCH, W., LANZER, G., GUELLY, C. & STRUNK, D. 2006. Blood monocytes mimic endothelial progenitor cells. *Stem cells,* 24**,** 357-67.

SCHIRALDI, M., RAUCCI, A., MUNOZ, L. M., LIVOTI, E., CELONA, B., VENEREAU, E., APUZZO, T., DE MARCHIS, F., PEDOTTI, M., BACHI, A., THELEN, M., VARANI, L., MELLADO, M., PROUDFOOT, A., BIANCHI, M. E. & UGUCCIONI, M. 2012. HMGB1 promotes recruitment of inflammatory cells to damaged tissues by forming a complex with CXCL12 and signaling via CXCR4. *Journal of Experimental Medicine,* 209**,** 551-63.

SCHRODER, S., PALINSKI, W. & SCHMID-SCHONBEIN, G. W. 1991. Activated monocytes and granulocytes, capillary nonperfusion, and neovascularization in diabetic retinopathy. *The American journal of pathology,* 139**,** 81-100.

SCHWAEBLE, W. J., STOVER, C. M., SCHALL, T. J., DAIRAGHI, D. J., TRINDER, P. K., LININGTON, C., IGLESIAS, A., SCHUBART, A., LYNCH, N. J., WEIHE, E. & SCHAFER, M. K. 1998. Neuronal expression of fractalkine in the presence and absence of inflammation. *FEBS letters,* 439**,** 203-7.

SEGAL, M. S., SHAH, R., AFZAL, A., PERRAULT, C. M., CHANG, K., SCHULER, A., BEEM, E., SHAW, L. C., LI CALZI, S., HARRISON, J. K., TRAN-SON-TAY, R. & GRANT, M. B. 2006. Nitric oxide cytoskeletal-induced alterations reverse the endothelial progenitor cell migratory defect associated with diabetes. *Diabetes,* 55**,** 102-9.

SERRA, A. M., WADDELL, J., MANIVANNAN, A., XU, H., COTTER, M. & FORRESTER, J. V. 2012. CD11b+ bone marrow-derived monocytes are the major leukocyte subset responsible for retinal capillary leukostasis in experimental diabetes in mouse and express high levels of CCR5 in the circulation. *The American journal of pathology,* 181**,** 719-27.

SMITH, L. I. 2002. A tutorial on principal components analysis.

SUBRAMANIAN, A., TAMAYO, P., MOOTHA, V. K., MUKHERJEE, S., EBERT, B. L., GILLETTE, M. A., PAULOVICH, A., POMEROY, S. L., GOLUB, T. R., LANDER, E. S. & MESIROV, J. P. 2005. Gene set enrichment analysis: a knowledge-based approach for interpreting genome-wide expression profiles. *Proceedings of the National Academy of Sciences of the United States of America,* 102**,** 15545-50.

SZKLARCZYK, D., FRANCESCHINI, A., WYDER, S., FORSLUND, K., HELLER, D., HUERTA-CEPAS, J., SIMONOVIC, M., ROTH, A., SANTOS, A., TSAFOU, K.

P., KUHN, M., BORK, P., JENSEN, L. J. & VON MERING, C. 2015. STRING v10: protein-protein interaction networks, integrated over the tree of life. *Nucleic Acids Research,* 43**,** D447-52.

TACKE, F., ALVAREZ, D., KAPLAN, T. J., JAKUBZICK, C., SPANBROEK, R., LLODRA, J., GARIN, A., LIU, J., MACK, M., VAN ROOIJEN, N., LIRA, S. A., HABENICHT, A. J. & RANDOLPH, G. J. 2007. Monocyte subsets differentially employ CCR2, CCR5, and CX3CR1 to accumulate within atherosclerotic plaques. *The Journal of clinical investigation,* 117**,** 185-94.

TAMURA, H., MIYAMOTO, K., KIRYU, J., MIYAHARA, S., KATSUTA, H., HIROSE, F., MUSASHI, K. & YOSHIMURA, N. 2005. Intravitreal injection of corticosteroid attenuates leukostasis and vascular leakage in experimental diabetic retina. *Investigative Ophthalmology and Visual Science,* 46**,** 1440-4.

TECILAZICH, F., DINH, T., PRADHAN-NABZDYK, L., LEAL, E., TELLECHEA, A., KAFANAS, A., GNARDELLIS, C., MAGARGEE, M. L., DEJAM, A., TOXAVIDIS, V., TIGGES, J. C., CARVALHO, E., LYONS, T. E. & VEVES, A. 2013. Role of endothelial progenitor cells and inflammatory cytokines in healing of diabetic foot ulcers. *PLoS One,* 8**,** e83314.

TESCH, G. H. 2007. Role of macrophages in complications of type 2 diabetes. *Clinical and experimental pharmacology & physiology,* 34**,** 1016-9.

TIRONE, M., TRAN, N. L., CERIOTTI, C., GORZANELLI, A., CANEPARI, M., BOTTINELLI, R., RAUCCI, A., DI MAGGIO, S., SANTIAGO, C., MELLADO, M., SACLIER, M., FRANCOIS, S., CARECCIA, G., HE, M., DE MARCHIS, F., CONTI, V., BEN LARBI, S., CUVELLIER, S., CASALGRANDI, M., PRETI, A., CHAZAUD, B., AL-ABED, Y., MESSINA, G., SITIA, G., BRUNELLI, S., BIANCHI, M. E. & VENEREAU, E. 2017. High mobility group box 1 orchestrates tissue

regeneration via CXCR4. *Journal of Experimental Medicine*.

TSUJIOKA, H., IMANISHI, T., IKEJIMA, H., KUROI, A., TAKARADA, S., TANIMOTO, T., KITABATA, H., OKOCHI, K., ARITA, Y., ISHIBASHI, K., KOMUKAI, K., KATAIWA, H., NAKAMURA, N., HIRATA, K., TANAKA, A. & AKASAKA, T. 2009. Impact of heterogeneity of human peripheral blood monocyte subsets on myocardial salvage in patients with primary acute myocardial infarction. *Journal of the American College of Cardiology,* 54**,** 130-8.

TUO, J., SMITH, B. C., BOJANOWSKI, C. M., MELETH, A. D., GERY, I., CSAKY, K. G., CHEW, E. Y. & CHAN, C. C. 2004. The involvement of sequence variation and expression of CX3CR1 in the pathogenesis of age-related macular degeneration. *FASEB journal : official publication of the Federation of American Societies for Experimental Biology*, 18**,** 1297-9.

VAN FURTH, R. 1989. Origin and turnover of monocytes and macrophages. *Current topics in pathology. Ergebnisse der Pathologie,* 79**,** 125-50.

VAN FURTH, R. & COHN, Z. A. 1968. The origin and kinetics of mononuclear phagocytes. *The Journal of experimental medicine,* 128**,** 415-35.

WANG, J., HOSSAIN, M., THANABALASURIAR, A., GUNZER, M., MEININGER, C. & KUBES, P. 2017. Visualizing the function and fate of neutrophils in sterile injury and repair. *Science,* 358**,** 111-116.

WILLIAMS, W. J. 1977. *Hematology,* New York, McGraw Hill.

WONG, S. L., DEMERS, M., MARTINOD, K., GALLANT, M., WANG, Y., GOLDFINE, A. B., KAHN, C. R. & WAGNER, D. D. 2015. Diabetes primes neutrophils to undergo NETosis, which impairs wound healing. *Nat Med,* 21**,** 815-9.

WOOLLARD, K. J. & GEISSMANN, F. 2010. Monocytes in atherosclerosis: subsets and functions. *Nat Rev Cardiol,* 7**,** 77-86.

YIPP, B. G. & KUBES, P. 2013. NETosis: how vital is it? *Blood,* 122**,** 2784-94.

YODER, M. C., MEAD, L. E., PRATER, D., KRIER, T. R., MROUEH, K. N., LI, F., KRASICH, R., TEMM, C. J., PRCHAL, J. T. & INGRAM, D. A. 2007. Redefining endothelial progenitor cells via clonal analysis and hematopoietic stem/progenitor cell principals. *Blood,* 109**,** 1801-9.

ZENG, H., QIN, L., ZHAO, D., TAN, X., MANSEAU, E. J., VAN HOANG, M., SENGER, D. R., BROWN, L. F., NAGY, J. A. & DVORAK, H. F. 2006. Orphan nuclear receptor TR3/Nur77 regulates VEGF-A-induced angiogenesis through its transcriptional activity. *Journal of Experimental Medicine,* 203**,** 719-29.

ZERBINI, G., MAESTRONI, A., PALINI, A., TREMOLADA, G., LATTANZIO, R., MAESTRONI, S., PASTORE, M. R., SECCHI, A., BONFANTI, R., GERHARDINGER, C. & LORENZI, M. 2012. Endothelial progenitor cells carrying monocyte markers are selectively abnormal in type 1 diabetic patients with early retinopathy. *Diabetes,* 61**,** 908-14.

ZHAO, C., TAN, Y. C., WONG, W. C., SEM, X., ZHANG, H., HAN, H., ONG, S. M., WONG, K. L., YEAP, W. H., SZE, S. K., KOURILSKY, P. & WONG, S. C. 2010. The CD14(+/low)CD16(+) monocyte subset is more susceptible to spontaneous and oxidant-induced apoptosis than the CD14(+)CD16(-) subset. *Cell death & disease,* 1**,** e95.

ZHAO, D., QIN, L., BOURBON, P. M., JAMES, L., DVORAK, H. F. & ZENG, H. 2011. Orphan nuclear transcription factor TR3/Nur77 regulates microvessel permeability by targeting endothelial nitric oxide synthase and destabilizing endothelial junctions. *Proceedings of the*

National Academy of Sciences of the United States of America, 108**,** 12066-71.

ZHENG, L., DU, Y., MILLER, C., GUBITOSI-KLUG, R. A., BALL, S., BERKOWITZ, B. A. & KERN, T. S. 2007. Critical role of inducible nitric oxide synthase in degeneration of retinal capillaries in mice with streptozotocin-induced diabetes. *Diabetologia,* 50**,** 1987-96.

ZIEGLER-HEITBROCK, L., ANCUTA, P., CROWE, S., DALOD, M., GRAU, V., HART, D. N., LEENEN, P. J., LIU, Y. J., MACPHERSON, G., RANDOLPH, G. J., SCHERBERICH, J., SCHMITZ, J., SHORTMAN, K., SOZZANI, S., STROBL, H., ZEMBALA, M., AUSTYN, J. M. & LUTZ, M. B. 2010. Nomenclature of monocytes and dendritic cells in blood. *Blood,* 116**,** e74-80.

TABLES

Table 1. Characteristics of the two principal monocyte subpopulations.

Table 2. A. Characteristics of study mice for the leukostasis experiments. *P=0.0001: vs. WT and Nr4a1$^{-/-}$. **B.** Characteristics of wild-type and Nr4a1-/- mice at 6, 14, and 18 months of age. Statistical analysis was performed with the unpaired t-test. **C.** Characteristics of wild-type and Nr4a1$^{-/-}$ mice after 4 months of diabetes. *P=0.05: vs. WT; **P<0.05: vs. Nr4a1$^{-/-}$; ***P<0.0001 vs. Nr4a1$^{-/-}$ and WT. **D.** Characteristics of wild-type and Nr4a1$^{-/-}$ mice after 6 months of diabetes. *P<0.0001 vs. WT-C and Nr4a1$^{-/-}$-C. C, control mice; DM, diabetic mice. Data are means ± SD. Statistical analysis was performed with ANOVA followed by Bonferroni's correction test.

Table 3. Characteristics of the mice used for the RNA experiments. C: controls; S-DM: short duration of diabetes; I-DM: intermediate duration of diabetes; L-DM long duration of diabetes; RIN: RNA integrity number; WBC: white blood cells. *P<0.0001 DM vc C; **P<0.0001 S-DM vs I-DM, L-DM; ***P<0.0001 L-DM vs S-DM, I-DM.

Table 4. Differentially expressed genes (DEGs) analyzed by RNA sequencing of three diabetic (D) mice vs three control (C) mice. FDR= false discovery rate.

Table 5. Differentially expressed genes (DEGs) from RNAsequencing clustered by gene function.

Table 6. Gene Set Ernrichment analysis (GSEA) performed on RNAsequencing data.

Table 7. Ingenuity Pathway analysis (IPA) performed on RNAsequencing data.

Table 8. Top 10 GO-Biological Processes identified by String program with corresponding genes. OGC: observed gene count. FDR: False Discovery Rate.

Table 1. Principal monocyte subsets in humans and rodents

Inflammatory		Patrollers	
Humans	Mouse	Humans	Mouse
$CD14^{hi}/CD16^{-}$	$Gr1^{+}/Ly\text{-}6C^{hi}$	$CD14^{lo}/CD16^{+}$	$Gr1^{-}/Ly\text{-}6c^{lo}$
Large size $CX3CR1^{lo}$ $CCR2^{+}$ $L\text{-}Selectin^{+}$ $LFA\text{-}1^{lo}$ $HLA\text{-}DR^{+}$ $FcγRIV^{-}$		Small size $CX3CR1^{hi}$ $CCR2^{-}$ $L\text{-}Selectin^{-}$ $LFA\text{-}1^{hi}$ $HLA\text{-}DR^{-}$ $FcγRIV^{+}$	

Table 2. Characteristics of experimental mice

A.

	n	Age at sacrifice (weeks)	Body weight at sacrifice (g)	Diabetes Duration (weeks)	Average Glucose throughout experiment	Glucose at sacrifice (mg/dl)	HbA1c at sacrifice (%)
WT	15	20 ± 6	31 ± 3	-	135 ± 15	130 ± 36	4.6 ± 0.3
WT + DM	10	21 ± 5	20 ± 3*	9 ± 6	544 ±39*	600 ± 0*	11.4 ± 1.6*
Nr4a1$^{-/-}$	6	21 ± 6	33 ± 5	-	151 ± 13	502 ± 85	4.3 ± 0.2
Nr4a1$^{-/-}$ + DM	5	23 ± 7	23 ± 2*	11 ± 4	544 ± 60*	524 ± 152*	11.8 ± 1.4*

B.

	n	Age (months)	Body weight (g)	Blood Glucose (mg/dl)	HbA1c (%)
WT	8	6 ± 1	39 ± 6	121 ± 18	4.8 ± 0.7
Nr4a1$^{-/-}$	8	6 ± 1	37 ± 5	106 ± 20	4.6 ± 0.3
WT	9	14 ± 1	40 ± 7	104 ± 17	4.4 ± 0.3
Nr4a1$^{-/-}$	9	14 ± 1	37 ± 6	110 ± 33	4.3 ± 0.2
WT	7	18 ± 0	41 ± 2	126 ± 26	4.6 ± 0.1
Nr4a1$^{-/-}$	7	18 ± 0	37± 1	95 ± 10	4.5 ± 0.2

C.

	n	Age (months)	Body weight (g)	Diabetes Duration (months)	Blood Glucose (mg/dl)	HbA1c (%)
WT-C	4	5 ± 1	34 ± 1	-	130 ± 19	4.4 ± 0.1
WT-DM	4	5 ± 1	25 ± 1*	4 ± 0	492 ± 76***	11.9 ± 1.2***
Nr4a1$^{-/-}$-C	4	6 ± 1	36 ± 7	-	105 ± 20	4.5 ± 0.4
Nr4a1$^{-/-}$-DM	4	5 ± 1	27 ± 3**	4 ± 0	424 ± 116***	11.1 ± 1.7***

D.

	n	Age (months)	Body weight (g)	Diabetes Duration (months)	Glucose (mg/dl)	HbA1c (%)
WT-C	19	10 ± 4	39 ± 7	-	111 ± 18	4.5 ± 0.5
WT-DM	6	7 ± 1	27 ± 1*	6 ± 0	554 ± 80*	12.2 ± 0.7*
Nr4a1$^{-/-}$-C	22	10 ± 4	38 ± 6	-	103 ± 28	4.5 ± 0.4
Nr4a1$^{-/-}$-DM	10	8 ± 1	26 ± 2*	6 ± 0	556 ± 93*	12.5 ± 1.0*

Table 3. Mice characteristics for RNA experiments

Mouse ID	Group	age (months)	DM duration (wks)	Glucose (mg/dl)	HbA1c (%)	WBC (per ml)	Blood (uL)	sorted PMo (#)	RIN
FT56-2	C	7		85	5	9,300	550	47408	9,7
FT51-3	C	8		104	4,3	5,300	500	27718	10,0
FT57-1	C	7		92	5	4,900	460	20945	9,6
FT57-2	C	7		92	4,7	6,700	440	28499	9,9
Jax4-0	C	7		82	5,3	8,300	350	25792	9,0
FT60-0	C	5				N/A	500	22600	8.8
Jax4-1	C	7		98	5	8,300	350	21948	9.3
ML219-1	C	10		73	4,3	4,100	500	48345	9,5
ML229-3	C	8		87	4,9	6,700	350	15372	N/A
FT56-0	I-DM	7	19**	432*	13*	5,000	500	24973	9,9
FT56-1	I-DM	7	19**	470*	13*	5,300	640	8344	8,3
FT55-1	I-DM	7	19**	422*	11,9*	3,100	650	7985	9,0
FT51-1	I-DM	8	19**	362*	11,9*	3,700	350	30306	10,0
Jax1-0	S-DM	5	10	337*	9,6*	4,600	460	50861	9,7
JAx1-3	S-DM	5	11	N/A	11,6*	4,500	250	7820	5,8
Jax2-0	S-DM	5	12	513*	11*	3,100	320	6255	7,9
Jax2-1	S-DM	5	11	310*	9,5*	4,700	350	32280	9,2
ML224-0	L-DM	9	28***	465*	14,2*	3,500	400	30488	9,1
ML224-1	L-DM	9	28***	438*	15*	3,400	730	9805	N/A
ML224-3	L-DM	9	28***	436*	14,7*	3,000	500	14915	8,2

Table 4. Differentially expressed genes (DEGs)

Name	Length	FT56-0 D1	FT55-1 D2	FT51-1 D3	FT56-2 C1	FT51-3 C2	FT57-1 C3	logFC	FDR
Ly6d	688	0	0	0	28,796	0,558	0,105	-10,733	9,87E-04
Gimap6	3254	0	0	0	24,820	3,905	0,210	-10,707	4,39E-05
Fcer2a	2970	0	0	0	27,540	0,101	0,000	-10,641	8,92E-03
Cd55	5068	0	0	0	22,978	0	1,261	-10,452	3,17E-03
Iglc2	604	0	0	0	19,839	0	0	-10,163	3,25E-02
Gimap4	1881	0	0	0	15,109	1,471	0,315	-9,932	5,06E-04
Tnfrsf13c	3532	0	0	0	14,649	0,355	0	-9,761	1,52E-02
Ccr7	1975	0	0	0	14,775	0	0	-9,738	4,99E-02
Trp53i11	3157	0	0	0	12,514	0	1,366	-9,649	9,15E-03
Iglc3	579	0	0	0	11,426	0,659	0	-9,449	1,85E-02
Gimap3	904	0	0	0	11,426	0,101	0	-9,381	3,78E-02
Niacr1	1937	0	0	0	1,256	6,136	4,152	-9,381	8,27E-05
Ebf1	9935	0	0	0	10,673	0,203	0,053	-9,305	2,05E-02
Fcrla	2259	0	0	0	8,413	1,116	0	-9,107	2,75E-02
Lef1	8641	0	0	0	8,706	0,406	0	-9,043	4,19E-02
Blnk	5974	0	0	0	8,329	0,761	0	-9,039	3,51E-02
Dhcr24	4019	0	0	0	1,590	5,274	2,102	-9,017	8,66E-04
Gmpr	1861	0	0	0	1,297	3,956	2,312	-8,773	3,25E-03
Ache	3962	0	0	0	2,762	2,130	2,628	-8,765	2,30E-03
Cd6	4077	0	0	0	4,520	0,964	1,104	-8,576	9,86E-03
Plxna3	7852	0	0	0	2,428	2,485	1,261	-8,481	7,30E-03
Rhbdf1	5288	0	0	0	4,144	1,014	0,420	-8,337	2,63E-02
Faim3	1844	0	0	0	19,671	0,101	0	-8,332	2,94E-02
Afap1l1	4033	0	0	0	2,469	2,586	0,368	-8,296	2,23E-02
Prrg1	10315	0	0	0	2,176	1,978	0,526	-8,084	2,76E-02
Galnt12	2683	0	0	0	1,465	1,116	1,892	-8,017	2,36E-02
Tcf7	4136	0	0	0,086	24,903	1,166	0,473	-7,976	9,91E-04
Xrcc5	2534	0	0	0	2,930	0,456	0,946	-7,974	3,99E-02
Cd28	6115	0	0	0	2,762	1,217	0,315	-7,961	4,31E-02
Prnp	2399	0	0	0	2,344	1,166	0,420	-7,834	4,61E-02
Tal1	4372	0	0	0	1,632	1,521	0,736	-7,818	3,67E-02
Scnn1g	2978	0	0,041	0,259	11,845	10,852	4,888	-6,411	1,32E-07
Igkc	322	0	0,455	0,735	97,353	0,558	0,841	-6,348	1,28E-02
Cxcr5	2612	0,101	0,041	0,086	18,709	0,051	0,315	-6,291	2,94E-02
Mrc2	6899	0	0	0,043	1,590	1,420	1,787	-6,289	3,99E-02
Tespa1	1740	0	0,124	0	4,771	0,659	2,260	-5,724	4,55E-02
Nanos1	3926	0	0,083	0,043	2,093	1,623	3,048	-5,524	2,94E-02
Prkcq	6732	0,101	0	0,086	5,190	0,862	2,102	-5,349	2,87E-02
Abhd14b	1573	0	0	0,303	2,469	3,296	5,361	-5,105	1,69E-02

Sdpr	3052	0,955	0,041	0,086	9,961	9,787	4,415	-4,484	4,37E-03
Cd33	2564	0	0,331	0,389	6,153	4,716	3,574	-4,275	8,02E-03
1110067 D22Rik	4275	0,050	0,496	0,562	2,846	4,615	6,307	-3,600	2,96E-02
Gp1bb	2489	3,218	0	1,340	11,510	19,118	14,663	-3,313	3,70E-02
Ube2c	2770	1,006	1,075	0,043	5,483	5,021	10,038	-3,265	4,53E-02
Egr1	5024	0,905	8,684	1,513	58,722	20,285	17,711	-3,118	3,76E-03
AU023871	2480	0,855	0,868	0,605	6,111	4,311	7,200	-2,911	1,63E-02
Ppbp	1077	17,097	2,192	6,355	51,397	67,549	57,337	-2,783	4,39E-05
Gp5	2194	5,531	1,323	2,075	27,331	17,344	11,667	-2,661	2,25E-03
Myl9	1210	13,979	1,406	2,464	28,335	40,265	34,476	-2,532	9,90E-03
Nab2	3470	2,866	0,496	2,940	10,380	15,416	8,882	-2,460	3,55E-02
Itga2b	5366	14,029	6,534	9,381	38,966	65,419	48,770	-2,356	1,02E-09
Alox12	3971	13,074	6,162	6,830	35,911	53,451	36,788	-2,277	8,71E-08
Mfsd2b	5675	2,213	6,782	1,902	16,239	20,640	15,871	-2,271	7,04E-03
Gp9	809	5,783	3,432	1,945	20,383	17,952	14,085	-2,233	2,98E-03
Pf4	583	12,420	1,820	6,268	30,219	35,803	29,115	-2,216	3,61E-03
Nrgn	1289	27,858	12,903	11,024	63,870	78,857	82,773	-2,124	1,63E-08
Clec4n	1561	1,659	3,887	3,631	15,570	13,337	7,673	-1,991	4,09E-02
Cd81	2225	34,143	39,204	19,151	126,735	119,174	90,393	-1,862	2,21E-10
Slc2a3	7010	3,118	7,072	7,695	22,434	16,025	25,489	-1,835	5,55E-03
Amz1	6713	14,633	17,038	14,223	53,364	38,592	57,284	-1,701	5,72E-08
Cyp51	3896	22,528	12,406	20,102	63,744	63,999	43,778	-1,641	2,07E-06
Abcb10	4293	8,699	7,402	3,199	20,634	19,930	17,448	-1,588	2,96E-02
Fdps	1223	14,482	18,320	16,557	44,910	65,013	35,369	-1,557	1,98E-05
Apbb1	2517	11,314	8,726	10,851	19,923	40,164	28,327	-1,517	2,73E-03
Ldlr	4707	90,915	40,776	117,890	254,976	260,559	187,671	-1,495	1,04E-04
Clu	3470	28,713	13,027	11,543	49,221	54,059	46,143	-1,489	1,76E-03
Tnf	2691	10,510	9,801	15,909	43,487	28,602	28,432	-1,472	1,76E-03
Sqle	6583	26,349	9,594	20,059	54,201	67,295	27,276	-1,410	2,11E-02
Tubb1	1402	20,717	23,324	6,658	57,424	40,418	32,373	-1,361	3,99E-02
Ctla2a	1368	39,876	15,632	19,497	59,475	70,591	59,439	-1,338	2,77E-03
Phlda3	1556	13,225	11,373	18,503	25,824	47,010	29,588	-1,248	1,52E-02
Cd24a	1811	8,297	9,801	8,603	17,704	19,321	25,594	-1,228	4,09E-02
Tspan17	1910	6,889	9,388	11,240	18,332	24,595	21,390	-1,223	4,74E-02
Cd40	3519	12,471	10,504	14,093	26,954	36,361	21,337	-1,191	2,22E-02
Sc4mol	7108	49,279	19,354	45,954	92,330	96,505	69,792	-1,175	8,02E-03
Mccc2	2213	14,080	22,042	26,673	33,944	51,321	49,927	-1,105	1,63E-02
Cd22	5557	39,323	19,726	34,757	48,467	97,114	54,394	-1,092	2,74E-02
Ets1	6411	83,020	59,096	96,231	208,811	140,168	158,083	-1,089	5,56E-05
Slamf9	1309	40,278	23,531	50,320	91,242	82,813	67,637	-1,083	4,12E-03
S100a11	508	47,067	48,592	56,935	111,583	99,345	108,157	-1,064	3,36E-07
Il1b	2017	69,695	48,633	96,231	118,950	146,507	170,486	-1,023	1,90E-03

Oxct1	3846	24,438	23,820	20,405	49,179	45,894	43,462	-1,013	2,77E-03
Spic	3907	25,897	20,057	22,610	35,744	61,159	40,257	-1,000	1,97E-02
Hp	1338	555,346	344,319	356,998	246,940	187,584	192,191	1,003	1,04E-04
Pcgf3	9670	62,454	49,212	43,966	25,029	25,153	26,277	1,025	1,76E-03
Cxcr4	2608	52,296	41,768	49,499	18,667	21,248	29,010	1,059	4,44E-03
Eif4e3	3988	21,824	37,054	28,489	13,059	16,126	12,403	1,071	4,33E-02
Map3k15	4319	53,805	66,333	34,066	28,503	26,624	17,816	1,079	1,64E-02
Hdgfrp3	9569	34,043	36,640	30,996	15,779	12,678	19,498	1,084	1,52E-02
Lyst	11757	128,528	129,192	147,330	72,073	70,997	43,883	1,115	1,45E-05
Mdm1	3134	597,837	575,574	562,257	283,856	243,976	233,867	1,188	5,33E-14
Rcn3	1590	28,763	38,749	23,172	13,142	11,917	9,092	1,408	3,35E-03
Syne2	25144	53,704	88,499	79,242	27,038	19,118	36,788	1,417	5,56E-05
Lyz1	1260	67,432	137,132	35,233	24,987	30,782	29,168	1,498	5,35E-03
Pbx1	13338	59,034	48,840	33,028	16,742	14,402	15,083	1,607	5,29E-06
Invs	11702	23,282	17,286	19,281	4,102	4,260	10,090	1,699	1,90E-02
RP23-127O4.4	3515	9,001	16,376	25,376	3,725	5,021	5,203	1,864	1,96E-02
Ddit4	1682	84,177	62,983	64,673	23,857	19,068	14,452	1,882	1,41E-11
4930506 M07Rik	4116	81,260	83,743	58,707	15,486	12,222	19,025	2,259	1,75E-16
Ifit2	4235	20,567	17,204	34,152	3,432	4,970	6,622	2,261	8,72E-05
Acpp	7778	15,186	13,895	6,571	1,967	1,116	4,257	2,279	3,79E-02
Fkbp5	8353	120,030	136,718	42,236	14,816	14,554	12,350	2,840	9,75E-13
Rims3	8265	78,495	119,308	65,105	1,842	8,215	10,196	3,701	7,28E-12
Slc37a2	6401	0,151	4,549	4,410	0,084	0	0,053	5,863	2,92E-02
Slc16a1	4421	2,967	6,865	1,081	0	0	0,158	6,025	5,93E-03
Ppp1r9a	14561	7,291	6,948	1,038	0	0	0,105	7,038	1,76E-04
Aldh1a3	4600	1,609	0,579	1,600	0	0	0	7,778	4,14E-02
Acot1	2025	1,307	1,075	1,513	0	0	0	7,819	3,32E-02
Cldn1	3243	2,213	1,530	1,340	0	0	0	8,201	1,51E-02
Tbc1d4	9921	5,129	1,323	0,086	0	0	0	8,562	3,59E-02
Angptl4	3850	5,028	3,846	0	0	0	0	9,003	2,82E-02
Pdk4	3500	5,883	6,989	0	0	0	0	9,539	7,04E-03
Clec4f	2549	38,568	0	0	0	0	0	11,120	2,10E-02

Table 5. Differentially expressed genes (DEGs) clustered by gene function.

Genes DOWN regulated in DM patrollers				
Gene	**LogFc**	**FC**	**FDR**	**Notes**
ANTI-INFLAMMATORY				
TNF	-1,47	-2,8	0,0012	TNFalfa. Pro-inflammatory.
IL1B	-1,022	-2,0	0,0019	Pro-inflammatory
CD40	-1,19	-2,3	0,022	TNF receptor
CD6	-8,58	-382,7	0,009	Mediates ischemia/reperfusion injury; Knock-outs have less IL6, hence anti-inflammatory. CD6 binds to ALCAM on other leukocytes (mainly CD19 lymphs) and activates them.
CD28	-7,96	-249,0	0,043	Is expressed in monos where it induces secretion of TNFalfa, IL4, IL2, IL10; Pro apoptotic.
Ppbp (aka CXCL7)	-2,78	-6,9	4E-05	Potent chemoattractant and activator of neutrophils.
PRKCQ (encodes PKC-θ)	-5,35	-40,8	0,028	Pro-inflamm as it increases IFN-γ, IL-2, IL-4, TNF-alfa, IL-6, IL-17. Treatment with PKC-θ inhibitor: (i) preserves tight junction integrity, (ii) reduces chemotaxis, and (iii) reduces inflammation.
EGR1	-3,11	-8,6	0,0037	Transcription factor: positive regulator of chemokyne biosynthesis. Increased expression during hypoxia. Pro-apoptotic (via p53), pro-inflammatory (IL-1b) and pro-atherosclerotic.
Clec4n (aka Dectin-2)	-1,99	-4,0	0,041	Membrane receptor; when stimulated initiates signaling that leads to the induction of cytokines
Niacr1	-9,38	-666,3	8E-05	Pro-apoptotic. Encodes GPR109a that increases secretion of PGE2 (vascular permeability) and PGD2. The gene expression is IFNgamma induced. Is the receptor for nicotinic acid (lipid lowering effect) and responsible for the flushing side effect. Shown also to possess anti-inflamamtory effects.
ACHE	-8,76	-433,5	0,0023	Acetylcholinesterase (catalyzes breakdown of Aceytlcholin). Its suppression is anti-apoptotic and anti-inflamm (by increase in acetylcholin levels)
NaNOS1	-5,52	-45,9	0,029	Nanos homolog 1. Expressed in macrophages derived from monos (more from CD16+ than CD14+). Nanos1 interfers with E-cadherin (reduces its proadhesive functions). E-cadherin has also antiinflammatory actions via activating PI3/akt pathway and suppressing NFkB, not known if Nanos1 interferes. Nanos1 also up-regulates the production of MMP14.
PF4 (aka CXCL4)	-2,21	-4,6	0,0036	angiostatic via (1) blocking VEGF and FGF; (2) displacing VEGF and FGF from their cognate receptors; (3) increasing CXCR3-B expression on EC; (4) by inhibiting pro-angiogeneic integrins. PF4 slows-down re-endothelialisation and inhibits intravascular neoangiogenesis (review 2010). PF4 facilitates monocyte differentiation to pro-inflammatory macrophages and increases the uptake and is pro-atherosclerotic via esterification of ox-LDL in lesional macrophages. PF4 upregulates IL4, 5, 13. PF4 is chemotactic and activator of PMN, and induces adhesion of PMN to EC (Bebawy paper) and is pro-inflammatory. PF4 regulates coagulation
CTLA2A	-1,34	-2,5	0,0027	Is a secreted protein, its expression is increased by IL4
Clu	-1,49	-2,8	0,0017	Pro-inflammatory by inducing NF-kappa-B expression and activity. Promotes apoptosis
ANTI-ADHESION				
CD81	-1.86	-3.6	2.1E-10	Reduces LFA-1 expression, therefore CD81 down-regulation results in increased LFA-1. CD81block reduces mono transmigr-reduces inflammation-ameliorates EAE. In addition mediates tight adhesion of leukocytes to EC (is associated to VLA4 that binds VCAM1).
ANGIOSTATIC				
PF4 (aka CXCL4)	-2,21	-4,6	0,0036	angiostatic via (1) blocking VEGF and FGF; (2) displacing VEGF and FGF from their cognate receptors; (3) increasing CXCR3-B expression on EC; (4) by inhibiting pro-angiogeneic integrins. PF4 slows-down re-endothelialisation and inhibits intravascular neoangiogenesis (review 2010). PF4 facilitates monocyte differentiation to pro-inflammatory macrophages and increases the uptake and is pro-atherosclerotic via esterification of ox-LDL in lesional macrophages. PF4 upregulates IL4, 5, 13. PF4 is chemotactic and activator of PMN, and induces adhesion of PMN to EC (Bebawy paper) and is pro-inflammatory. PF4 regulates coagulation
ANTI-APOPTOTIC				
Niacr1	-9,38	-666,3	8E-05	Pro-apoptotic. Encodes GPR109a that increases secretion of PGE2 (vascular permeability) and PGD2. The gene expression is IFNgamma induced. Is the receptor for nicotinic acid (lipid lowering effect) and responsible for the flushing side effect. Shown also to possess anti-inflamamtory effects.
ACHE	-8,76	-433,5	0,0023	acetylcholinesterase (catalyzes breakdown of Aceytlcholin). Its suppression is anti-apoptotic and anti-inflamm (by increase in acetylcholin levels)
CD28	-7,96	-249,0	0,043	Is expressed in monos where it induces secretion of TNFalfa, IL4, IL2, IL10; Pro apoptotic.
EGR1	-3,11	-8,6	0,0037	Transcription factor: positive regulator of chemokyne biosynthesis. Increased expression during hypoxia. Pro-apoptotic (via p53), pro-inflammatory (IL-1b) and pro-atherosclerotic.
NAB2	-2,46	-5,5	0,035	Transcriptional regulator NGFI-A binding protein 2. Is pro-apoptotic by activating TRAIL (TNF-related apoptosis inducing ligand)

Clu	-1,49	-2,8	0,0017	Proinflammatory by inducing NF-kappa-B expression and activity. Promotes apoptosis
Apbb1	-1,5	-2,8	0,0027	DNA damage; translocates to the nucleus and induces apoptosis by recruiting other pro-apoptosis factors such as MAPK8/JNK1
Clu	-1,49	-2,8	0,0017	Proinflammatory by inducing NF-kappa-B expression and activity. Promotes apoptosis
Phlda3	-1,25	-2,4	0,015	Pro-apoptotic, Mediates of hypoxia-induced p53-dependent apoptosis also by inhibiting AKT pro-survivor signaling
CD24a (aka CD24)	-1,23	-2,3	0,041	Pro-apoptotic
Ets1	-1,08	2,1	5E-05	Role in haematopoietic cell differentiation. PKC is a major regulator of Ets1. Conflicting data on role of Ets1 in apoptosis: Ets1-deficiency increases T-cells apoptosis and overexpression of Ets1 protects VSMCs from undergoing apoptosis (via p21 activation); on the other hand Ets1 is pro-apoptotic via p53, and stimulates expression of proapoptotic genes (such as bid).
Genes UP regulated in DM patrollers				
Gene	**LogFc**	**FC**	**FDR**	**Notes**
ANTI-INFLAMMATORY				
IFIT2 (aka isg54)	2,26	4,79	8,7E-05	inhibitory effects after infection; inhibits LPS-induced expression of tumor necrosis factor (TNF), interleukin-6 (IL-6) and CXCL2 (also known as MIP2), this effect was mediated post-ranscriptionally, possibly by affecting mRNA stability
Eif4e3	1,07	2,10	0,043	expressed in human peripheral mononuclear cells; inhibits Eif4e1 upregulation by HIF, and that results in increased NFkB. EIF4E3 represses target expression and oncogenic transformation, in direct contrast to EIF4E1, which stimulates these processes. EIF4E3 overexpression decreases expression of VEGF, c-Myc, Cyclin D1, and NBS1
Hp	1,003	2,00	0,0001	is a member of the acute phase plasma proteins. Is expressed in monos. It reduces expression of pro-inflamm cytokines by monos. In addition Hp 2-2 genotype (less efficient) associated with increased risk of CVD and retinopathy in DM patients
PRO-MIGRATORY/PRO-ADHEVIVE				
CXCR4	1,06	2,08	0,0044	positive regulator of chemotaxis and migration. Binding to SDF1 is pro-phagocytic signal
PPP1r9a	7,04	131,60	0,00018	encodes Neurabin I, mediator of repair post stroke (by Sigma-1R). NrbI targets PP1 activity to actin-rich structures in cultured cells to promote filopodia and disassemble the stress fiber network.
Claudin1	8,2	294,07	0,015	Expressed in Monos and increased by DM. Cldn 1 activates MMP2 (and MT-MMP1) which increases motility via enhanced responsee to CXCL12. Cldn is also anti-apoptotic (JCI, 2005). Possibly angiogenic via interaction with MMPs (Claudin 1 interacts direclty with MMPs). Claudin 1 also activates Notch signaling (directly and via MMPs) that is required for generation and formation of PMO; Notch signaling in Monos reduces IL-8.
Shootin1	2,26	4,79	1,8E-16	shootin1 is widely expressed: also in dendritic cells (myelo-monocitic lineage). Shootin1 promotes the polarization of migrating neurons. Twio isorms a (only neuronal) and b (also in other cells) acts as a clutch molecule to couple actin filaments and cell adhesions, thereby generating the force underlying these processes. Shootin accumulates at cell–cell contact sites of some epithelial cells, where it colocalizes with E-cadherin and the actin-binding protein cortactin. Also important is axonal growth.
VASCULO-PROTECTIVE				
ANGPTL4	9	512,00	0,028	Expressed in PBMC. is secreted. Hypoxia increases expression via HIF. Vasculoprotective. Promotes EC survival. Angptl4-/- mice have higher monos and neutrophils. Reduced levels causes increase atherosclerosis and leukocytes, and decreased leukocyte apoptosis. Protective anti-ischemia by increasing EC surface, blocking EC junctions breackdown, redcuing inflammation via reduction of ICAM on EC. Consistent reports on role in inbiting vascular permeability. Contradictory data on role in atherosclerosis).
RCN3	1,41	2.82	0.003	inhibition of several proteins in the endoplasmic or sarcoplasmic reticulum membrane. Increases activity and secretion of PACE4 (aka PCSK6) that is anti-apoptotic, and via CORIN activation is anti-hypertensive and cardioprotective. Corin deficiency leads to endothelial dysfunction and vascular remodeling.
ANTI-APOPTOTIC				
Claudin1	8,2	294,07	0,015	Expressed in Monos and increased by DM. Cldn 1 activates MMP2 (and MT-MMP1) which increases motility via enhanced responsee to CXCL12. Cldn is also anti-apoptotic (JCI, 2005). Possibly angiogenic via interaction with MMPs (Claudin 1 interacts direclty with MMPs). Claudin 1 also activates Notch signaling (directly and via MMPs) that is required for generation and formation of Pats (Nat comm, 2016); Notch signaling in Monos reduces IL-8. CHECK meaning of increase in claudin 1 by phorbol ester via PKC.
ddit4	1,88	3,68	1,4E-11	role in responses to cellular energy levels and cellular stress, including responses to hypoxia and DNA damage. It is a HIF-1 target gene. Inhibits mTOR apoptosis.
RCN3	1,41	2,82	0,0033	inhibition of several proteins in the endoplasmic or sarcoplasmic reticulum membrane. Increases activity and secretion of PACE4 (aka PCSK6) that is anti-apoptotic, and via CORIN activation is anti-hypertensive and cardioprotective. Corin deficiency leads to endothelial dysfunction and vascular remodeling.

Table 6. Gene Set Ernrichment analysis (GSEA)

	GS	SIZE	ES	NES	NOM p-val	FDR q-val	FWER p-val	RANK AT MAX
1	GSE10325_LUPUS_CD4_TCELL_VS_LUPUS_BCELL_UP	22	0,71	3,11	0,000	0,000	0,000	58
2	GO_REGULATION_OF_CELL_CELL_ADHESION	27	0,60	2,78	0,000	0,000	0,001	52
3	GO_LYMPHOCYTE_ACTIVATION	25	0,62	2,77	0,000	0,000	0,001	70
4	GO_POSITIVE_REGULATION_OF_IMMUNE_RESPONSE	24	0,60	2,74	0,000	0,000	0,001	48
5	GO_REGULATION_OF_HOMOTYPIC_CELL_CELL_ADHESION	24	0,59	2,70	0,000	0,000	0,001	52
6	GO_LEUKOCYTE_ACTIVATION	27	0,56	2,69	0,000	0,000	0,001	70
7	GO_LYMPHOCYTE_DIFFERENTIATION	18	0,65	2,69	0,000	0,000	0,001	66
8	GO_ACTIVATION_OF_IMMUNE_RESPONSE	18	0,65	2,69	0,000	0,000	0,001	48
9	GO_REGULATION_OF_IMMUNE_RESPONSE	35	0,52	2,67	0,000	0,000	0,001	70
10	GSE22886_NAIVE_TCELL_VS_NKCELL_UP	16	0,67	2,64	0,000	0,000	0,002	58
11	GO_REGULATION_OF_CELL_ADHESION	34	0,53	2,64	0,000	0,000	0,002	55
12	GO_ANTIGEN_RECEPTOR_MEDIATED_SIGNALING_PATHWAY	16	0,66	2,63	0,000	0,000	0,002	48
13	GO_IMMUNE_SYSTEM_DEVELOPMENT	23	0,59	2,63	0,000	0,000	0,002	66
14	GO_LEUKOCYTE_CELL_CELL_ADHESION	18	0,63	2,61	0,000	0,000	0,002	70
15	GO_POSITIVE_REGULATION_OF_CELL_ADHESION	23	0,57	2,54	0,000	0,000	0,004	55
16	GO_IMMUNE_RESPONSE_REGULATING_CELL_SURFACE_RECEPTOR_SIGNALING_PATHWAY	17	0,63	2,54	0,000	0,000	0,004	48
17	GO_LEUKOCYTE_DIFFERENTIATION	22	0,57	2,52	0,000	0,000	0,004	66
18	GO_REGULATION_OF_CELL_ACTIVATION	35	0,49	2,50	0,000	0,000	0,006	84
19	GO_POSITIVE_REGULATION_OF_CELL_CELL_ADHESION	19	0,59	2,46	0,000	0,001	0,010	48
20	SMID_BREAST_CANCER_NORMAL_LIKE_UP	36	0,48	2,46	0,000	0,001	0,010	58
21	GSE22886_NAIVE_TCELL_VS_MONOCYTE_UP	18	0,59	2,45	0,000	0,000	0,010	77
22	GO_CELL_ACTIVATION	30	0,50	2,43	0,000	0,001	0,017	70
23	GO_POSITIVE_REGULATION_OF_CELL_ACTIVATION	29	0,50	2,41	0,000	0,001	0,024	84
24	GO_REGULATION_OF_IMMUNE_SYSTEM_PROCESS	55	0,42	2,40	0,000	0,001	0,025	54
25	SANSOM_APC_TARGETS_DN	16	0,61	2,39	0,000	0,001	0,025	51
26	GSE3982_MEMORY_CD4_TCELL_VS_BCELL_UP	21	0,55	2,38	0,000	0,001	0,031	67
27	GSE10325_LUPUS_CD4_TCELL_VS_LUPUS_MYELOID_UP	19	0,57	2,37	0,000	0,001	0,032	58
28	GSE22886_CD4_TCELL_VS_BCELL_NAIVE_UP	15	0,59	2,31	0,000	0,002	0,048	58
29	GO_IMMUNE_RESPONSE	44	0,42	2,31	0,000	0,002	0,051	50
30	KUMAR_TARGETS_OF_MLL_AF9_FUSION	39	0,44	2,30	0,001	0,002	0,051	126
31	GO_IMMUNE_SYSTEM_PROCESS	74	0,36	2,25	0,000	0,003	0,078	58
32	GO_CELL_CELL_ADHESION	30	0,46	2,24	0,000	0,003	0,085	70
33	GSE4748_CYANOBACTERIUM_LPSLIKE_VS_LPS_AND_CYANOBACTERIUM_LPSLIKE_STIM_DC_3H_UP	16	0,57	2,23	0,000	0,003	0,100	51
34	GO_REGULATION_OF_CYTOKINE_PRODUCTION	22	0,51	2,22	0,000	0,003	0,103	86
35	WALLACE_PROSTATE_CANCER_RACE_UP	24	0,47	2,22	0,002	0,003	0,107	58
36	GO_POSITIVE_REGULATION_OF_IMMUNE_SYSTEM_PROCESS	43	0,42	2,20	0,000	0,004	0,126	84
37	GO_BIOLOGICAL_ADHESION	49	0,39	2,19	0,000	0,004	0,133	87
38	GSE10325_CD4_TCELL_VS_BCELL_UP	17	0,54	2,17	0,000	0,005	0,157	58
39	GSE22886_NAIVE_CD4_TCELL_VS_MONOCYTE_UP	19	0,51	2,15	0,000	0,006	0,198	58
40	GSE22886_NAIVE_CD8_TCELL_VS_MONOCYTE_UP	23	0,48	2,11	0,000	0,008	0,269	58
41	HADDAD_B_LYMPHOCYTE_PROGENITOR	17	0,52	2,09	0,001	0,009	0,294	106
42	JAATINEN_HEMATOPOIETIC_STEM_CELL_DN	19	0,50	2,08	0,000	0,009	0,323	58
43	GO_PROTEIN_COMPLEX_BIOGENESIS	20	0,48	2,04	0,001	0,013	0,421	90
44	GO_PROTEIN_COMPLEX_ASSEMBLY	20	0,48	2,04	0,001	0,013	0,439	90
45	GSE16266_LPS_VS_HEATSHOCK_AND_LPS_STIM_MEF_UP	15	0,51	2,03	0,004	0,014	0,474	37
46	GO_SINGLE_ORGANISM_CELL_ADHESION	25	0,44	2,02	0,000	0,014	0,485	84

47	GSE32901_NAIVE_VS_TH17_NEG_CD4_TCELL_UP	15	0,52	2,01	0,004	0,015	0,515	55
48	GSE3039_ALPHAALPHA_VS_ALPHABETA_CD8_TCELL_DN	22	0,45	2,01	0,002	0,015	0,527	92
49	REACTOME_IMMUNE_SYSTEM	23	0,44	1,99	0,001	0,017	0,565	48
50	GSE23568_CTRL_TRANSDUCED_VS_WT_CD8_TCELL_DN	16	0,50	1,98	0,004	0,019	0,612	51
51	GO_POSITIVE_REGULATION_OF_RESPONSE_TO_STIMULUS	55	0,34	1,96	0,002	0,021	0,666	50
52	MARSON_BOUND_BY_FOXP3_UNSTIMULATED	25	0,42	1,93	0,006	0,027	0,754	83
53	GO_MACROMOLECULAR_COMPLEX_ASSEMBLY	21	0,44	1,92	0,005	0,029	0,780	90
54	ZHOU_INFLAMMATORY_RESPONSE_LPS_UP	15	0,49	1,90	0,008	0,032	0,814	111
55	KIM_ALL_DISORDERS_CALB1_CORR_UP	16	0,47	1,89	0,005	0,034	0,841	87
56	MCLACHLAN_DENTAL_CARIES_UP	16	0,46	1,87	0,010	0,039	0,878	50
57	GSE20715_0H_VS_24H_OZONE_TLR4_KO_LUNG_UP	16	0,46	1,85	0,006	0,044	0,910	58
58	GO_REGULATION_OF_CELL_DEATH	45	0,34	1,83	0,006	0,049	0,935	170
59	GSE3039_NKT_CELL_VS_ALPHAALPHA_CD8_TCELL_DN	22	0,41	1,81	0,011	0,059	0,965	73
60	GO_POSITIVE_REGULATION_OF_CYTOKINE_PRODUCTION	16	0,45	1,80	0,016	0,061	0,969	82
61	GO_RESPONSE_TO_HORMONE	19	0,43	1,80	0,004	0,060	0,970	43
62	CASORELLI_ACUTE_PROMYELOCYTIC_LEUKEMIA_DN	15	0,46	1,78	0,012	0,067	0,982	69
63	GSE10325_BCELL_VS_MYELOID_UP	17	0,44	1,78	0,010	0,068	0,985	91
64	GSE24142_EARLY_THYMIC_PROGENITOR_VS_DN2_THYMOCYTE_DN	16	0,45	1,77	0,016	0,071	0,988	58
65	GO_PROTEIN_COMPLEX_SUBUNIT_ORGANIZATION	24	0,39	1,77	0,017	0,070	0,988	110
66	SMID_BREAST_CANCER_LUMINAL_B_DN	39	0,33	1,76	0,006	0,075	0,990	58
67	GO_KINASE_BINDING	24	0,38	1,76	0,012	0,074	0,990	150
68	GO_REGULATION_OF_ORGANELLE_ORGANIZATION	32	0,35	1,75	0,012	0,075	0,992	121
69	GO_NEGATIVE_REGULATION_OF_CELL_DEATH	30	0,37	1,75	0,016	0,076	0,993	64
70	ZHENG_BOUND_BY_FOXP3	22	0,40	1,74	0,018	0,079	0,996	58
71	GSE4984_UNTREATED_VS_GALECTIN1_TREATED_DC_DN	17	0,44	1,73	0,021	0,086	0,999	91
72	GSE21546_WT_VS_SAP1A_KO_AND_ELK1_KO_ANTI_CD3_STIM_DP_THYMOCYTES_DN	17	0,42	1,73	0,017	0,085	0,999	85
73	GO_CELL_SURFACE	45	0,32	1,72	0,016	0,090	1,000	101
74	REACTOME_ADAPTIVE_IMMUNE_SYSTEM	19	0,41	1,69	0,023	0,102	1,000	48
75	GSE24142_EARLY_THYMIC_PROGENITOR_VS_DN3_THYMOCYTE_DN	17	0,42	1,68	0,017	0,108	1,000	58
76	GO_IMMUNE_EFFECTOR_PROCESS	17	0,42	1,68	0,023	0,111	1,000	50
77	GO_DEFENSE_RESPONSE	37	0,32	1,68	0,021	0,109	1,000	37
78	GSE29618_BCELL_VS_MONOCYTE_DAY7_FLU_VACCINE_UP	18	0,41	1,67	0,025	0,112	1,000	91
79	GO_IDENTICAL_PROTEIN_BINDING	22	0,38	1,65	0,036	0,123	1,000	73
80	POOLA_INVASIVE_BREAST_CANCER_UP	17	0,40	1,64	0,036	0,135	1,000	50
81	GO_NEGATIVE_REGULATION_OF_PROTEIN_METABOLIC_PROCESS	28	0,35	1,63	0,033	0,136	1,000	167
82	GSE11057_PBMC_VS_MEM_CD4_TCELL_DN	15	0,42	1,63	0,039	0,139	1,000	48
83	GO_NEGATIVE_REGULATION_OF_MOLECULAR_FUNCTION	25	0,36	1,61	0,022	0,152	1,000	167
84	MARSON_BOUND_BY_FOXP3_STIMULATED	19	0,39	1,61	0,050	0,153	1,000	57
85	GO_ENZYME_BINDING	41	0,30	1,60	0,049	0,158	1,000	90
86	TARTE_PLASMA_CELL_VS_PLASMABLAST_UP	17	0,40	1,60	0,053	0,160	1,000	155
87	ACEVEDO_METHYLATED_IN_LIVER_CANCER_DN	16	0,40	1,58	0,040	0,174	1,000	179
88	BOSCO_TH1_CYTOTOXIC_MODULE	17	0,38	1,57	0,045	0,189	1,000	122
89	GSE7218_UNSTIM_VS_ANTIGEN_STIM_THROUGH_IGG_BCELL_DN	17	0,38	1,56	0,048	0,191	1,000	33
90	GO_RESPONSE_TO_ABIOTIC_STIMULUS	21	0,36	1,56	0,044	0,189	1,000	155
91	GO_RESPONSE_TO_EXTERNAL_STIMULUS	54	0,27	1,55	0,040	0,197	1,000	104
92	GO_TRANSMEMBRANE_RECEPTOR_PROTEIN_TYROSINE_KINASE_SIGNALING_PATHWAY	16	0,39	1,55	0,059	0,197	1,000	37
93	GO_EXTERNAL_SIDE_OF_PLASMA_MEMBRANE	25	0,34	1,54	0,031	0,202	1,000	48
94	GSE24142_EARLY_THYMIC_PROGENITOR_VS_DN2_THYMOCYTE_ADULT_DN	16	0,39	1,54	0,056	0,202	1,000	58

95	GO_NEGATIVE_REGULATION_OF_GENE_EXPRESSION	29	0,32	1,54	0,040	0,201	1,000	104
96	GO_ENZYME_LINKED_RECEPTOR_PROTEIN_SIGNALING_PATHWAY	21	0,35	1,53	0,053	0,212	1,000	37
97	GO_NEGATIVE_REGULATION_OF_CATALYTIC_ACTIVITY	21	0,35	1,53	0,049	0,210	1,000	167
98	GSE16450_IMMATURE_VS_MATURE_NEURON_CELL_LINE_12H_IFNA_STIM_UP	15	0,39	1,53	0,068	0,209	1,000	87
99	GO_REGULATION_OF_CELL_PROLIFERATION	48	0,28	1,52	0,057	0,215	1,000	90
100	GO_SIDE_OF_MEMBRANE	29	0,32	1,52	0,051	0,219	1,000	48
101	GO_PLASMA_MEMBRANE_PROTEIN_COMPLEX	17	0,38	1,52	0,055	0,217	1,000	147
102	GO_POSITIVE_REGULATION_OF_ORGANELLE_ORGANIZATION	21	0,35	1,51	0,065	0,220	1,000	121
103	YANG_BCL3_TARGETS_UP	15	0,39	1,50	0,063	0,228	1,000	104
104	RUTELLA_RESPONSE_TO_CSF2RB_AND_IL4_UP	15	0,39	1,50	0,064	0,228	1,000	86
105	GO_CHEMICAL_HOMEOSTASIS	21	0,35	1,49	0,083	0,236	1,000	209
106	GO_HOMEOSTATIC_PROCESS	31	0,31	1,49	0,078	0,235	1,000	54
107	GRAESSMANN_APOPTOSIS_BY_DOXORUBICIN_DN	29	0,31	1,49	0,071	0,236	1,000	144
108	GSE4590_LARGE_PRE_BCELL_VS_VPREB_POS_LARGE_PRE_BCELL_DN	15	0,38	1,49	0,072	0,237	1,000	77
109	GSE33374_CD8_ALPHAALPHA_VS_ALPHABETA_CD161_HIGH_TCELL_DN	15	0,39	1,48	0,054	0,240	1,000	150
110	GO_REGULATION_OF_RESPONSE_TO_EXTERNAL_STIMULUS	29	0,31	1,48	0,062	0,244	1,000	163
111	GO_REGULATION_OF_HOMEOSTATIC_PROCESS	16	0,36	1,47	0,078	0,246	1,000	163
112	GSE29618_BCELL_VS_MONOCYTE_UP	17	0,36	1,46	0,077	0,258	1,000	36
113	CUI_TCF21_TARGETS_2_DN	28	0,30	1,46	0,107	0,263	1,000	167
114	GO_INNATE_IMMUNE_RESPONSE	15	0,38	1,46	0,080	0,260	1,000	21
115	GO_POSITIVE_REGULATION_OF_BIOSYNTHETIC_PROCESS	39	0,28	1,45	0,071	0,263	1,000	104
116	GO_NEGATIVE_REGULATION_OF_CELLULAR_COMPONENT_ORGANIZATION	16	0,37	1,45	0,076	0,266	1,000	150
117	GO_RESPONSE_TO_ENDOGENOUS_STIMULUS	27	0,31	1,44	0,083	0,271	1,000	104
118	GO_NEGATIVE_REGULATION_OF_RESPONSE_TO_STIMULUS	41	0,27	1,44	0,077	0,274	1,000	158
119	GO_REGULATION_OF_PROTEOLYSIS	16	0,37	1,44	0,091	0,275	1,000	84
120	GO_REGULATION_OF_DEFENSE_RESPONSE	18	0,35	1,42	0,099	0,292	1,000	82
121	GO_REGULATION_OF_CELL_CYCLE	19	0,34	1,42	0,089	0,293	1,000	104
122	GO_CELLULAR_RESPONSE_TO_ENDOGENOUS_STIMULUS	17	0,35	1,42	0,114	0,295	1,000	104
123	GSE22886_NAIVE_BCELL_VS_MONOCYTE_UP	16	0,36	1,42	0,112	0,293	1,000	91
124	GO_REGULATION_OF_KINASE_ACTIVITY	19	0,34	1,41	0,091	0,304	1,000	167
125	GO_REGULATION_OF_TRANSFERASE_ACTIVITY	21	0,32	1,41	0,100	0,305	1,000	167
126	GO_REGULATION_OF_RESPONSE_TO_WOUNDING	15	0,36	1,41	0,091	0,305	1,000	180
127	GO_CELLULAR_RESPONSE_TO_CYTOKINE_STIMULUS	24	0,31	1,40	0,110	0,313	1,000	149
128	GO_CELLULAR_RESPONSE_TO_LIPID	15	0,36	1,39	0,112	0,330	1,000	104
129	GO_SIGNALING_RECEPTOR_ACTIVITY	42	0,26	1,38	0,108	0,330	1,000	65
130	GO_REGULATION_OF_PROTEIN_LOCALIZATION	29	0,29	1,38	0,124	0,336	1,000	103
131	KAECH_DAY15_EFF_VS_MEMORY_CD8_TCELL_UP	17	0,34	1,37	0,118	0,338	1,000	23
132	VERHAAK_AML_WITH_NPM1_MUTATED_DN	19	0,33	1,37	0,137	0,336	1,000	109
133	GO_GUANYL_NUCLEOTIDE_BINDING	16	0,34	1,37	0,122	0,341	1,000	75
134	GO_DEFENSE_RESPONSE_TO_OTHER_ORGANISM	15	0,36	1,37	0,130	0,345	1,000	37
135	GO_CELLULAR_CHEMICAL_HOMEOSTASIS	15	0,34	1,36	0,134	0,350	1,000	199
136	GO_CELLULAR_LIPID_METABOLIC_PROCESS	20	0,32	1,35	0,119	0,358	1,000	146
137	GO_CELLULAR_HOMEOSTASIS	15	0,34	1,35	0,130	0,359	1,000	199
138	CHICAS_RB1_TARGETS_SENESCENT	15	0,35	1,35	0,118	0,359	1,000	181
139	BOYLAN_MULTIPLE_MYELOMA_C_D_DN	20	0,32	1,34	0,127	0,366	1,000	82
140	GO_RESPONSE_TO_NITROGEN_COMPOUND	18	0,32	1,34	0,144	0,373	1,000	104
141	DELYS_THYROID_CANCER_UP	18	0,32	1,32	0,153	0,399	1,000	157
142	GO_FOREBRAIN_DEVELOPMENT	15	0,34	1,32	0,148	0,399	1,000	90

143	FOSTER_TOLERANT_MACROPHAGE_DN	15	0,34	1,32	0,159	0,401	1,000	126
144	GO_CELLULAR_RESPONSE_TO_ORGANIC_SUBSTANCE	46	0,24	1,31	0,155	0,403	1,000	104
145	DIAZ_CHRONIC_MEYLOGENOUS_LEUKEMIA_UP	15	0,33	1,30	0,176	0,418	1,000	54
146	GO_MEMBRANE_PROTEIN_COMPLEX	21	0,30	1,30	0,170	0,421	1,000	147
147	GO_MEMBRANE_MICRODOMAIN	15	0,34	1,29	0,166	0,429	1,000	168
148	GO_PROTEOLYSIS	22	0,29	1,29	0,180	0,429	1,000	194
149	JAEGER_METASTASIS_DN	16	0,33	1,29	0,177	0,431	1,000	143
150	GO_CELLULAR_RESPONSE_TO_OXYGEN_CONTAINING_COMPOUND	21	0,30	1,29	0,183	0,428	1,000	104
151	GO_RECEPTOR_BINDING	47	0,23	1,29	0,178	0,426	1,000	104
152	GO_RECEPTOR_ACTIVITY	63	0,22	1,28	0,174	0,436	1,000	57
153	GO_RESPONSE_TO_EXTRACELLULAR_STIMULUS	18	0,31	1,28	0,177	0,439	1,000	155
154	GO_RNA_POLYMERASE_II_TRANSCRIPTION_FACTOR_ACTIVITY_SEQUENCE_SPECIFIC_DNA_BINDING	16	0,33	1,27	0,191	0,445	1,000	99
155	GO_RESPONSE_TO_BACTERIUM	20	0,30	1,27	0,186	0,444	1,000	23
156	GO_POSITIVE_REGULATION_OF_GENE_EXPRESSION	37	0,25	1,27	0,179	0,443	1,000	104
157	GO_RESPONSE_TO_CYTOKINE	25	0,28	1,27	0,197	0,447	1,000	149
158	GO_SIGNAL_TRANSDUCER_ACTIVITY	50	0,23	1,26	0,200	0,456	1,000	170
159	GO_RESPONSE_TO_BIOTIC_STIMULUS	27	0,27	1,26	0,192	0,456	1,000	37
160	GO_KINASE_ACTIVITY	20	0,29	1,25	0,195	0,465	1,000	94
161	GO_POSITIVE_REGULATION_OF_ESTABLISHMENT_OF_PROTEIN_LOCALIZATION	16	0,31	1,25	0,203	0,473	1,000	103
162	ZWANG_TRANSIENTLY_UP_BY_2ND_EGF_PULSE_ONLY	32	0,25	1,24	0,201	0,482	1,000	135
163	SENESE_HDAC3_TARGETS_UP	16	0,31	1,24	0,211	0,481	1,000	88
164	MASSARWEH_TAMOXIFEN_RESISTANCE_UP	17	0,31	1,23	0,219	0,488	1,000	190
165	DODD_NASOPHARYNGEAL_CARCINOMA_UP	51	0,22	1,23	0,208	0,485	1,000	75
166	GO_MACROMOLECULAR_COMPLEX_BINDING	41	0,23	1,23	0,222	0,493	1,000	137
167	GO_SMALL_MOLECULE_BIOSYNTHETIC_PROCESS	15	0,32	1,22	0,229	0,494	1,000	155
168	GO_PROTEIN_KINASE_ACTIVITY	17	0,30	1,21	0,232	0,509	1,000	77
169	ONDER_CDH1_TARGETS_2_DN	22	0,27	1,21	0,230	0,514	1,000	153
170	GO_SMALL_MOLECULE_METABOLIC_PROCESS	34	0,24	1,21	0,232	0,512	1,000	158
171	GO_NEURON_DIFFERENTIATION	27	0,25	1,21	0,235	0,511	1,000	155
172	GO_SEQUENCE_SPECIFIC_DNA_BINDING	19	0,29	1,20	0,243	0,520	1,000	99
173	VECCHI_GASTRIC_CANCER_EARLY_DN	16	0,30	1,20	0,257	0,520	1,000	19
174	GO_POSITIVE_REGULATION_OF_PROTEIN_METABOLIC_PROCESS	33	0,24	1,20	0,245	0,522	1,000	121
175	GO_REGULATION_OF_PHOSPHORUS_METABOLIC_PROCESS	43	0,22	1,19	0,279	0,532	1,000	167
176	GO_RESPONSE_TO_LIPID	26	0,25	1,19	0,249	0,533	1,000	170
177	GO_TRANSFERASE_ACTIVITY_TRANSFERRING_PHOSPHORUS_CONTAINING_GROUPS	21	0,28	1,19	0,242	0,531	1,000	94
178	GO_NEGATIVE_REGULATION_OF_PROTEIN_MODIFICATION_PROCESS	16	0,30	1,19	0,240	0,532	1,000	119
179	GO_CELL_CYCLE	20	0,28	1,19	0,254	0,530	1,000	99
180	GO_PROTEIN_DIMERIZATION_ACTIVITY	30	0,24	1,17	0,285	0,557	1,000	56
181	GO_POSITIVE_REGULATION_OF_TRANSCRIPTION_FROM_RNA_POLYMERASE_II_PROMOTER	22	0,27	1,17	0,271	0,559	1,000	104
182	NABA_MATRISOME	27	0,25	1,16	0,295	0,569	1,000	242
183	CHEN_METABOLIC_SYNDROM_NETWORK	38	0,22	1,16	0,289	0,571	1,000	98
184	GO_REGULATION_OF_PROTEIN_MODIFICATION_PROCESS	40	0,22	1,16	0,275	0,572	1,000	167
185	GO_NEGATIVE_REGULATION_OF_TRANSPORT	15	0,30	1,15	0,301	0,581	1,000	138
186	GO_REGULATION_OF_PROTEIN_SECRETION	20	0,26	1,15	0,293	0,584	1,000	84
187	GO_PROTEIN_HOMODIMERIZATION_ACTIVITY	16	0,29	1,15	0,293	0,583	1,000	73
188	GSE8921_UNSTIM_VS_TLR1_2_STIM_MONOCYTE_24H_UP	15	0,29	1,15	0,290	0,580	1,000	48
189	SENGUPTA_NASOPHARYNGEAL_CARCINOMA_DN	20	0,27	1,14	0,313	0,588	1,000	119
190	YOSHIMURA_MAPK8_TARGETS_UP	45	0,21	1,14	0,311	0,592	1,000	148
191	GO_REGULATION_OF_TRANSCRIPTION_FROM_RNA_POLYMERASE_II_PROMOTER	30	0,24	1,14	0,311	0,590	1,000	104
192	GO_ORGANIC_ACID_METABOLIC_PROCESS	20	0,27	1,14	0,300	0,589	1,000	111

193	GO_MEMBRANE_ORGANIZATION	28	0,24	1,13	0,305	0,592	1,000	84
194	GO_LIPID_METABOLIC_PROCESS	25	0,25	1,13	0,303	0,597	1,000	155
195	GO_NEGATIVE_REGULATION_OF_CELL_COMMUNICATION	38	0,21	1,12	0,316	0,610	1,000	167
196	SCHUETZ_BREAST_CANCER_DUCTAL_INVASIVE_UP	22	0,25	1,11	0,342	0,629	1,000	184
197	KRAS.600.LUNG.BREAST_UP.V1_DN	15	0,29	1,11	0,328	0,629	1,000	169
198	GRAESSMANN_RESPONSE_TO_MC_AND_DOXORUBICIN_UP	15	0,28	1,10	0,350	0,644	1,000	8
199	GO_TAXIS	16	0,27	1,09	0,348	0,664	1,000	133
200	GO_ENZYME_REGULATOR_ACTIVITY	15	0,28	1,08	0,367	0,666	1,000	98
201	MATSUDA_NATURAL_KILLER_DIFFERENTIATION	23	0,24	1,08	0,351	0,675	1,000	107
202	GO_POSITIVE_REGULATION_OF_CELL_COMMUNICATION	34	0,21	1,07	0,384	0,685	1,000	50
203	SHEDDEN_LUNG_CANCER_GOOD_SURVIVAL_A12	16	0,27	1,07	0,384	0,683	1,000	179
204	DURAND_STROMA_S_UP	19	0,25	1,06	0,377	0,693	1,000	119
205	GO_RESPONSE_TO_OXYGEN_CONTAINING_COMPOUND	36	0,21	1,06	0,395	0,698	1,000	104
206	KOINUMA_TARGETS_OF_SMAD2_OR_SMAD3	20	0,25	1,06	0,374	0,695	1,000	172
207	GO_RECEPTOR_MEDIATED_ENDOCYTOSIS	19	0,26	1,05	0,380	0,711	1,000	21
208	GO_PROTEIN_LOCALIZATION	32	0,22	1,05	0,398	0,711	1,000	84
209	GO_TISSUE_DEVELOPMENT	46	0,19	1,05	0,405	0,710	1,000	172
210	GO_POSITIVE_REGULATION_OF_MULTICELLULAR_ORGANISMAL_PROCESS	50	0,18	1,05	0,426	0,708	1,000	90
211	GO_POSITIVE_REGULATION_OF_TRANSPORT	33	0,21	1,05	0,397	0,707	1,000	138
212	GSE20366_TREG_VS_NAIVE_CD4_TCELL_DN	16	0,26	1,04	0,403	0,711	1,000	75
213	FORTSCHEGGER_PHF8_TARGETS_DN	15	0,27	1,04	0,390	0,709	1,000	224
214	GO_EXTRACELLULAR_SPACE	32	0,21	1,04	0,418	0,709	1,000	242
215	GO_CIRCULATORY_SYSTEM_DEVELOPMENT	19	0,25	1,04	0,428	0,713	1,000	155
216	PUJANA_BRCA1_PCC_NETWORK	18	0,25	1,03	0,419	0,716	1,000	102
217	GSE14699_NAIVE_VS_DELETIONAL_TOLERANCE_CD8_TCELL_DN	16	0,26	1,03	0,416	0,714	1,000	77
218	SMID_BREAST_CANCER_BASAL_UP	25	0,23	1,03	0,425	0,724	1,000	177
219	GO_NEGATIVE_REGULATION_OF_NITROGEN_COMPOUND_METABOLIC_PROCESS	28	0,22	1,03	0,433	0,721	1,000	104
220	LINDGREN_BLADDER_CANCER_CLUSTER_2B	15	0,27	1,02	0,427	0,731	1,000	151
221	GO_CARDIOVASCULAR_SYSTEM_DEVELOPMENT	19	0,25	1,02	0,444	0,735	1,000	155
222	GO_POSITIVE_REGULATION_OF_CELL_PROLIFERATION	31	0,21	1,01	0,461	0,734	1,000	242
223	PEDRIOLI_MIR31_TARGETS_DN	21	0,23	1,01	0,449	0,733	1,000	172
224	GO_POSITIVE_REGULATION_OF_PHOSPHATE_METABOLIC_PROCESS	27	0,22	1,01	0,457	0,736	1,000	163
225	WEST_ADRENOCORTICAL_TUMOR_DN	17	0,25	1,00	0,448	0,745	1,000	114
226	GO_SENSORY_ORGAN_DEVELOPMENT	18	0,25	1,00	0,446	0,747	1,000	104
227	GO_POSITIVE_REGULATION_OF_DEVELOPMENTAL_PROCESS	37	0,19	1,00	0,474	0,751	1,000	110
228	GO_POSITIVE_REGULATION_OF_PHOSPHORUS_METABOLIC_PROCESS	27	0,22	1,00	0,490	0,753	1,000	163
229	NABA_MATRISOME_ASSOCIATED	16	0,25	0,99	0,469	0,756	1,000	62
230	HELLER_SILENCED_BY_METHYLATION_UP	16	0,25	0,99	0,464	0,754	1,000	126
231	GO_REGULATION_OF_RESPONSE_TO_STRESS	31	0,20	0,99	0,469	0,752	1,000	82
232	ENK_UV_RESPONSE_EPIDERMIS_DN	17	0,25	0,99	0,465	0,752	1,000	97
233	GRAESSMANN_APOPTOSIS_BY_DOXORUBICIN_UP	24	0,22	0,98	0,476	0,759	1,000	135
234	GO_NUCLEIC_ACID_BINDING_TRANSCRIPTION_FACTOR_ACTIVITY	22	0,23	0,98	0,480	0,761	1,000	99
235	RIGGI_EWING_SARCOMA_PROGENITOR_UP	16	0,25	0,98	0,476	0,763	1,000	141
236	GO_CENTRAL_NERVOUS_SYSTEM_DEVELOPMENT	26	0,21	0,98	0,483	0,760	1,000	101
237	GO_REGULATION_OF_TRANSPORT	61	0,17	0,98	0,517	0,762	1,000	279
238	GO_CELL_PROLIFERATION	26	0,21	0,97	0,496	0,762	1,000	143
239	GO_ESTABLISHMENT_OF_PROTEIN_LOCALIZATION	26	0,21	0,97	0,498	0,765	1,000	84
240	GO_REGULATION_OF_CELLULAR_LOCALIZATION	45	0,18	0,97	0,508	0,766	1,000	112
241	GO_GOLGI_APPARATUS	41	0,18	0,95	0,523	0,793	1,000	212

242	GO_RIBONUCLEOTIDE_BINDING	44	0,18	0,95	0,542	0,790	1,000	75
243	GO_PHOSPHATE_CONTAINING_COMPOUND_METABOLIC_PROCESS	42	0,18	0,95	0,544	0,793	1,000	157
244	GO_NEGATIVE_REGULATION_OF_PHOSPHATE_METABOLIC_PROCESS	19	0,22	0,95	0,510	0,790	1,000	167
245	KINSEY_TARGETS_OF_EWSR1_FLII_FUSION_UP	18	0,23	0,95	0,532	0,788	1,000	270
246	GO_NEGATIVE_REGULATION_OF_PHOSPHORUS_METABOLIC_PROCESS	19	0,22	0,95	0,530	0,788	1,000	167
247	GO_SINGLE_ORGANISM_BIOSYNTHETIC_PROCESS	27	0,20	0,95	0,525	0,787	1,000	158
248	GO_CELL_DEVELOPMENT	40	0,18	0,94	0,524	0,787	1,000	165
249	GO_REGULATION_OF_INTRACELLULAR_SIGNAL_TRANSDUCTION	37	0,18	0,94	0,541	0,795	1,000	104
250	GO_ENDOCYTOSIS	31	0,19	0,94	0,536	0,795	1,000	21
251	BENPORATH_ES_WITH_H3K27ME3	34	0,18	0,94	0,536	0,792	1,000	173
252	WONG_ADULT_TISSUE_STEM_MODULE	34	0,18	0,94	0,559	0,790	1,000	181
253	GO_NEGATIVE_REGULATION_OF_MULTICELLULAR_ORGANISMAL_PROCESS	29	0,19	0,93	0,526	0,790	1,000	163
254	GO_HYDROLASE_ACTIVITY_ACTING_ON_ACID_ANHYDRIDES	17	0,23	0,93	0,529	0,793	1,000	212
255	GO_VACUOLE	22	0,22	0,93	0,555	0,793	1,000	194
256	GO_REGULATION_OF_HYDROLASE_ACTIVITY	29	0,19	0,91	0,562	0,818	1,000	22
257	GO_ENDOPLASMIC_RETICULUM	28	0,19	0,91	0,576	0,830	1,000	188
258	GO_GOLGI_MEMBRANE	16	0,23	0,90	0,584	0,841	1,000	44
259	GO_INFLAMMATORY_RESPONSE	16	0,23	0,90	0,585	0,838	1,000	21
260	GO_PROTEIN_DOMAIN_SPECIFIC_BINDING	22	0,21	0,90	0,583	0,835	1,000	140
261	GO_CATABOLIC_PROCESS	23	0,20	0,89	0,580	0,846	1,000	98
262	GO_PROTEIN_COMPLEX_BINDING	33	0,18	0,89	0,590	0,844	1,000	132
263	GO_POSITIVE_REGULATION_OF_PROTEIN_MODIFICATION_PROCESS	24	0,19	0,89	0,621	0,844	1,000	110
264	NUYTTEN_EZH2_TARGETS_UP	26	0,19	0,89	0,619	0,843	1,000	190
265	IVANOVA_HEMATOPOIESIS_STEM_CELL_AND_PROGENITOR	21	0,21	0,88	0,598	0,844	1,000	143
266	GO_VESICLE_MEDIATED_TRANSPORT	51	0,16	0,88	0,602	0,841	1,000	22
267	MIKKELSEN_MCV6_HCP_WITH_H3K27ME3	18	0,22	0,88	0,608	0,843	1,000	251
268	LEE_BMP2_TARGETS_UP	19	0,21	0,87	0,602	0,851	1,000	134
269	GO_REGULATION_OF_INTRACELLULAR_TRANSPORT	16	0,23	0,87	0,620	0,848	1,000	103
270	MEISSNER_NPC_HCP_WITH_H3K4ME2	28	0,19	0,87	0,611	0,848	1,000	62
271	GO_NEURON_DEVELOPMENT	22	0,20	0,87	0,636	0,845	1,000	155
272	GO_PHOSPHORYLATION	29	0,18	0,87	0,624	0,849	1,000	157
273	PEREZ_TP53_TARGETS	41	0,16	0,87	0,642	0,847	1,000	265
274	GO_ORGANONITROGEN_COMPOUND_METABOLIC_PROCESS	28	0,18	0,86	0,644	0,857	1,000	160
275	GO_NEUROGENESIS	48	0,16	0,86	0,655	0,854	1,000	170
276	CHYLA_CBFA2T3_TARGETS_UP	23	0,19	0,86	0,620	0,852	1,000	178
277	GO_LEUKOCYTE_MIGRATION	15	0,22	0,86	0,630	0,852	1,000	209
278	DUTERTRE_ESTRADIOL_RESPONSE_24HR_DN	16	0,22	0,85	0,645	0,854	1,000	114
279	GO_ION_TRANSPORT	28	0,18	0,85	0,656	0,852	1,000	214
280	GO_ADENYL_NUCLEOTIDE_BINDING	30	0,18	0,85	0,655	0,855	1,000	170
281	GO_RESPONSE_TO_WOUNDING	20	0,20	0,85	0,644	0,853	1,000	246
282	GO_POSITIVE_REGULATION_OF_INTRACELLULAR_SIGNAL_TRANSDUCTION	20	0,20	0,85	0,654	0,853	1,000	48
283	GO_DEVELOPMENTAL_PROCESS_INVOLVED_IN_REPRODUCTION	16	0,21	0,84	0,646	0,855	1,000	69
284	FEVR_CTNNB1_TARGETS_UP	21	0,20	0,84	0,679	0,857	1,000	60
285	GO_POSITIVE_REGULATION_OF_CELLULAR_COMPONENT_ORGANIZATION	38	0,16	0,84	0,657	0,857	1,000	110
286	GO_POSITIVE_REGULATION_OF_SECRETION	20	0,19	0,83	0,665	0,868	1,000	138
287	GO_G_PROTEIN_COUPLED_RECEPTOR_SIGNALING_PATHWAY	20	0,19	0,83	0,667	0,865	1,000	219
288	GO_ESTABLISHMENT_OF_LOCALIZATION_IN_CELL	37	0,16	0,81	0,705	0,897	1,000	84
289	GO_PEPTIDYL_AMINO_ACID_MODIFICATION	20	0,19	0,81	0,696	0,898	1,000	178
290	GO_GOLGI_APPARATUS_PART	23	0,18	0,81	0,691	0,897	1,000	158
291	GO_EMBRYONIC_MORPHOGENESIS	23	0,18	0,80	0,709	0,895	1,000	56
292	GO_EMBRYONIC_ORGAN_DEVELOPMENT	19	0,19	0,80	0,717	0,900	1,000	56
293	BRUINS_UVC_RESPONSE_VIA_TP53_GROUP_A	24	0,18	0,80	0,709	0,899	1,000	76

294	GO_CARBOHYDRATE_DERIVATIVE_METABOLIC_PROCESS	19	0,19	0,80	0,737	0,898	1,000	246
295	GO_CELL_MORPHOGENESIS_INVOLVED_IN_DIFFERENTIATION	15	0,20	0,80	0,728	0,898	1,000	58
296	BRUINS_UVC_RESPONSE_LATE	23	0,18	0,79	0,744	0,898	1,000	178
297	BLALOCK_ALZHEIMERS_DISEASE_UP	34	0,16	0,79	0,713	0,902	1,000	184
298	MIKKELSEN_MEF_HCP_WITH_H3K27ME3	16	0,20	0,78	0,719	0,905	1,000	68
299	BENPORATH_SUZ12_TARGETS	30	0,16	0,78	0,733	0,906	1,000	173
300	GO_MUSCLE_STRUCTURE_DEVELOPMENT	16	0,20	0,78	0,741	0,906	1,000	165
301	GO_HEAD_DEVELOPMENT	23	0,18	0,76	0,763	0,926	1,000	114
302	GO_ENDOPLASMIC_RETICULUM_PART	18	0,19	0,76	0,768	0,924	1,000	39
303	GO_REGULATION_OF_TRANSMEMBRANE_TRANSPORT	16	0,19	0,76	0,751	0,924	1,000	269
304	MARTENS_TRETINOIN_RESPONSE_UP	25	0,17	0,76	0,767	0,922	1,000	207
305	GO_LOCOMOTION	44	0,14	0,76	0,760	0,919	1,000	34
306	GO_REGULATION_OF_CYTOSKELETON_ORGANIZATION	16	0,19	0,76	0,777	0,917	1,000	110
307	GO_MOLECULAR_FUNCTION_REGULATOR	24	0,17	0,76	0,755	0,916	1,000	253
308	GO_ION_TRANSMEMBRANE_TRANSPORT	22	0,17	0,76	0,760	0,916	1,000	191
309	BENPORATH_EED_TARGETS	27	0,16	0,75	0,763	0,916	1,000	239
310	GO_REGULATION_OF_ION_TRANSPORT	19	0,18	0,75	0,760	0,920	1,000	153
311	GO_PROTEIN_PHOSPHORYLATION	26	0,16	0,75	0,776	0,920	1,000	170
312	GO_INTRINSIC_COMPONENT_OF_PLASMA_MEMBRANE	71	0,13	0,75	0,799	0,919	1,000	65
313	GO_CELLULAR_MACROMOLECULE_LOCALIZATION	19	0,18	0,73	0,799	0,932	1,000	84
314	GO_REGULATION_OF_SECRETION	35	0,14	0,73	0,792	0,936	1,000	276
315	GSE37301_CD4_TCELL_VS_GRANULOCYTE_MONOCYTE_PROGENITOR_UP	18	0,18	0,73	0,799	0,935	1,000	234
316	REACTOME_DEVELOPMENTAL_BIOLOGY	18	0,18	0,72	0,795	0,936	1,000	90
317	GO_REGULATION_OF_MULTICELLULAR_ORGANISMAL_DEVELOPMENT	59	0,13	0,72	0,816	0,935	1,000	113
318	GO_REGULATION_OF_CELLULAR_COMPONENT_MOVEMENT	25	0,16	0,72	0,802	0,938	1,000	152
319	GO_REGULATION_OF_ANATOMICAL_STRUCTURE_SIZE	20	0,17	0,71	0,835	0,942	1,000	190
320	GO_NEUROLOGICAL_SYSTEM_PROCESS	24	0,16	0,71	0,810	0,940	1,000	199
321	GO_INTRACELLULAR_VESICLE	36	0,14	0,71	0,823	0,939	1,000	141
322	PUJANA_ATM_PCC_NETWORK	17	0,17	0,70	0,838	0,946	1,000	232
323	GO_POSITIVE_REGULATION_OF_CATALYTIC_ACTIVITY	30	0,14	0,70	0,828	0,946	1,000	159
324	GO_INTRACELLULAR_PROTEIN_TRANSPORT	15	0,18	0,69	0,822	0,949	1,000	84
325	GO_TRANSMEMBRANE_TRANSPORT	28	0,15	0,69	0,846	0,947	1,000	214
326	BENPORATH_PRC2_TARGETS	19	0,17	0,69	0,832	0,944	1,000	239
327	GO_INTRACELLULAR_SIGNAL_TRANSDUCTION	49	0,12	0,69	0,848	0,944	1,000	212
328	GO_REGULATION_OF_GROWTH	15	0,18	0,69	0,844	0,942	1,000	93
329	GO_NEGATIVE_REGULATION_OF_TRANSCRIPTION_FROM_RNA_POLYMERASE_II_PROMOTER	16	0,17	0,69	0,836	0,941	1,000	242
330	GO_INORGANIC_ION_TRANSMEMBRANE_TRANSPORT	16	0,17	0,69	0,848	0,941	1,000	191
331	NUYTTEN_NIPP1_TARGETS_UP	15	0,18	0,68	0,872	0,943	1,000	273
332	GO_RESPONSE_TO_ORGANIC_CYCLIC_COMPOUND	20	0,16	0,68	0,852	0,942	1,000	23
333	GO_EPITHELIUM_DEVELOPMENT	26	0,15	0,68	0,865	0,941	1,000	242
334	GO_ANATOMICAL_STRUCTURE_FORMATION_INVOLVED_IN_MORPHOGENESIS	30	0,14	0,67	0,861	0,943	1,000	155
335	GO_SINGLE_ORGANISM_CATABOLIC_PROCESS	17	0,17	0,67	0,865	0,942	1,000	142
336	GO_MEMBRANE_REGION	37	0,13	0,66	0,861	0,948	1,000	80
337	GO_REGULATION_OF_BODY_FLUID_LEVELS	18	0,16	0,66	0,872	0,946	1,000	237
338	GO_POSITIVE_REGULATION_OF_MOLECULAR_FUNCTION	35	0,13	0,66	0,867	0,951	1,000	208
339	GO_CATION_TRANSPORT	18	0,16	0,65	0,875	0,954	1,000	191
340	GO_CELLULAR_RESPONSE_TO_STRESS	27	0,14	0,65	0,885	0,951	1,000	157
341	SATO_SILENCED_BY_METHYLATION_IN_PANCREATIC_CANCER_1	15	0,17	0,65	0,903	0,950	1,000	45
342	GO_EMBRYO_DEVELOPMENT_ENDING_IN_BIRTH_OR_EGG_HATCHING	20	0,15	0,63	0,890	0,960	1,000	158
343	GSE21063_WT_VS_NFATC1_KO_BCELL_UP	15	0,16	0,63	0,907	0,965	1,000	208

344	LIU_PROSTATE_CANCER_DN	18	0,15	0,62	0,885	0,963	1,000	190
345	IVANOVA_HEMATOPOIESIS_STEM_CELL_LONG_TERM	15	0,16	0,62	0,904	0,962	1,000	165
346	GO_REGULATION_OF_CELL_DEVELOPMENT	34	0,12	0,62	0,904	0,959	1,000	170
347	SMID_BREAST_CANCER_BASAL_DN	20	0,14	0,61	0,913	0,965	1,000	211
348	CHICAS_RB1_TARGETS_CONFLUENT	29	0,13	0,60	0,917	0,969	1,000	255
349	GO_TISSUE_MORPHOGENESIS	18	0,15	0,60	0,926	0,970	1,000	56
350	GO_REGULATION_OF_CELLULAR_COMPONENT_BIOGENESIS	21	0,14	0,60	0,921	0,970	1,000	110
351	GO_REGULATION_OF_MAPK_CASCADE	17	0,15	0,59	0,928	0,975	1,000	104
352	GO_REGULATION_OF_VESICLE_MEDIATED_TRANSPORT	18	0,14	0,59	0,931	0,972	1,000	138
353	GO_ORGANONITROGEN_COMPOUND_BIOSYNTHETIC_PROCESS	16	0,15	0,58	0,936	0,971	1,000	158
354	CHARAFE_BREAST_CANCER_LUMINAL_VS_BASAL_DN	15	0,15	0,58	0,930	0,970	1,000	186
355	GO_ORGAN_MORPHOGENESIS	29	0,11	0,56	0,957	0,983	1,000	242
356	GO_TRANSITION_METAL_ION_BINDING	21	0,12	0,53	0,967	0,994	1,000	68
357	GO_CELL_DEATH	27	0,11	0,52	0,974	0,996	1,000	50
358	GO_REGULATION_OF_CELL_DIFFERENTIATION	52	0,09	0,51	0,967	0,996	1,000	113
359	GO_TUBE_DEVELOPMENT	21	0,12	0,50	0,985	0,997	1,000	163
360	GO_SECRETION	23	0,11	0,50	0,976	0,997	1,000	279
361	GO_EMBRYO_DEVELOPMENT	31	0,10	0,48	0,975	0,999	1,000	69
362	GO_SECRETION_BY_CELL	22	0,11	0,48	0,986	0,997	1,000	279
363	ZWANG_TRANSIENTLY_UP_BY_1ST_EGF_PULSE_ONLY	37	0,09	0,47	0,991	0,996	1,000	13
364	GO_POSITIVE_REGULATION_OF_CELL_DIFFERENTIATION	25	0,10	0,46	0,986	0,995	1,000	170
365	GO_NEGATIVE_REGULATION_OF_DEVELOPMENTAL_PROCESS	26	0,10	0,45	0,991	0,995	1,000	167
366	GO_MOVEMENT_OF_CELL_OR_SUBCELLULAR_COMPONENT	47	0,08	0,42	0,995	0,997	1,000	180
367	GO_CELL_JUNCTION	40	0,08	0,42	0,995	0,995	1,000	115

Table 7. Ingenuity Pathway analysis (IPA).

Ingenuity Canonical Pathways	-log (p-value)	Ratio	z-score	Molecules
Primary Immunodeficiency Signaling	7.79E00	2.08E-01	NaN	IL7R,BLNK,CD19,CD40LG,CD3E,CD4,CD8A,TNFRSF13C,CD3D,AICDA
Dermatan Sulfate Biosynthesis	3.9E00	1.17E-01	NaN	UST,CHST3,CHST11,HS3ST1,CHST10,DSEL,CSGALNACT1
Dermatan Sulfate Biosynthesis (Late Stages)	3.69E00	1.3E-01	NaN	UST,CHST3,CHST11,HS3ST1,CHST10,DSEL
T Cell Receptor Signaling	3.68E00	8.26E-02	NaN	CD3G,CD28,PRKCQ,CD3E,CD4,FGFR1,CD8A,CD3D,CD8B
Hematopoiesis from Pluripotent Stem Cells	3.63E00	1.28E-01	NaN	CD3G,CD3E,CD4,CD8A,CD3D,CD8B
Chondroitin Sulfate Biosynthesis (Late Stages)	3.53E00	1.22E-01	NaN	UST,CHST3,CHST11,HS3ST1,CHST10,CSGALNACT1
CTLA4 Signaling in Cytotoxic T Lymphocytes	3.26E00	8.08E-02	NaN	CD3G,CD28,CD3E,AP1M2,FGFR1,CD8A,CD3D,CD8B
Chondroitin Sulfate Biosynthesis	3.13E00	1.03E-01	NaN	UST,CHST3,CHST11,HS3ST1,CHST10,CSGALNACT1
PKCŒ[Signaling in T Lymphocytes	3.07E00	6.82E-02	2.449	CD3G,CD28,PRKCQ,CD3E,MAP3K6,CD4,FGFR1,RAC3,CD3D
Communication between Innate and Adaptive Immune Cells	2.85E00	7.87E-02	NaN	CD28,CD40LG,CD4,CD8A,TNFRSF13C,CD8B,CCR7
CCR5 Signaling in Macrophages	2.74E00	8.7E-02	NaN	CD3G,PRKCQ,CD3E,CD4,MAPK12,CD3D
iCOS-iCOSL Signaling in T Helper Cells	2.68E00	6.56E-02	2.236	CD3G,CD28,CD40LG,PRKCQ,CD3E,CD4,FGFR1,CD3D
Hepatic Fibrosis / Hepatic Stellate Cell Activation	2.62E00	5.46E-02	NaN	COL5A1,CD40LG,VCAM1,EDNRB,EDN1,IL1RL1,FGFR1,CCR7,COL15A1,IL18RAP
Cytotoxic T Lymphocyte-mediated Apoptosis of Target Cells	2.54E00	1.25E-01	-1.000	CD3G,PRF1,CD3E,CD3D
Xenobiotic Metabolism Signaling	2.52E00	4.55E-02	NaN	PRKCQ,UST,MAP3K6,ALDH1A3,FGFR1,GSTM3,CHST3,CHST11,CHST10,HS3ST1,UGT2B10,MAPK12,PPARGC1A
CD28 Signaling in T Helper Cells	2.48E00	6.11E-02	2.236	CD3G,CD28,PRKCQ,CD3E,CD4,FGFR1,MAPK12,CD3D
Type I Diabetes Mellitus Signaling	2.33E00	6.36E-02	-1.000	CD3G,CD28,PRF1,CD3E,GAD1,MAPK12,CD3D
Axonal Guidance Signaling	2.31E00	3.79E-02	NaN	PLXNA3,PRKCQ,BMP2,FGFR1,ADAM11,KEL,FZD1,PLCH2,ABLIM1,RAC3,SEMA4C,EPHB6,GNAT1,ADAM19,ADAM23,GLI1,EPHA2
Factors Promoting Cardiogenesis in Vertebrates	2.12E00	6.52E-02	NaN	PRKCQ,BMP2,TDGF1,LEF1,FZD1,Tcf7
Calcium-induced T Lymphocyte Apoptosis	2.11E00	7.58E-02	2.236	CD3G,PRKCQ,CD3E,CD4,CD3D
Role of NFAT in Regulation of the Immune Response	2.08E00	4.86E-02	3.000	BLNK,CD3G,CD28,PRKCQ,GNAT1,CD3E,CD4,FGFR1,CD3D
Heparan Sulfate Biosynthesis (Late Stages)	2.05E00	7.35E-02	NaN	UST,CHST3,CHST11,HS3ST1,CHST10
LPS/IL-1 Mediated Inhibition of RXR Function	2.05E00	4.52E-02	NaN	UST,ALDH1A3,IL1RL1,GSTM3,CHST3,CHST11,HS3ST1,CHST10,PPARGC1A,IL18RAP
Basal Cell Carcinoma Signaling	1.95E00	6.94E-02	2.236	BMP2,LEF1,FZD1,GLI1,Tcf7
Heparan Sulfate Biosynthesis	1.86E00	6.58E-02	NaN	UST,CHST3,CHST11,HS3ST1,CHST10
Regulation of IL-2 Expression in Activated and Anergic T Lymphocytes	1.79E00	6.33E-02	NaN	CD3G,CD28,CD3E,MAPK12,CD3D
Human Embryonic Stem Cell Pluripotency	1.74E00	4.9E-02	NaN	FGFR1,BMP2,TDGF1,S1PR1,LEF1,FZD1,Tcf7
Granulocyte Adhesion and Diapedesis	1.73E00	4.52E-02	NaN	VCAM1,SELP,CLDN1,IL1RL1,THY1,CCL24,SDC4,IL18RAP
B Cell Receptor Signaling	1.63E00	4.32E-02	2.449	BLNK,PAX5,CD19,EBF1,PRKCQ,MAP3K6,FGFR1,MAPK12
Nur77 Signaling in T Lymphocytes	1.61E00	6.78E-02	NaN	CD3G,CD28,CD3E,CD3D
HER-2 Signaling in Breast Cancer	1.61E00	5.68E-02	NaN	PRKCQ,FGFR1,PARD6B,PARD6G,ITGB4
Retinoate Biosynthesis I	1.6E00	8.82E-02	NaN	ALDH1A3,BMP2,ADH1C

Crosstalk between Dendritic Cells and Natural Killer Cells	1.59E00	5.62E-02	NaN	CD28,PRF1,CD40LG,TLN2,CCR7
OX40 Signaling Pathway	1.59E00	5.62E-02	-1.342	CD3G,CD3E,CD4,MAPK12,CD3D
PCP pathway	1.52E00	6.35E-02	NaN	VANGL1,FZD1,SDC4,MAPK12
Salvage Pathways of Pyrimidine Ribonucleotides	1.52E00	5.38E-02	NaN	AK1,PRKCQ,MAP3K6,PRKAA2,AICDA
Anandamide Degradation	1.43E00	5,00E-01	NaN	FAAH
Glutamate Dependent Acid Resistance	1.43E00	5,00E-01	NaN	GAD1
Thyroid Cancer Signaling	1.41E00	7.5E-02	NaN	GDNF,LEF1,Tcf7
Virus Entry via Endocytic Pathways	1.37E00	4.9E-02	NaN	CD55,PRKCQ,FGFR1,ITGB4,RAC3
Caveolar-mediated Endocytosis Signaling	1.36E00	5.63E-02	NaN	CD55,ITGA9,ITGB4,PTRF
Role of JAK1 and JAK3 in Œ≥c Cytokine Signaling	1.36E00	5.63E-02	NaN	IL7R,BLNK,IL9R,FGFR1
T Helper Cell Differentiation	1.32E00	5.48E-02	NaN	CD28,CD40LG,CXCR5,TBX21
Mouse Embryonic Stem Cell Pluripotency	1.31E00	4.72E-02	2.236	FGFR1,LEF1,FZD1,MAPK12,Tcf7
Serotonin Degradation	1.3E00	5.41E-02	NaN	ALDH1A3,ADH1C,UGT2B10,CSGALNACT1
IL-15 Signaling	1.27E00	5.26E-02	NaN	VCAM1,FGFR1,MAPK12,RAC3
GDNF Family Ligand-Receptor Interactions	1.27E00	5.26E-02	2.000	GDNF,GFRA1,FGFR1,MAPK12
Autoimmune Thyroid Disease Signaling	1.24E00	6.38E-02	NaN	CD28,PRF1,CD40LG
CD40 Signaling	1.23E00	5.13E-02	1.000	CD40LG,FGFR1,MAPK12,FCER2
Paxillin Signaling	1.21E00	4.42E-02	NaN	TLN2,ITGA9,FGFR1,ITGB4,MAPK12
Systemic Lupus Erythematosus Signaling	1.21E00	3.56E-02	NaN	CD3G,CD28,CD40LG,CD3E,FGFR1,C6,TNFRSF13C,CD3D
Endothelin-1 Signaling	1.2E00	3.74E-02	2.646	PRKCQ,GNAT1,EDNRB,EDN1,FGFR1,PLCH2,MAPK12
Role of Macrophages, Fibroblasts and Endothelial Cells in Rheumatoid Arthritis	1.18E00	3.24E-02	NaN	VCAM1,PRKCQ,IL1RL1,FGFR1,LEF1,FZD1,PLCH2,Tcf7,PRSS1,IL18RAP
RAR Activation	1.17E00	3.68E-02	NaN	PRKCQ,ALDH1A3,BMP2,ADH1C,SORBS3,MAPK12,PPARGC1A
Role of Osteoblasts, Osteoclasts and Chondrocytes in Rheumatoid Arthritis	1.15E00	3.45E-02	NaN	IL1RL1,FGFR1,BMP2,LEF1,FZD1,MAPK12,Tcf7,IL18RAP
Uracil Degradation II (Reductive)	1.14E00	2.5E-01	NaN	DPYS
Thymine Degradation	1.14E00	2.5E-01	NaN	DPYS
IL-22 Signaling	1.13E00	8.33E-02	NaN	IL22RA2,MAPK12
FcŒ≥RIIB Signaling in B Lymphocytes	1.11E00	5.66E-02	NaN	BLNK,FGFR1,MAPK12
NF-ŒʃB Activation by Viruses	1.11E00	4.65E-02	NaN	PRKCQ,CD4,FGFR1,CXCR5
Natural Killer Cell Signaling	1.1E00	4.1E-02	NaN	PRKCQ,FGFR1,KLRB1,Klra7 (includes others),RAC3
phagosome formation	1.1E00	4.1E-02	NaN	PRKCQ,MRC2,FGFR1,PLCH2,FCER2
Tyrosine Degradation I	1.05E00	2,00E-01	NaN	HGD
Glutamate Degradation III (via 4-aminobutyrate)	1.05E00	2,00E-01	NaN	GAD1
Reelin Signaling in Neurons	1.03E00	4.35E-02	NaN	BLK,MAPT,FGFR1,MAPK12
14-3-3-mediated Signaling	1.01E00	3.85E-02	NaN	PRKCQ,MAPT,FGFR1,PLCH2,MAPK12
p70S6K Signaling	1,00E+00	3.82E-02	2.236	CD19,PRKCQ,MAPT,FGFR1,PLCH2
Leukocyte Extravasation Signaling	9.98E-01	3.33E-02	2.000	VCAM1,PRKCQ,CLDN1,FGFR1,THY1,MAPK12,CTTN
Tec Kinase Signaling	9.98E-01	3.53E-02	2.236	BLK,PRKCQ,GNAT1,FGFR1,MAPK12,TNFRSF10A
Chondroitin and Dermatan Biosynthesis	9.7E-01	1.67E-01	NaN	CSGALNACT1
Adipogenesis pathway	9.7E-01	3.73E-02	NaN	EBF1,EGR2,FGFR1,BMP2,FZD1
Sonic Hedgehog Signaling	9.67E-01	6.67E-02	NaN	GLI1,CCNB1
Pyridoxal 5'-phosphate Salvage Pathway	9.28E-01	4.69E-02	NaN	PRKCQ,MAP3K6,PRKAA2

Phosphatidylcholine Biosynthesis I	9.07E-01	1.43E-01	NaN	PCYT1B
UVB-Induced MAPK Signaling	8.99E-01	4.55E-02	NaN	PRKCQ,FGFR1,MAPK12
Eicosanoid Signaling	8.85E-01	4.48E-02	NaN	PTGIS,PTGER3,TBXA2R
SAPK/JNK Signaling	8.83E-01	3.85E-02	2.000	SH2D2A,FGFR1,MAPK12,RAC3
Ovarian Cancer Signaling	8.74E-01	3.47E-02	NaN	EDN1,FGFR1,LEF1,FZD1,Tcf7
IL-10 Signaling	8.71E-01	4.41E-02	NaN	IL1RL1,MAPK12,IL18RAP
Agrin Interactions at Neuromuscular Junction	8.57E-01	4.35E-02	NaN	MAPK12,RAC3,CTTN
Coagulation System	8.57E-01	5.71E-02	NaN	F9,F7
B Cell Development	8.57E-01	5.71E-02	NaN	IL7R,CD19
Histidine Degradation III	8.53E-01	1.25E-01	NaN	HAL
Salvage Pathways of Pyrimidine Deoxyribonucleotides	8.53E-01	1.25E-01	NaN	AICDA
Regulation of the Epithelial-Mesenchymal Transition Pathway	8.4E-01	3.17E-02	NaN	FGFR1,PARD6B,LEF1,PARD6G,FZD1,Tcf7
Ethanol Degradation II	8.18E-01	5.41E-02	NaN	ALDH1A3,ADH1C
Complement System	8.18E-01	5.41E-02	NaN	CD55,C6
Prostanoid Biosynthesis	8.06E-01	1.11E-01	NaN	PTGIS
Ephrin B Signaling	8.05E-01	4.11E-02	NaN	EPHB6,GNAT1,RAC3
Notch Signaling	8,00E-01	5.26E-02	NaN	DTX1,HEY1
ILK Signaling	7.89E-01	3.06E-02	2.000	FBLIM1,FGFR1,BMP2,LEF1,ITGB4,MAPK12
Netrin Signaling	7.82E-01	5.13E-02	NaN	RAC3,ABLIM1
HGF Signaling	7.72E-01	3.48E-02	2.000	PRKCQ,MAP3K6,FGFR1,MAPK12
Role of Wnt/GSK-3Œ≤ Signaling in the Pathogenesis of Influenza	7.69E-01	3.95E-02	NaN	LEF1,FZD1,Tcf7
B Cell Activating Factor Signaling	7.65E-01	5,00E-02	NaN	MAPK12,TNFRSF13C
Thyroid Hormone Metabolism II (via Conjugation and/or Degradation)	7.65E-01	5,00E-02	NaN	UGT2B10,CSGALNACT1
Noradrenaline and Adrenaline Degradation	7.65E-01	5,00E-02	NaN	ALDH1A3,ADH1C
IL-17A Signaling in Airway Cells	7.57E-01	3.9E-02	NaN	FGFR1,MUC5B,MAPK12
p38 MAPK Signaling	7.53E-01	3.42E-02	NaN	IL1RL1,MAPT,MAPK12,IL18RAP
Thrombin Signaling	7.41E-01	2.96E-02	2.236	PRKCQ,GNAT1,FGFR1,PLCH2,MAPK12,GATA2
Fc Epsilon RI Signaling	7.35E-01	3.36E-02	2.000	PRKCQ,FGFR1,MAPK12,RAC3
UVC-Induced MAPK Signaling	7.32E-01	4.76E-02	NaN	PRKCQ,MAPK12
GŒ±i Signaling	7.27E-01	3.33E-02	2.000	PTGER3,TBXA2R,CHRM4,S1PR1
Macropinocytosis Signaling	7.13E-01	3.7E-02	NaN	PRKCQ,FGFR1,ITGB4
Role of Tissue Factor in Cancer	7.09E-01	3.28E-02	NaN	BLK,FGFR1,F7,MAPK12
CXCR4 Signaling	7.05E-01	3.03E-02	2.000	PRKCQ,GNAT1,CD4,FGFR1,MAPK12
Histidine Degradation VI	6.93E-01	8.33E-02	NaN	HAL
Cdc42 Signaling	6.9E-01	2.99E-02	-0.447	CD3G,CD3E,CDC42EP5,MAPK12,CD3D
IL-9 Signaling	6.87E-01	4.44E-02	NaN	IL9R,FGFR1
Triacylglycerol Degradation	6.87E-01	4.44E-02	NaN	FAAH,CEL
Allograft Rejection Signaling	6.82E-01	3.57E-02	NaN	CD28,PRF1,CD40LG
PEDF Signaling	6.82E-01	3.57E-02	NaN	GDNF,FGFR1,MAPK12
IL-17 Signaling	6.72E-01	3.53E-02	NaN	FGFR1,MUC5B,MAPK12
Type II Diabetes Mellitus Signaling	6.68E-01	3.15E-02	1.000	PRKCQ,FGFR1,PRKAA2,MAPK12
IL-6 Signaling	6.68E-01	3.15E-02	2.000	IL1RL1,FGFR1,MAPK12,IL18RAP
Choline Biosynthesis III	6.62E-01	7.69E-02	NaN	PCYT1B
Oleate Biosynthesis II (Animals)	6.62E-01	7.69E-02	NaN	Scd4
Cholesterol Biosynthesis I	6.62E-01	7.69E-02	NaN	DHCR24
Cholesterol Biosynthesis II (via 24,25-dihydrolanosterol)	6.62E-01	7.69E-02	NaN	DHCR24

Cholesterol Biosynthesis III (via Desmosterol)	6.62E-01	7.69E-02	NaN	DHCR24
LPS-stimulated MAPK Signaling	6.62E-01	3.49E-02	NaN	PRKCQ,FGFR1,MAPK12
PI3K Signaling in B Lymphocytes	6.6E-01	3.12E-02	NaN	BLNK,BLK,CD19,PLCH2
Graft-versus-Host Disease Signaling	6.45E-01	4.17E-02	NaN	CD28,PRF1
CCR3 Signaling in Eosinophils	6.45E-01	3.08E-02	NaN	PRKCQ,FGFR1,CCL24,MAPK12
Integrin Signaling	6.42E-01	2.74E-02	2.449	TLN2,ITGA9,FGFR1,ITGB4,RAC3,CTTN
DNA Double-Strand Break Repair by Non-Homologous End Joining	6.34E-01	7.14E-02	NaN	XRCC5
Altered T Cell and B Cell Signaling in Rheumatoid Arthritis	6.24E-01	3.33E-02	NaN	CD28,CD40LG,TNFRSF13C
PPARŒ±/RXRŒ± Activation	6.18E-01	2.81E-02	0.000	IL1RL1,PRKAA2,PLCH2,PPARGC1A,IL18RAP
Acute Myeloid Leukemia Signaling	6.15E-01	3.3E-02	NaN	FGFR1,LEF1,Tcf7
Telomere Extension by Telomerase	6.08E-01	6.67E-02	NaN	XRCC5
Amyloid Processing	6.07E-01	3.92E-02	NaN	MAPT,MAPK12
Superpathway of Inositol Phosphate Compounds	6.03E-01	2.65E-02	NaN	CD28,CD19,PPP1R16B,FGFR1,PLCH2,DUSP14
FcŒ≥ Receptor-mediated Phagocytosis in Macrophages and Monocytes	5.98E-01	3.23E-02	NaN	TLN2,PRKCQ,RAC3
PPAR Signaling	5.98E-01	3.23E-02	NaN	IL1RL1,PPARGC1A,IL18RAP
CD27 Signaling in Lymphocytes	5.95E-01	3.85E-02	NaN	MAP3K6,MAPK12
Granzyme B Signaling	5.84E-01	6.25E-02	NaN	PRF1
Extrinsic Prothrombin Activation Pathway	5.84E-01	6.25E-02	NaN	F7
Methionine Degradation I (to Homocysteine)	5.84E-01	6.25E-02	NaN	NSUN4
Parkinson's Signaling	5.84E-01	6.25E-02	NaN	MAPK12
Nicotine Degradation III	5.72E-01	3.7E-02	NaN	UGT2B10,CSGALNACT1
Molecular Mechanisms of Cancer	5.72E-01	2.41E-02	NaN	PRKCQ,GNAT1,FGFR1,BMP2,LEF1,FZD1,MAPK12,RAC3,GLI1
3-phosphoinositide Biosynthesis	5.7E-01	2.69E-02	NaN	CD28,CD19,PPP1R16B,FGFR1,DUSP14
TR/RXR Activation	5.56E-01	3.06E-02	NaN	FGFR1,SYT2,PPARGC1A
ErbB Signaling	5.56E-01	3.06E-02	NaN	PRKCQ,FGFR1,MAPK12
AMPK Signaling	5.53E-01	2.65E-02	2.000	AK1,FGFR1,PRKAA2,MAPK12,PPARGC1A
Agranulocyte Adhesion and Diapedesis	5.53E-01	2.65E-02	NaN	VCAM1,SELP,CLDN1,CCL24,SDC4
Dendritic Cell Maturation	5.47E-01	2.63E-02	2.236	CD40LG,FGFR1,PLCH2,MAPK12,CCR7
Cysteine Biosynthesis III (mammalia)	5.4E-01	5.56E-02	NaN	NSUN4
Wnt/Ca+ pathway	5.39E-01	3.51E-02	NaN	FZD1,PLCH2
Glucocorticoid Receptor Signaling	5.35E-01	2.44E-02	NaN	CD3G,VCAM1,CD3E,FGFR1,PRKAA2,MAPK12,CD3D
IL-12 Signaling and Production in Macrophages	5.35E-01	2.74E-02	NaN	CD40LG,PRKCQ,FGFR1,MAPK12
RANK Signaling in Osteoclasts	5.33E-01	2.97E-02	NaN	MAP3K6,FGFR1,MAPK12
UVA-Induced MAPK Signaling	5.26E-01	2.94E-02	NaN	FGFR1,PLCH2,MAPK12
GADD45 Signaling	5.21E-01	5.26E-02	NaN	CCNB1
Histamine Degradation	5.21E-01	5.26E-02	NaN	ALDH1A3
DNA damage-induced 14-3-3œÉ Signaling	5.21E-01	5.26E-02	NaN	CCNB1
IL-8 Signaling	5.1E-01	2.54E-02	2.236	VCAM1,PRKCQ,FGFR1,MAPK12,RAC3
Ephrin A Signaling	5.09E-01	3.33E-02	NaN	FGFR1,EPHA2
Cardiomyocyte Differentiation via BMP Receptors	5.02E-01	5,00E-02	NaN	BMP2
Granzyme A Signaling	5.02E-01	5,00E-02	NaN	PRF1
Colorectal Cancer Metastasis Signaling	4.99E-01	2.43E-02	2.449	PTGER3,FGFR1,LEF1,FZD1,MAPK12,Tcf7

Melatonin Degradation I	4.9E-01	3.23E-02	NaN	UGT2B10,CSGALNACT1
Oxidative Ethanol Degradation III	4.85E-01	4.76E-02	NaN	ALDH1A3
eNOS Signaling	4.81E-01	2.58E-02	NaN	AQP3,PRKCQ,FGFR1,PRKAA2
Nicotine Degradation II	4.81E-01	3.17E-02	NaN	UGT2B10,CSGALNACT1
Endometrial Cancer Signaling	4.72E-01	3.12E-02	NaN	FGFR1,LEF1
Fatty Acid Œ±-oxidation	4.68E-01	4.55E-02	NaN	ALDH1A3
Thrombopoietin Signaling	4.63E-01	3.08E-02	NaN	PRKCQ,FGFR1
Hypoxia Signaling in the Cardiovascular System	4.63E-01	3.08E-02	NaN	EDN1,UBE2E2
Amyotrophic Lateral Sclerosis Signaling	4.63E-01	2.7E-02	NaN	GDNF,FGFR1,SLC1A2
p53 Signaling	4.63E-01	2.7E-02	NaN	FGFR1,PERP,TNFRSF10A
Corticotropin Releasing Hormone Signaling	4.63E-01	2.7E-02	NaN	PRKCQ,MAPK12,GLI1
Hepatic Cholestasis	4.6E-01	2.52E-02	NaN	PRKCQ,IL1RL1,MAPK12,IL18RAP
Glioblastoma Multiforme Signaling	4.6E-01	2.52E-02	2.000	FGFR1,LEF1,FZD1,PLCH2
Pyrimidine Deoxyribonucleotides De Novo Biosynthesis I	4.53E-01	4.35E-02	NaN	AK1
Putrescine Degradation III	4.53E-01	4.35E-02	NaN	ALDH1A3
Lymphotoxin Œ≤ Receptor Signaling	4.47E-01	2.99E-02	NaN	VCAM1,FGFR1
Role of IL-17A in Arthritis	4.47E-01	2.99E-02	NaN	FGFR1,MAPK12
Superpathway of Melatonin Degradation	4.47E-01	2.99E-02	NaN	UGT2B10,CSGALNACT1
GABA Receptor Signaling	4.47E-01	2.99E-02	NaN	GABRR2,GAD1
Neuropathic Pain Signaling In Dorsal Horn Neurons	4.44E-01	2.63E-02	NaN	PRKCQ,FGFR1,PLCH2
EGF Signaling	4.38E-01	2.94E-02	NaN	FGFR1,MAPK12
Tumoricidal Function of Hepatic Natural Killer Cells	4.38E-01	4.17E-02	NaN	PRF1
CDP-diacylglycerol Biosynthesis I	4.38E-01	4.17E-02	NaN	GPAT3
HIF1Œ± Signaling	4.38E-01	2.61E-02	NaN	EDN1,FGFR1,MAPK12
NGF Signaling	4.26E-01	2.56E-02	NaN	MAP3K6,FGFR1,MAPK12
IL-17A Signaling in Gastric Cells	4.24E-01	4,00E-02	NaN	MAPK12
Role of JAK family kinases in IL-6-type Cytokine Signaling	4.24E-01	4,00E-02	NaN	MAPK12
Tryptophan Degradation X (Mammalian, via Tryptamine)	4.24E-01	4,00E-02	NaN	ALDH1A3
Ethanol Degradation IV	4.24E-01	4,00E-02	NaN	ALDH1A3
Aldosterone Signaling in Epithelial Cells	4.24E-01	2.41E-02	2.000	SCNN1G,PRKCQ,FGFR1,PLCH2
Myc Mediated Apoptosis Signaling	4.23E-01	2.86E-02	NaN	FGFR1,MAPK12
Melatonin Signaling	4.15E-01	2.82E-02	NaN	PRKCQ,PLCH2
Chemokine Signaling	4.15E-01	2.82E-02	NaN	CCL24,MAPK12
Lipid Antigen Presentation by CD1	4.11E-01	3.85E-02	NaN	CD3E
Phosphatidylglycerol Biosynthesis II (Non-plastidic)	4.11E-01	3.85E-02	NaN	GPAT3
Renin-Angiotensin Signaling	4.09E-01	2.5E-02	NaN	PRKCQ,FGFR1,MAPK12
ErbB4 Signaling	4.08E-01	2.78E-02	NaN	PRKCQ,FGFR1
G-Protein Coupled Receptor Signaling	4.05E-01	2.22E-02	NaN	PDE4C,PTGER3,FGFR1,TBXA2R,CHRM4,S1PR1
STAT3 Pathway	4,00E-01	2.74E-02	NaN	FGFR1,MAPK12
cAMP-mediated signaling	4,00E-01	2.26E-02	2.236	PDE4C,PTGER3,TBXA2R,CHRM4,S1PR1
D-myo-inositol (1,4,5)-Trisphosphate Biosynthesis	3.98E-01	3.7E-02	NaN	PLCH2
Role of NANOG in Mammalian Embryonic Stem Cell Pluripotency	3.98E-01	2.46E-02	NaN	FGFR1,BMP2,FZD1
Sphingosine-1-phosphate Signaling	3.98E-01	2.46E-02	NaN	FGFR1,S1PR1,PLCH2

RhoA Signaling	3.98E-01	2.46E-02	NaN	RHPN2,CDC42EP5,SEPT1
Toll-like Receptor Signaling	3.93E-01	2.7E-02	NaN	IL1RL1,MAPK12
Germ Cell-Sertoli Cell Junction Signaling	3.91E-01	2.31E-02	NaN	MAP3K6,FGFR1,MAPK12,RAC3
Ephrin Receptor Signaling	3.87E-01	2.3E-02	NaN	EPHB6,GNAT1,RAC3,EPHA2
TREM1 Signaling	3.86E-01	2.67E-02	NaN	NLRP6,IL1RL1
Superpathway of Cholesterol Biosynthesis	3.86E-01	3.57E-02	NaN	DHCR24
Sperm Motility	3.82E-01	2.4E-02	NaN	PRKCQ,PDE4C,PLCH2
BMP signaling pathway	3.8E-01	2.63E-02	NaN	BMP2,MAPK12
Intrinsic Prothrombin Activation Pathway	3.75E-01	3.45E-02	NaN	F9
Glutathione-mediated Detoxification	3.75E-01	3.45E-02	NaN	GSTM3
Angiopoietin Signaling	3.73E-01	2.6E-02	NaN	FGFR1,TIE1
Estrogen-Dependent Breast Cancer Signaling	3.73E-01	2.6E-02	NaN	FGFR1,HSD17B1
Atherosclerosis Signaling	3.71E-01	2.36E-02	NaN	CD40LG,VCAM1,SELP
VDR/RXR Activation	3.66E-01	2.56E-02	NaN	PRKCQ,IL1RL1
GNRH Signaling	3.61E-01	2.33E-02	NaN	PRKCQ,MAP3K6,MAPK12
NF-ŒÍB Signaling	3.61E-01	2.22E-02	2.000	CD40LG,PRKCQ,FGFR1,BMP2
Erythropoietin Signaling	3.6E-01	2.53E-02	NaN	PRKCQ,FGFR1
GŒ±12/13 Signaling	3.57E-01	2.31E-02	NaN	FGFR1,TBXA2R,MAPK12
ATM Signaling	3.54E-01	2.5E-02	NaN	MAPK12,CCNB1
4-1BB Signaling in T Lymphocytes	3.53E-01	3.23E-02	NaN	MAPK12
Superpathway of Methionine Degradation	3.53E-01	3.23E-02	NaN	NSUN4
Growth Hormone Signaling	3.48E-01	2.47E-02	NaN	PRKCQ,FGFR1
Cardiac Hypertrophy Signaling	3.48E-01	2.13E-02	2.000	GNAT1,MAP3K6,FGFR1,PLCH2,MAPK12
P2Y Purigenic Receptor Signaling Pathway	3.47E-01	2.27E-02	NaN	PRKCQ,FGFR1,PLCH2
CREB Signaling in Neurons	3.45E-01	2.17E-02	NaN	PRKCQ,GNAT1,FGFR1,PLCH2
Pyrimidine Ribonucleotides Interconversion	3.43E-01	3.12E-02	NaN	AK1
HMGB1 Signaling	3.42E-01	2.26E-02	NaN	VCAM1,FGFR1,MAPK12
Phospholipase C Signaling	3.41E-01	2.11E-02	NaN	BLNK,CD3G,PRKCQ,CD3E,CD3D
IL-3 Signaling	3.36E-01	2.41E-02	NaN	PRKCQ,FGFR1
Prolactin Signaling	3.36E-01	2.41E-02	NaN	PRKCQ,FGFR1
Role of Pattern Recognition Receptors in Recognition of Bacteria and Viruses	3.24E-01	2.19E-02	NaN	PRKCQ,FGFR1,MAPK12
FLT3 Signaling in Hematopoietic Progenitor Cells	3.24E-01	2.35E-02	NaN	FGFR1,MAPK12
Leptin Signaling in Obesity	3.24E-01	2.35E-02	NaN	FGFR1,PLCH2
Inhibition of Angiogenesis by TSP1	3.24E-01	2.94E-02	NaN	MAPK12
Pyrimidine Ribonucleotides De Novo Biosynthesis	3.24E-01	2.94E-02	NaN	AK1
GPCR-Mediated Nutrient Sensing in Enteroendocrine Cells	3.24E-01	2.35E-02	NaN	PRKCQ,PLCH2
IL-17A Signaling in Fibroblasts	3.15E-01	2.86E-02	NaN	MAPK12
Dopamine Degradation	3.15E-01	2.86E-02	NaN	ALDH1A3
Stearate Biosynthesis I (Animals)	3.15E-01	2.86E-02	NaN	DHCR24
Role of NFAT in Cardiac Hypertrophy	3.14E-01	2.08E-02	2.000	PRKCQ,FGFR1,PLCH2,MAPK12
TGF-Œ≤ Signaling	3.13E-01	2.3E-02	NaN	BMP2,MAPK12
Production of Nitric Oxide and Reactive Oxygen Species in Macrophages	3.11E-01	2.07E-02	2.000	PRKCQ,MAP3K6,FGFR1,MAPK12
G Beta Gamma Signaling	3.08E-01	2.27E-02	NaN	PRKCQ,GNAT1

VEGF Family Ligand-Receptor Interactions	3.08E-01	2.27E-02	NaN	PRKCQ,FGFR1
Signaling by Rho Family GTPases	3.08E-01	2.02E-02	2.000	GNAT1,CDC42EP5,FGFR1,MAPK12,SEPT1
IL-4 Signaling	3.03E-01	2.25E-02	NaN	FGFR1,FCER2
tRNA Splicing	2.98E-01	2.7E-02	NaN	PDE4C
FGF Signaling	2.97E-01	2.22E-02	NaN	FGFR1,MAPK12
Clathrin-mediated Endocytosis Signaling	2.97E-01	2.03E-02	NaN	MYO6,FGFR1,ITGB4,CTTN
IL-1 Signaling	2.92E-01	2.2E-02	NaN	GNAT1,MAPK12
April Mediated Signaling	2.9E-01	2.63E-02	NaN	MAPK12
mTOR Signaling	2.9E-01	2.01E-02	1.000	PRKCQ,FGFR1,PRKAA2,PRR5
Synaptic Long Term Depression	2.87E-01	2.05E-02	NaN	PRKCQ,GNAT1,PLCH2
Epithelial Adherens Junction Signaling	2.87E-01	2.05E-02	NaN	FGFR1,LEF1,Tcf7
Estrogen Biosynthesis	2.83E-01	2.56E-02	NaN	HSD17B1
Ceramide Signaling	2.83E-01	2.15E-02	NaN	FGFR1,S1PR1
Prostate Cancer Signaling	2.78E-01	2.13E-02	NaN	FGFR1,LEF1
D-myo-inositol-5-phosphate Metabolism	2.76E-01	2.01E-02	NaN	PPP1R16B,PLCH2,DUSP14
Neuroprotective Role of THOP1 in Alzheimer's Disease	2.75E-01	2.5E-02	NaN	MAPT
Retinol Biosynthesis	2.75E-01	2.5E-02	NaN	CEL
Relaxin Signaling	2.72E-01	2,00E-02	NaN	PDE4C,GNAT1,FGFR1
MIF Regulation of Innate Immunity	2.68E-01	2.44E-02	NaN	MAPK12
Mechanisms of Viral Exit from Host Cells	2.68E-01	2.44E-02	NaN	PRKCQ
CDK5 Signaling	2.55E-01	2.02E-02	NaN	MAPT,MAPK12
FAK Signaling	2.55E-01	2.02E-02	NaN	TLN2,FGFR1
Role of p14/p19ARF in Tumor Suppression	2.55E-01	2.33E-02	NaN	FGFR1
Serotonin Receptor Signaling	2.55E-01	2.33E-02	NaN	SLC6A4
iNOS Signaling	2.48E-01	2.27E-02	NaN	MAPK12
Triacylglycerol Biosynthesis	2.48E-01	2.27E-02	NaN	GPAT3
Cholecystokinin/Gastrin-mediated Signaling	2.47E-01	1.98E-02	NaN	PRKCQ,MAPK12
PAK Signaling	2.47E-01	1.98E-02	NaN	FGFR1,MAPK12
Antioxidant Action of Vitamin C	2.39E-01	1.94E-02	NaN	PLCH2,MAPK12
VEGF Signaling	2.39E-01	1.94E-02	NaN	SH2D2A,FGFR1
nNOS Signaling in Neurons	2.3E-01	2.13E-02	NaN	PRKCQ
Cell Cycle: G2/M DNA Damage Checkpoint Regulation	2.19E-01	2.04E-02	NaN	CCNB1
Docosahexaenoic Acid (DHA) Signaling	2.03E-01	1.92E-02	NaN	FGFR1
Phototransduction Pathway	1.99E-01	1.89E-02	NaN	GNAT1

Table 8. STRING analysis comparing significantly enriched genes

Pathway ID	Pathway description	OGC	FDR	matching proteins
GO.0043123	positive regulation of I-kappaB kinase/NF-kappaB signaling	12	1.85e-15	Cd40,Clec4n,Il1b,Map3k7,Myd88,Prkcq,Tab2, Ticam1,Tlr4,Tnf,Traf2,Traf6
GO.0001817	regulation of cytokine production	15	2.45e-15	Cd24a,Cd40,Cd40lg,Clec4n,Clu,Il1b,Myd88,Pf4, Prkcq,Ticam1,Tlr4,Tnf,Traf2,Traf3,Traf6
GO.0001819	positive regulation of cytokine production	13	1.84e-14	Cd40,Cd40lg,Clec4n,Clu,Il1b,Myd88,Pf4,Prkcq, Ticam1,Tlr4,Tnf,Traf2,Traf6
GO.0051092	positive regulation of NF-kappaB transcription factor activity	10	3.84e-14	Cd40,Clu,Il1b,Myd88,Prkcq,Ticam1,Tlr4,Tnf,Traf2,Traf6
GO.0051240	positive regulation of multicellular organismal process	17	6.29e-12	Cd24a,Cd40,Cd40lg,Clec4n,Clu,Cxcr4,Egr1,Il1b, Myd88,Niacr1,Pf4,Prkcq,Ticam1,Tlr4,Tnf,Traf2,Traf6
GO.0051239	regulation of multicellular organismal process	20	6.78e-12	Apbb1,App,Cd24a,Cd40,Cd40lg,Clec4n,Clu,Cxcr4,Egr1, Il1b,Myd88,Nab2,Niacr1,Pf4,Ticam1,Tlr4,Tnf,Traf2,Traf3,Traf6
GO.0051090	regulation of sequence-specific DNA binding transcription factor activity	11	5.58e-11	Cd40,Clu,Il1b,Myd88,Prkcq,Ticam1,Tlr4,Tnf,Traf2,Traf3,Traf6
GO.0080134	regulation of response to stress	15	9.89e-11	Apbb1,Cd24a,Clu,Ets1,Hp,Il1b,Map3k7,Myd88,Prkcq,Ticam1, Tlr4,Tnf,Traf2,Traf3,Traf6
GO.0048583	regulation of response to stimulus	20	1.96e-10	Apbb1,App,Cd24a,Clec4n,Clu,Cxcr4,Egr1,Ets1,Hp,Il1b,Map3k7, Myd88,Pf4,Tab2,Ticam1,Tlr4,Tnf,Traf2,Traf3,Traf6
GO.0010942	positive regulation of cell death	12	2.53e-10	Apbb1,Cd24a,Cd40,Cd40lg,Clu,Egr1,Hp,Ifit2,Il1b,Niacr1,Tnf,Traf2

IX. FIGURES

Figure 1. A. Representation of flowcytometry experiments for the definition of the circulating monocyte subsets in non-diabetic control (left) and diabetic (right) wild-type mice. **B.** Full flowcytometry gating strategy with antibody panel used, and number of events of the principal leukocyte populations.

Figure 2. Absolute number of circulating leukocytes in the peripheral blood of diabetic (DM) and control (C) mice, measured by hemocytometer. *P=0.0001

Figure 3. Lymphocytes, granulocytes and total monocytes expressed as percentage of circulating leukocytes in diabetic (DM) and control (C) mice, measured by flowcytometry. *P=0.02

Figure 4. Percent of monocyte subpopulations in wild-type diabetic and control mice. Bars represent mean ± SD for the indicated number of observations. Statistical analysis was performed using ANOVA, followed by post-hoc testing with the Bonferroni test. INF, Inflammatory monocytes; INT, Intermediate monocytes; PAT, Patroller monocytes. *P<0.0001 vs intermediate monocytes in controls. **P=0.015 vs patroller monocytes in controls

Figure 5. Retinal microvessels immunostained for FITC-ConcanavalinA (green, to identify adherent cells) and for Cy3-CD45 (red, to identify WBCs) show co-localization of the two fluorochromes.

Figure 6. Scatterplot and Pearson correlation between FITC-ConA and Cy3-CD45 measurements performed in the four experimental animal groups.

Figure 7. Number of FITC-ConA+ cells per retina in wild-type and NR4A1$^{-/-}$ mice. Bars represent mean ± SD for the indicated number of observations. Statistical analysis was performed using ANOVA for the 4 groups, followed by post-hoc testing with the Bonferroni

test. C, control mice; DM, diabetic mice. *P<0.001 vs WT-C and KO-DM; **P=0.02 vs WT-DM.

Figure 8. Retinal microvessels immunostained for FITC-ConcanavalinA (green, to identify leukocytes) and for Cy3-CD16.2 (red, to identify Patroller monocytes) show co-localization of the two fluorochromes in a subset of adherent cells.

Figure 9. CD16.2 (aka FcgRIV) Median Fluorescence Intensity of circulating leukocyte subpopulations from wild-type control (WT-C), wild type diabetic (WT-DM), and Nr4A1-/- control (KO) mice, measured by flowcytometry.

Figure 10. Enumeration of $CD16.2^{+}$ cells in perfused retinal microvessels. Panel A, pie graph representing the relative proportion of FITC-ConA+/CD16.2+ cells (black) of total FITC-ConA+ cells. Panel B, absolute number of leukocytes (FITC-ConA+ cells, white bars) and patrolling monocytes (CD16.2+ cells, black bars). For each mouse, counts are the mean of the two eyes, counted by masked observers. C, control mice (n=15 FITC-ConA+ cells/n=4 CD16.2+ cells); DM, diabetic mice (n=10 FITC-ConA+ cells/n=5 CD16.2+ cells). *P<0.001; *P<0.0001.

Figure 11. Retinal fluorescein angiograms in wild-type and $Nr4a1^{-/-}$ mice at 3 and 16 months of age. In parentheses the mouse identification code.

Figure 12. Acellular capillaries in retinal trypsin digests of two wild-type and two Nr4a1-/- mice at 5 and 18 months of age. In parentheses the mouse identification code. The acellular capillaries are identified by the red filling. The red numbers represent the length of the acellular segments, which must meet the criterion of being > 40µm.

Figure 13. Enumeration of Retinal Acellular Capillaries in at 6, 14, and 18 months of age in wild-type and Nr4A1-/- mice.

Figure 14. Retinal fluorescein angiograms in one wild-type and one NR4A1-/- mouse after 4 months of diabetes. In parentheses the mouse identification code. OS, left eye; OD, right eye.

Figure 15. Number of acellular capillaries per mm^2 retinal trypsin digest in wild-type and $NR4A1^{-/-}$ mice after 4 months of diabetes. Bars represent mean ± SD for the indicated number of observations. Statistical analysis was performed using ANOVA for the 4 groups, followed by post-hoc testing with the Bonferroni test. C, control mice; DM, diabetic mice.

Figure 16. Representative images of Fluorescein Angiograms from WT (Panel A) and $NR4A1^{-/-}$ (Panel B) mice after 6 months of diabetes. In parentheses the mouse identification code.

Figure 17. Acellular capillaries in retinal trypsin digests of two wild-type and two NR4A1-/- mice after 6 months of diabetes. In parentheses the mouse identification code. The acellular capillaries are identified by the red filling. The red numbers represent the length of the acellular segments, which must meet the criterion of being > 40µm.

Figure 18. Number of acellular capillaries per mm2 retinal trypsin digest in wild-type and NR4A1-/- mice after 6 months of diabetes. Bars represent mean ± SD for the indicated number of observations. Statistical analysis was performed using ANOVA for the 4 groups, followed by post-hoc testing with the Bonferroni test. C, control mice; DM, diabetic mice. *P<0.0001 vs WT-DM, NR4A-/--C, and WT-C; **P=0.006 vs WT-C.

Figure 19. Principal Component Analysis (PCA) of the RNAsequencing data.

Figure 20. Heat Map of the RNAsequencing data.

Figure 21. STRING analysis comparing genes significantly enriched. Edges in the graph represent protein-protein interactions.

Edge colors are from STRING: teal, interactions from curated databases; purple, experimentally determined interactions; green, gene neighborhood; blue, databases; red, gene fusions; dark blue, gene co-occurrence; pale green, text-mining; black, coexpression; lavender, protein homology.

Figure 1. Representation of flowcytometry experiments

A.

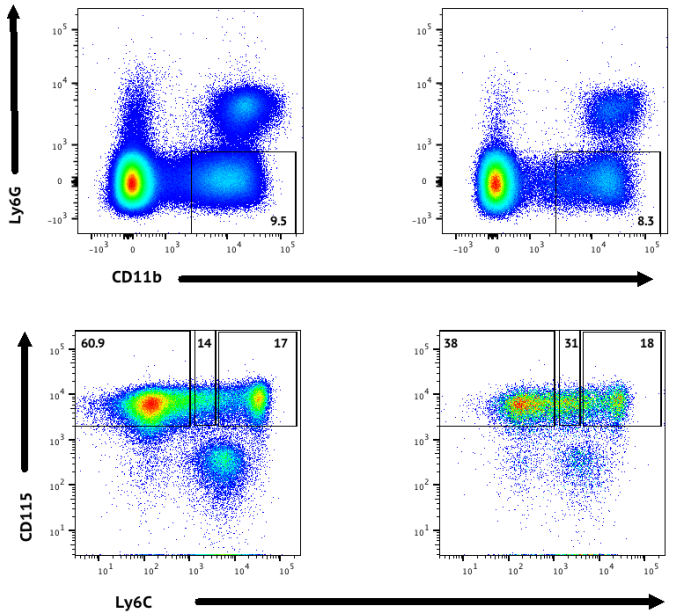

B.

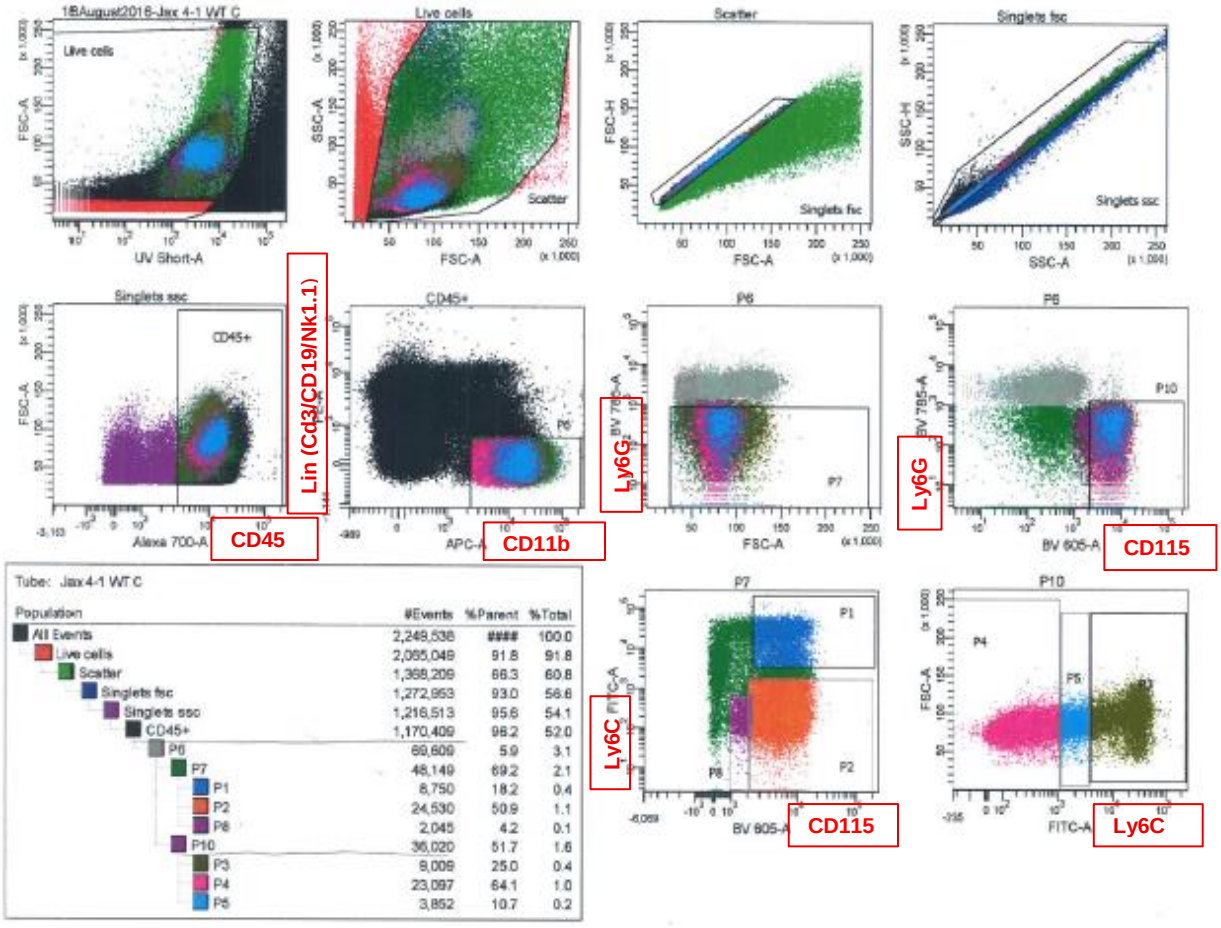

Figure 2. Circulating leukocytes in peripheral blood

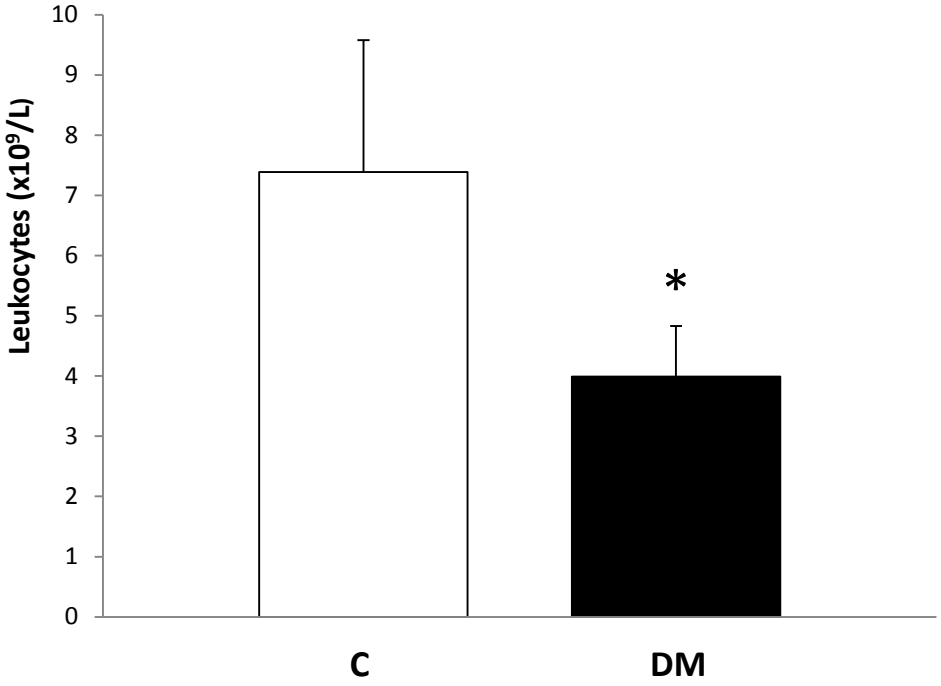

Figure 3. Leukocyte subpopulations

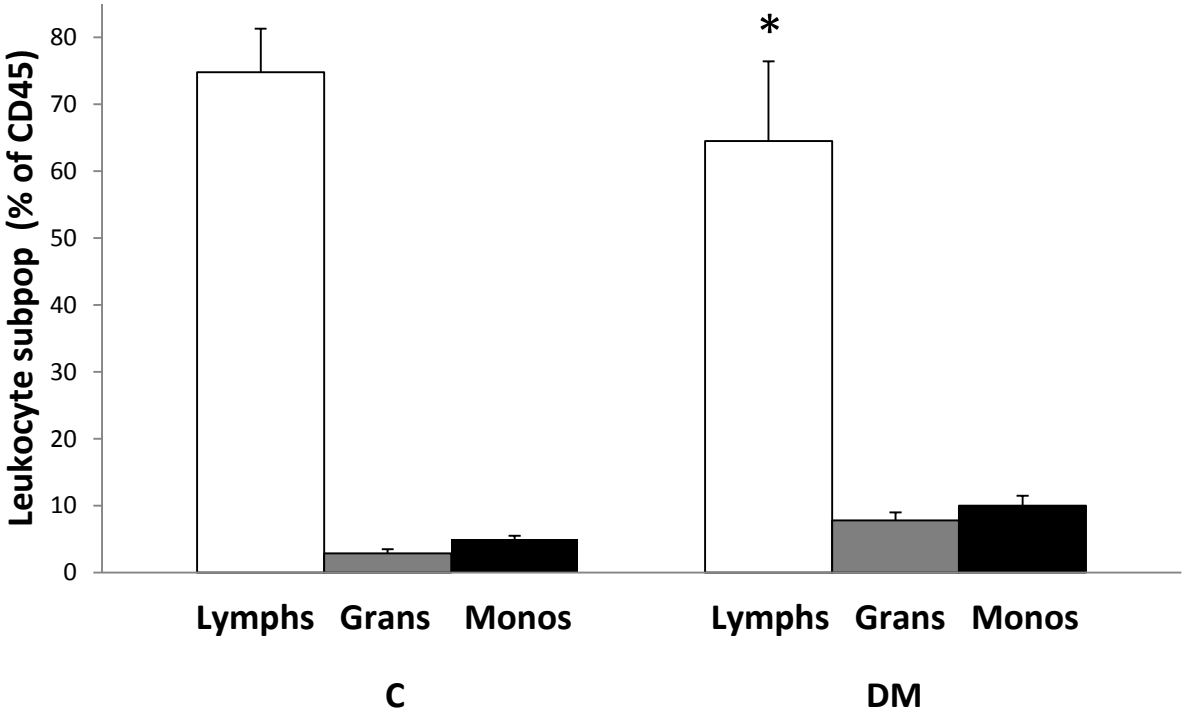

Figure 4. Monocyte subpopulations

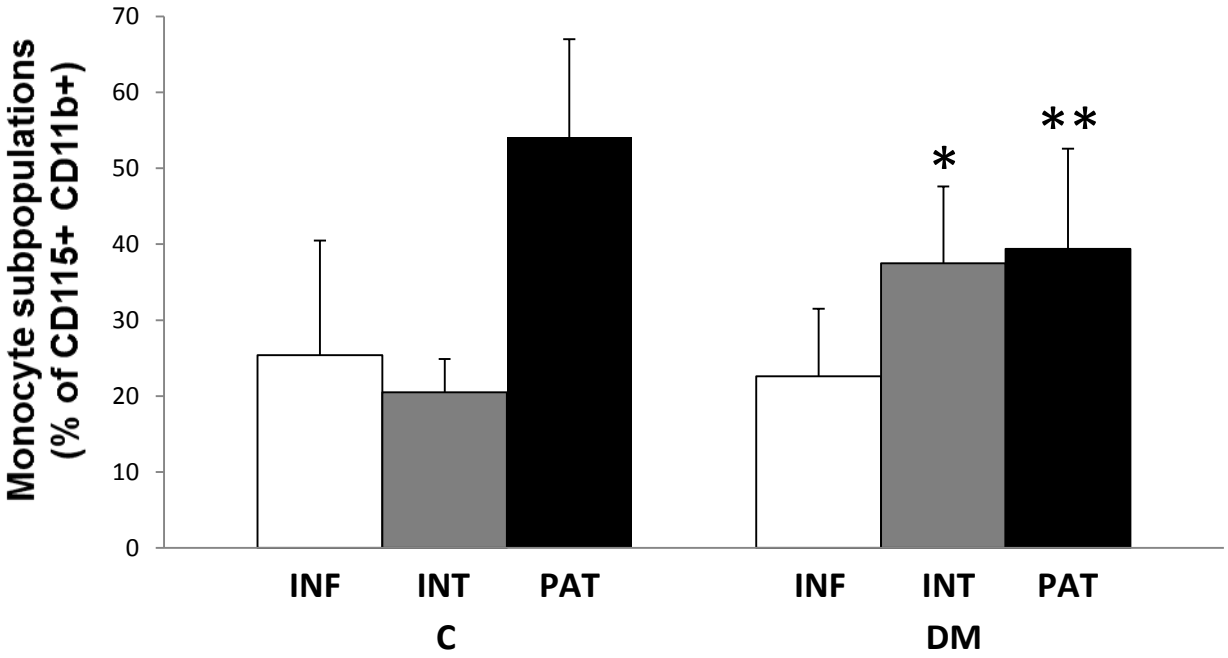

Figure 5. Adherent cells in retinal microvessels are CD45+

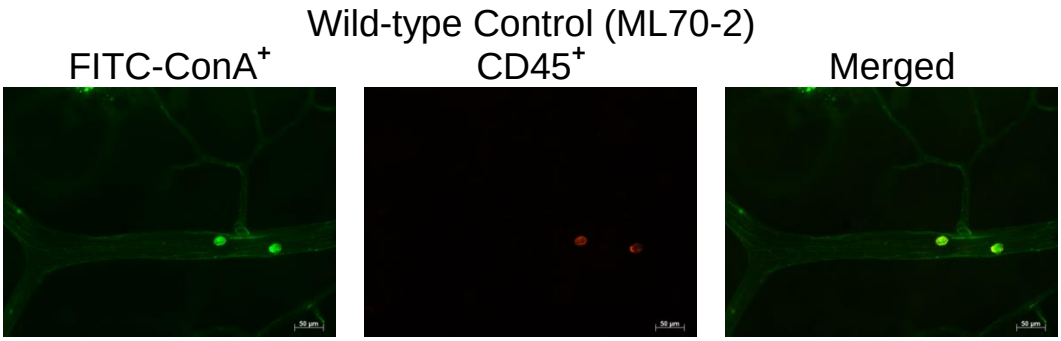

Figure 6. Correlation between FITC-ConA and CD45

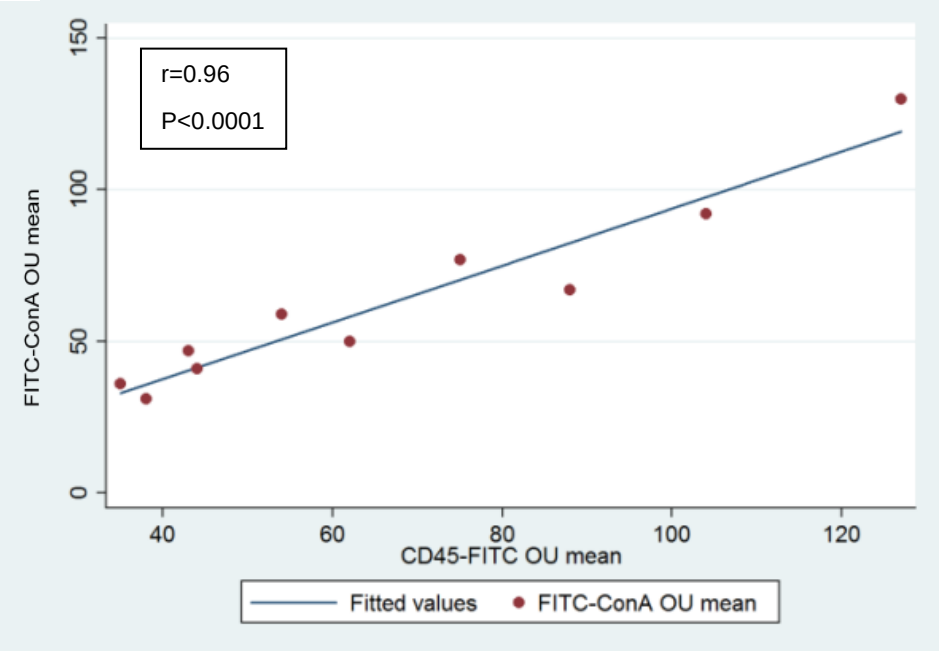

Figure 7. FITC-ConA+ cells counted on retinal whole mounts

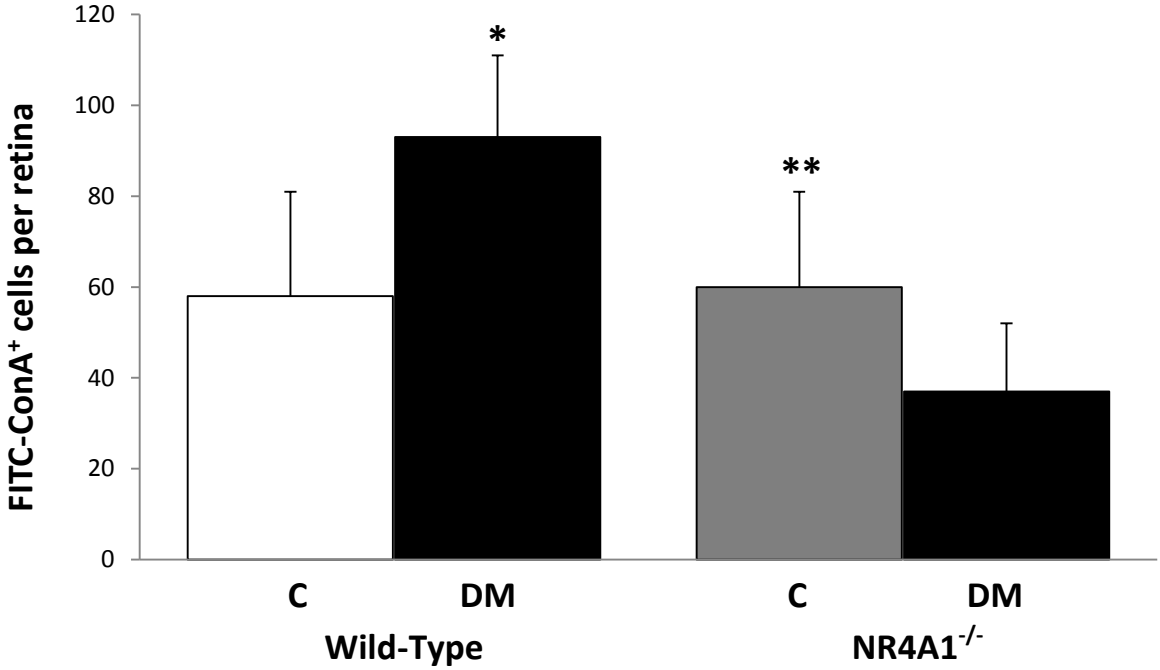

Figure 8. A subset of adherent cells (leukostasis) in retinal microvessels are Patrolling monocytes

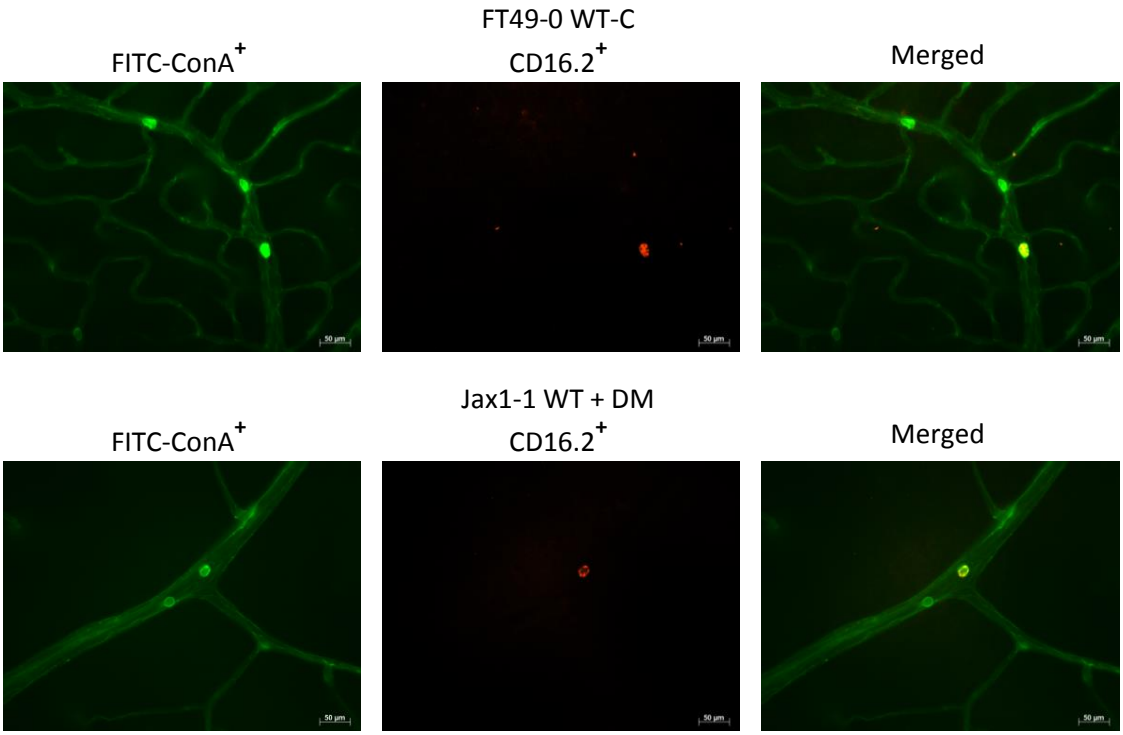

Figure 9: CD16.2 Median Fluorescence Intensity in leukocyte subpopulations

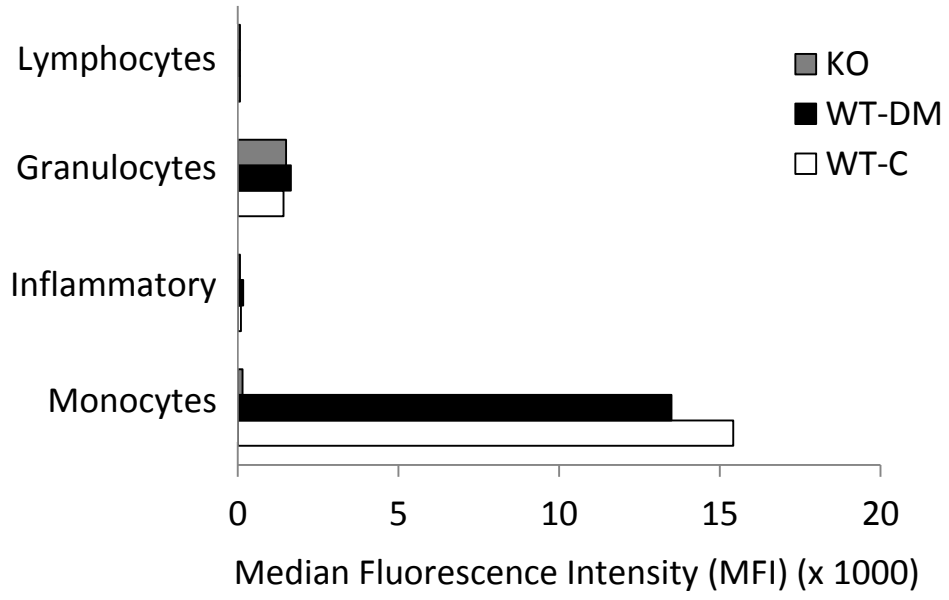

Figure 10. Enumeration of CD16.2+ cells in perfused retinas

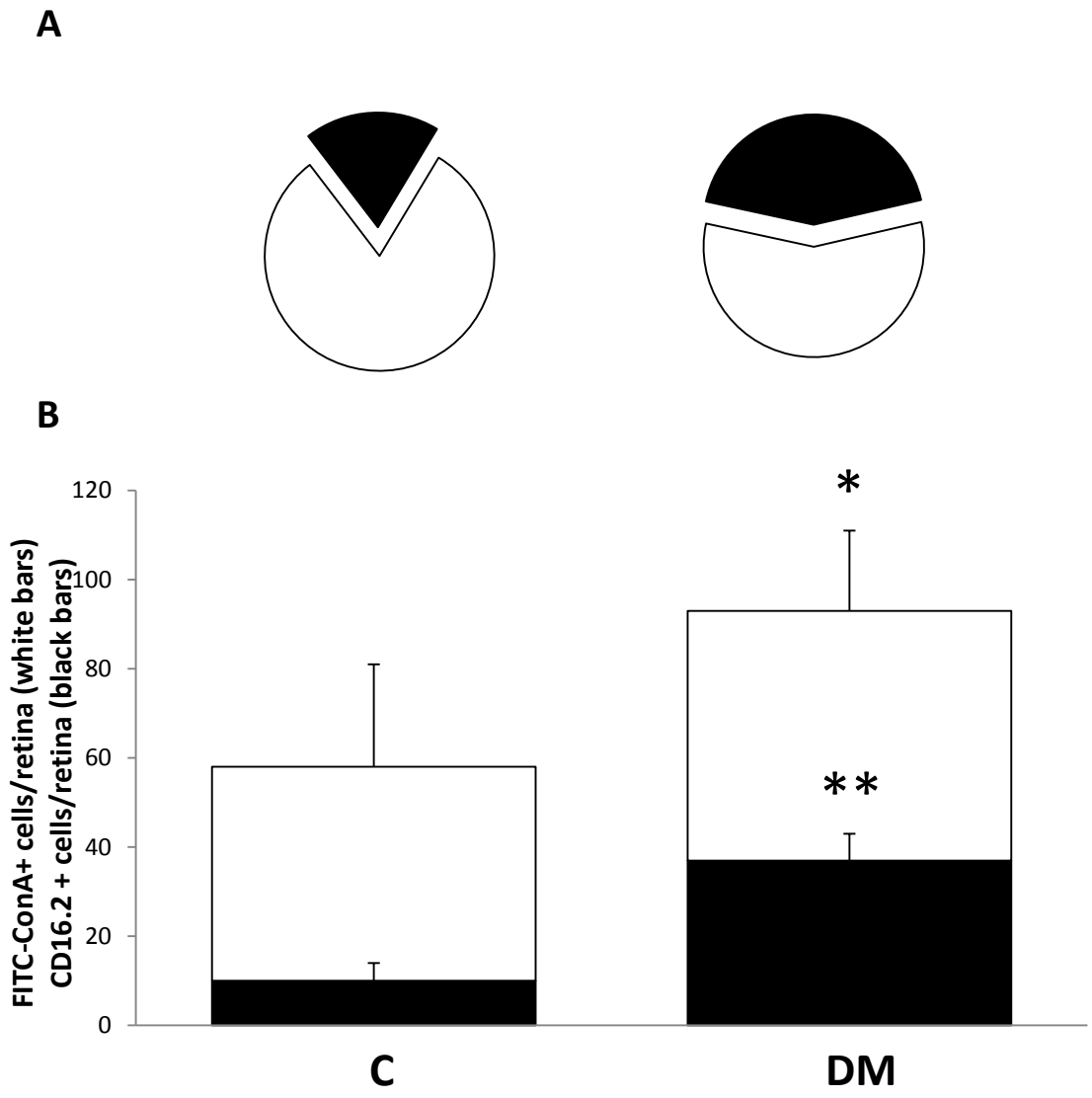

Figure 11. Retinal Fluorescein Angiography in healthy aging

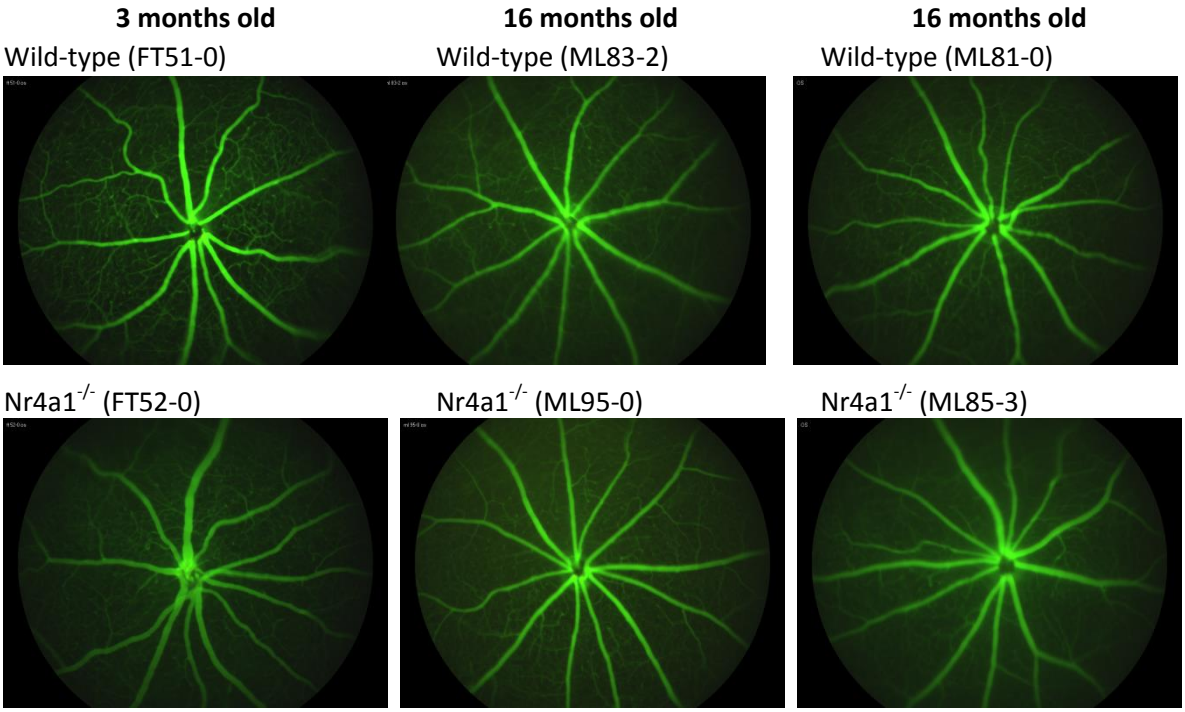

Figure 12. Retinal Acellular Capillaries in healthy aging

5 Months Old

Wild-type (ML23-1)

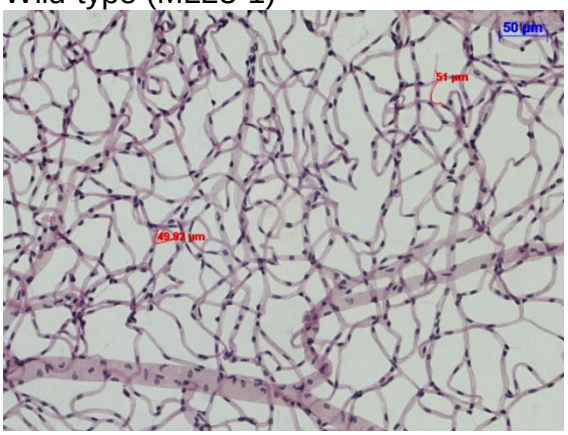

Nr4A1-/- (ML18-3)

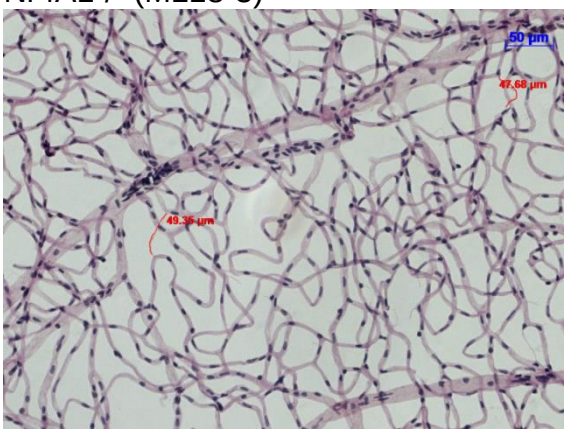

18 Months Old

Wild-type (ML47-3)

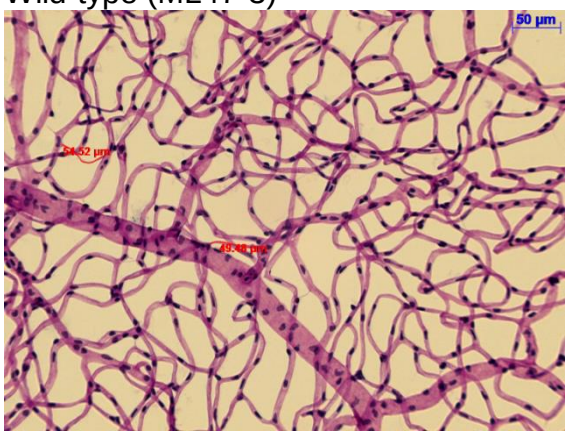

Nr4A1-/- (ML39-3)

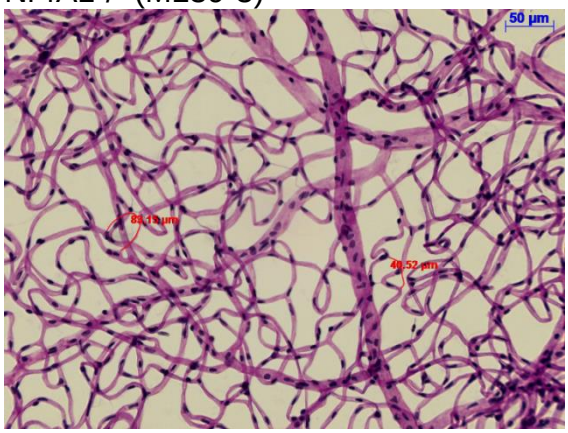

Figure 13. Enumeration of Retinal Acellular Capillaries in healthy aging.

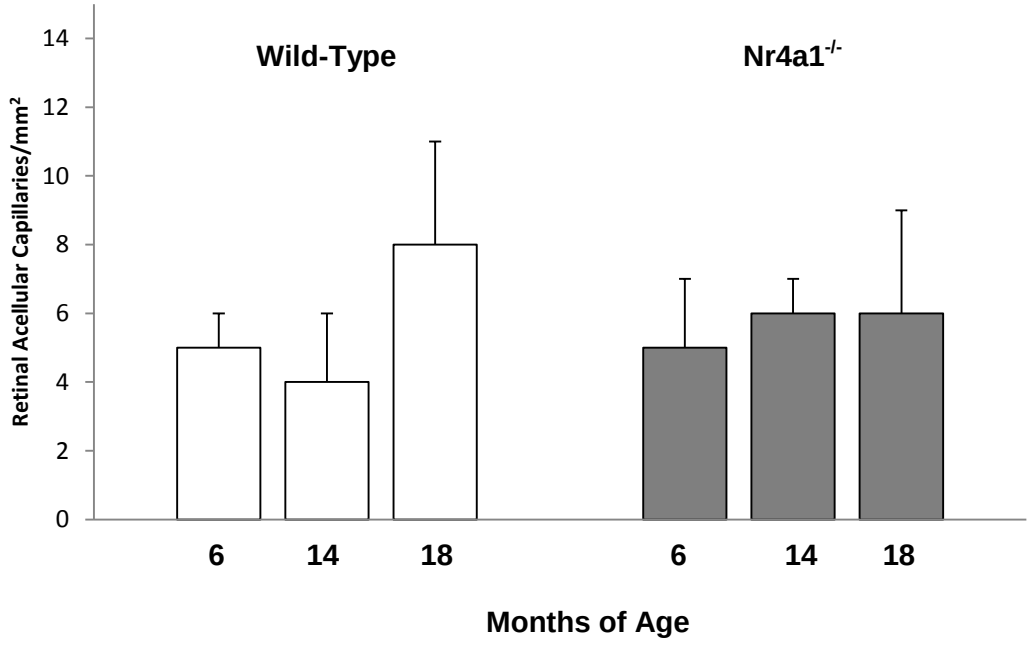

Figure 14. Fluorescein Angiography after 4 months of Diabetes

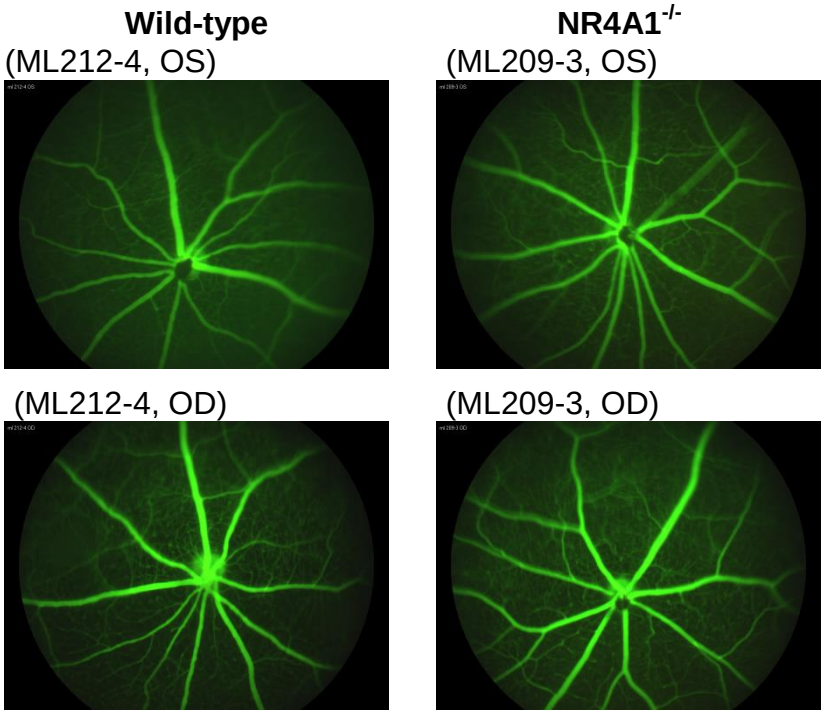

Figure 15. Enumeration of Retinal Acellular Capillaries after 4 Months of Diabetes

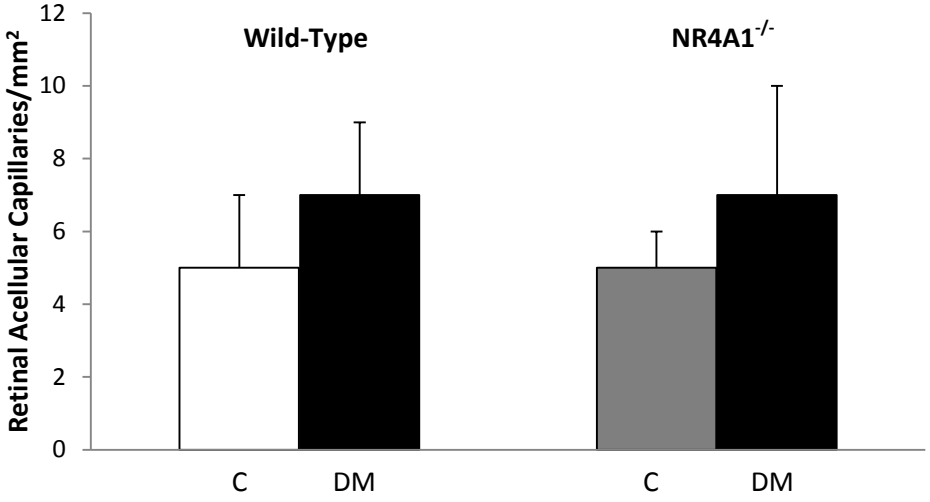

Figure 16. Fluorescein Angiography after 6 months of Diabetes

A. WT mice

Wild-type
(ML224-2, OS)

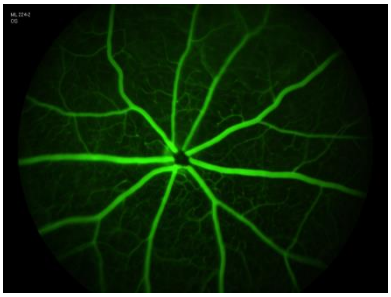

Wild-type
(ML224-3, OS)

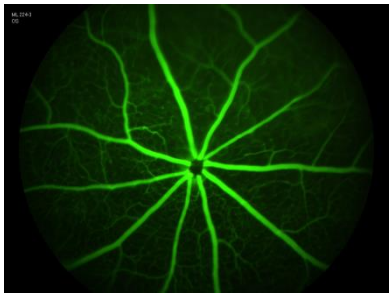

(ML224-2, OD)

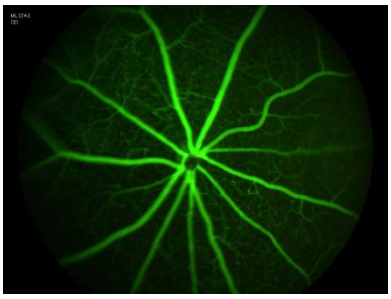

(ML224-3, OD)

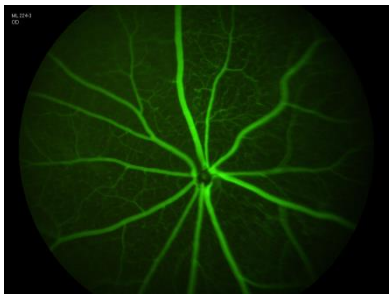

B. NR4A1$^{-/-}$ mice

NR4A1$^{-/-}$
(FT44-0 OS)

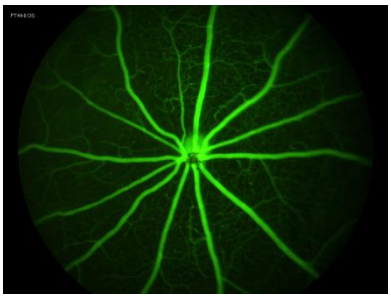

NR4A1$^{-/-}$
(FT44-1 OS)

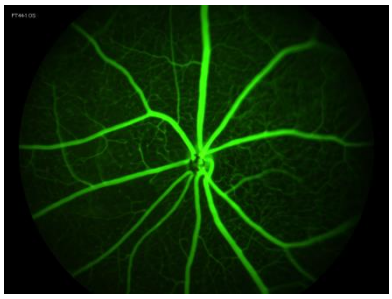

(FT44-0 OD)

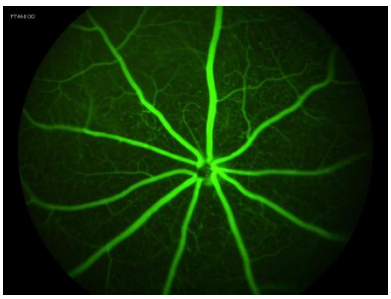

(FT44-1 OD)

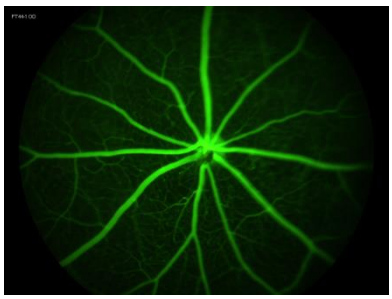

Figure 17. Retinal Acellular Capillaries after 6 months of DM

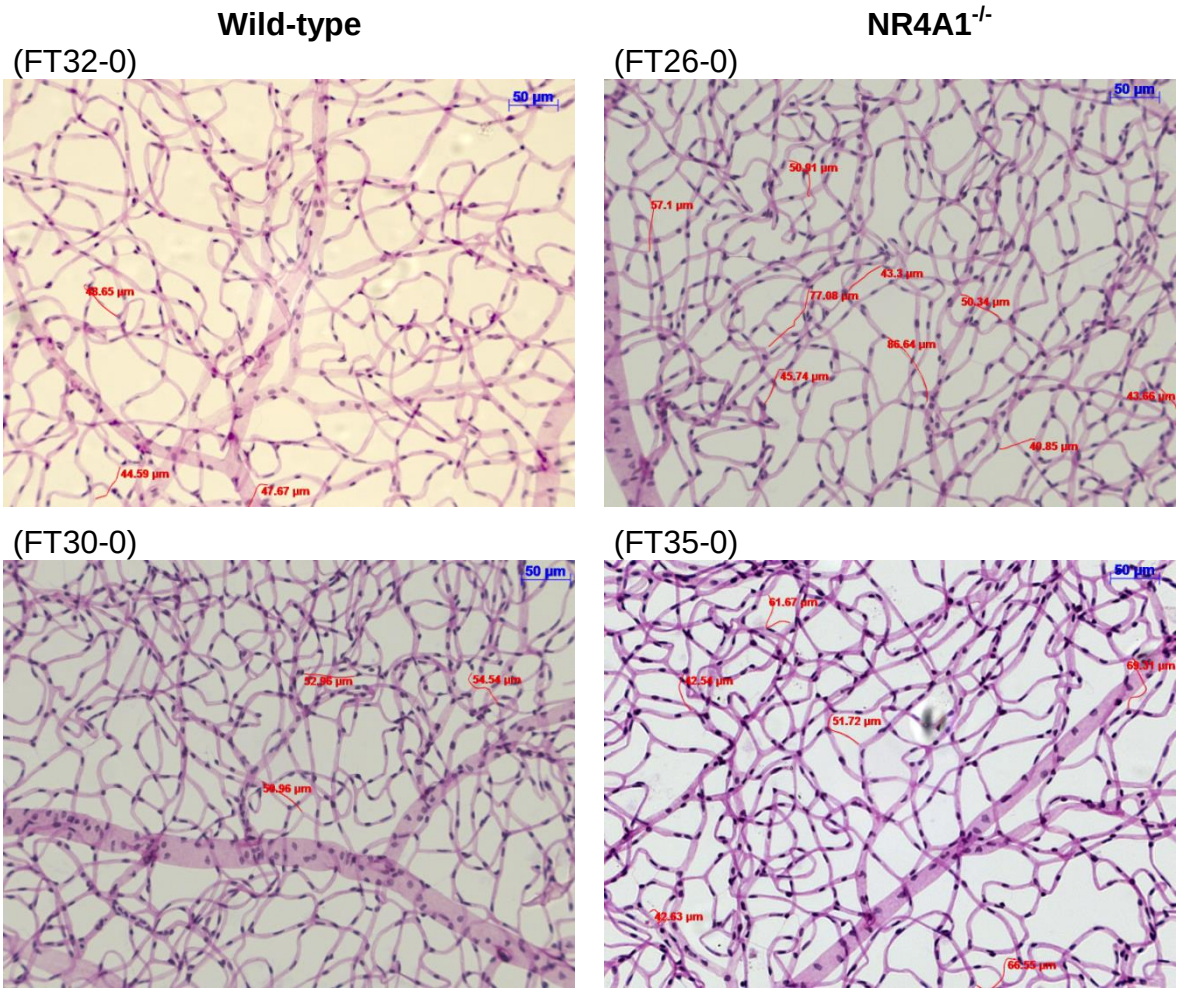

Figure 18. Enumeration of Retinal Acellular Capillaries after 6 Months of Diabetes

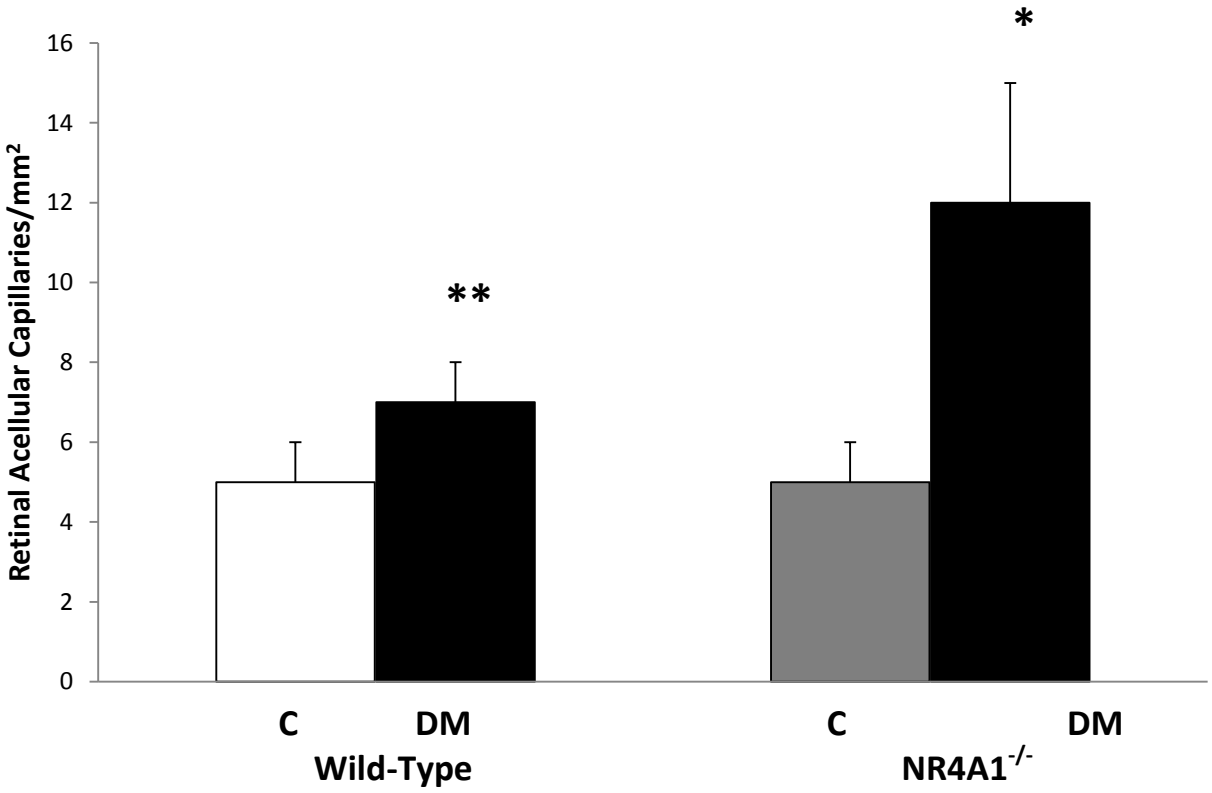

Figure 19. Principal Compinent Analysis (PCA)

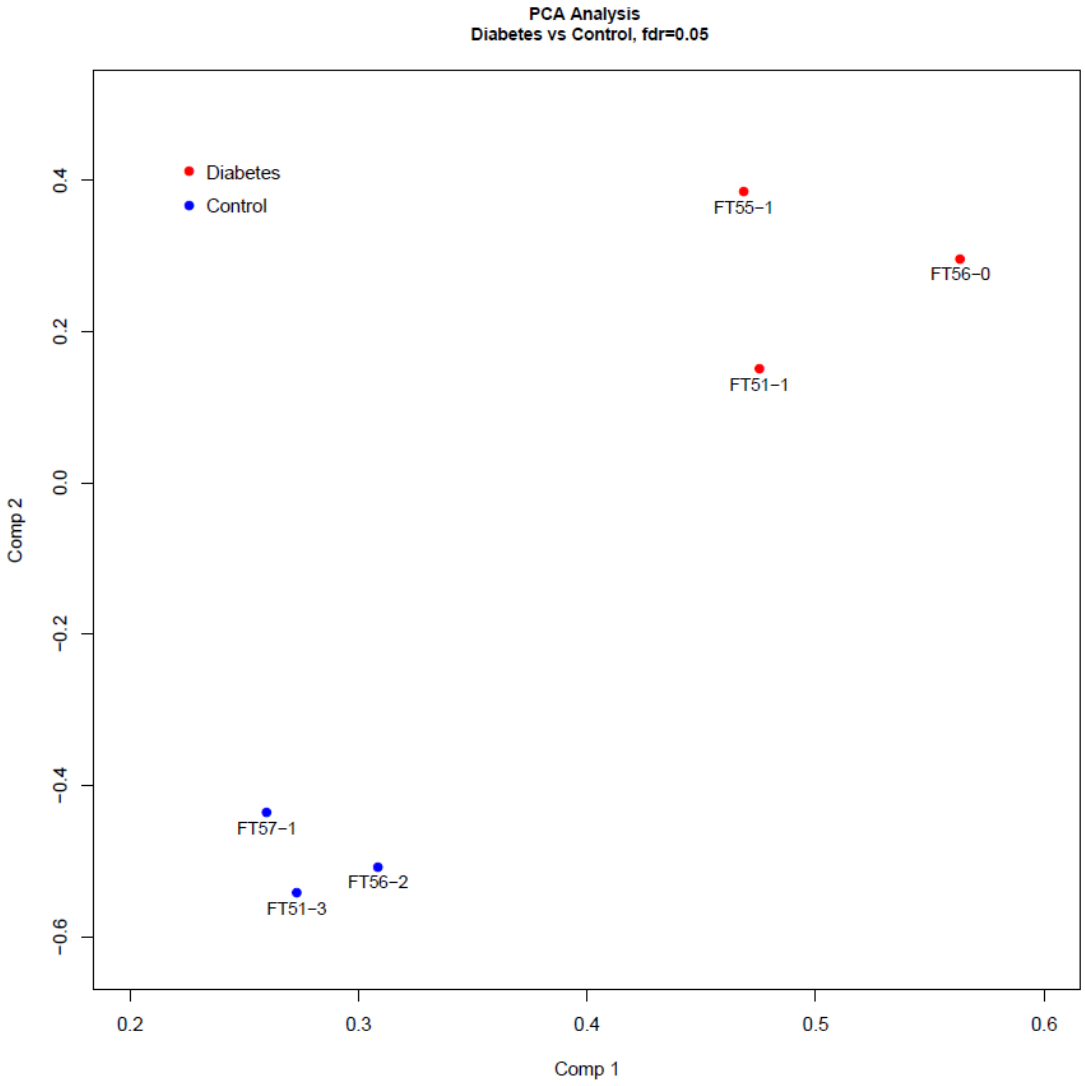

Figure 20. Heat Map

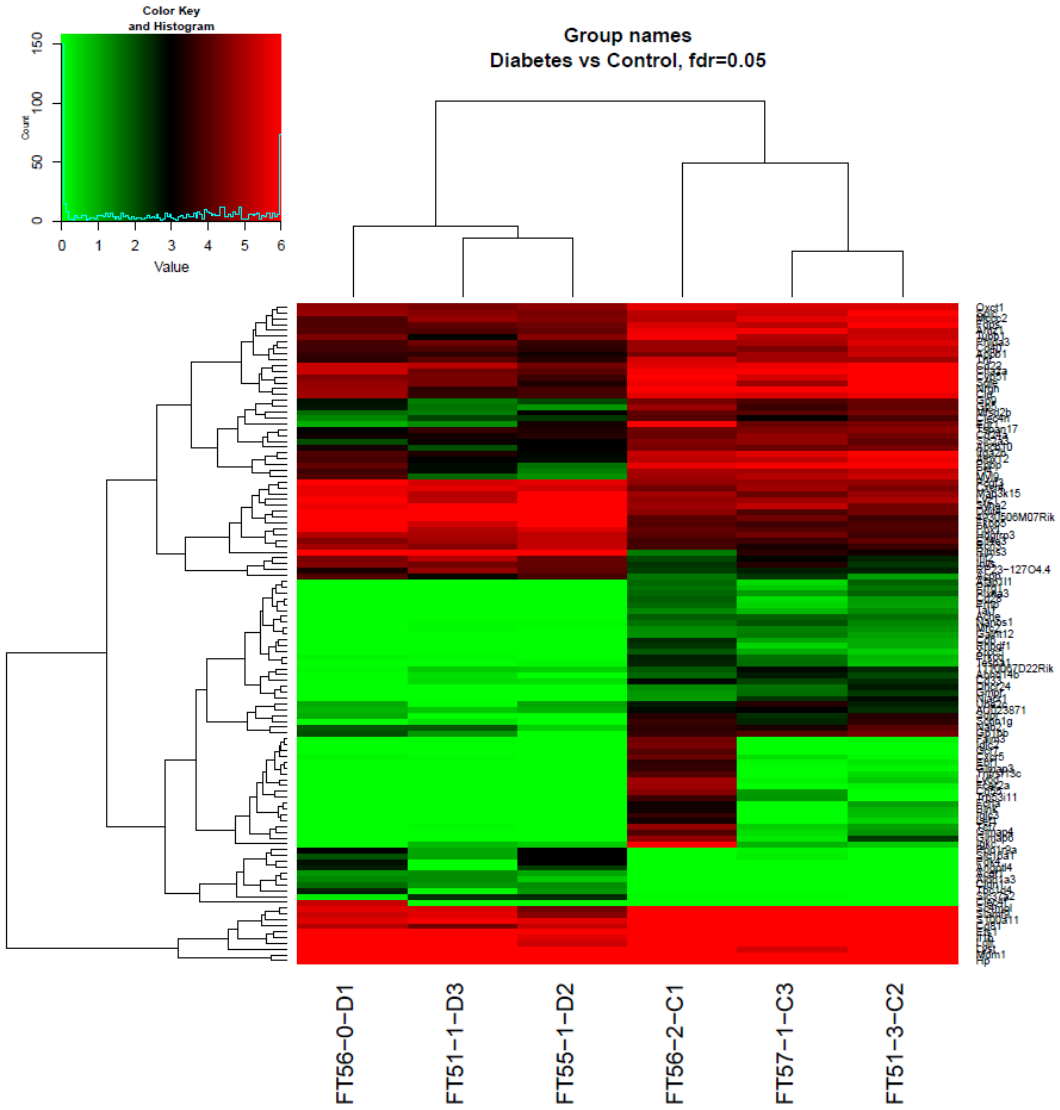

Figure 21. STRING analysis comparing genes significantly enriched